

## A GOLDEN STANDARD TYPE IA SUPERNOVA SN 2005CF: OBSERVATIONS FROM THE ULTRAVIOLET TO THE NEAR-INFRARED WAVEBANDS

X. F. WANG<sup>1,2</sup>, W. D. LI<sup>1</sup>, A. V. FILIPPENKO<sup>1</sup>, R. J. FOLEY<sup>1,3,4</sup>, R. P. KIRSHNER<sup>3</sup>, M. MODJAZ<sup>3,1,5</sup>, J. BLOOM<sup>1</sup>, P. J. BROWN<sup>6</sup>, D. CARTER<sup>7</sup>, A. S. FRIEDMAN<sup>3</sup>, A. GAL-YAM<sup>8</sup>, M. GANESHALINGAM<sup>1</sup>, M. HICKEN<sup>3</sup>, K. KRISCIUNAS<sup>9</sup>, P. MILNE<sup>10</sup>, N. B. SUNTZEFF<sup>9</sup>, W. M. WOOD-VASEY<sup>3,11</sup>, S. B. CENKO<sup>1,12</sup>, P. CHALLIS<sup>3</sup>, D. B. FOX<sup>6</sup>, D. KIRKMAN<sup>14</sup>, J. Z. LI<sup>2</sup>, T. P. LI<sup>2</sup>, M. A. MALKAN<sup>15</sup>, D. B. REITZEL<sup>15</sup>, R. M. RICH<sup>15</sup>, F. J. D. SERDUKE<sup>1</sup>, R. C. SHANG<sup>2</sup>, J. M. SILVERMAN<sup>1</sup>, T. N. STEELE<sup>1</sup>, B. J. SWIFT<sup>1</sup>, C. TAO<sup>16</sup>, D. S. WONG<sup>1</sup>, AND S. N. ZHANG<sup>2</sup>

*Draft version October 27, 2018*

### ABSTRACT

We present extensive photometry at ultraviolet (UV), optical, and near-infrared (NIR) wavelengths, as well as dense sampling of optical spectra, for the normal type Ia supernova (SN Ia) 2005cf. The optical photometry, performed at eight different telescopes, shows a  $1\sigma$  scatter of  $\lesssim 0.03$  mag after proper corrections for the instrument responses. From the well-sampled light curves, we find that SN 2005cf reached a  $B$ -band maximum at  $13.63 \pm 0.02$  mag, with an observed luminosity decline rate  $\Delta m_{15}(B) = 1.05 \pm 0.03$  mag. The correlations between the decline rate and various color indexes, recalibrated on the basis of an expanded SN Ia sample, yield a consistent estimate for the host-galaxy reddening of SN 2005cf, e.g.,  $E(B - V)_{\text{host}} = 0.09 \pm 0.03$  mag. The UV photometry was obtained with the *Hubble Space Telescope* and the *Swift* Ultraviolet/Optical Telescope, and the results match each other to within 0.1–0.2 mag. The UV light curves show similar evolution to the broadband  $U$ , with an exception in the 2000–2500 Å spectral range (corresponding to the F220W/uvw2 filters), where the light curve appears broader and much fainter than that on either side (likely owing to the intrinsic spectral evolution). Combining the UV data with the ground-based optical and NIR data, we establish the generic UV-optical-NIR bolometric light curve for SN 2005cf and derive the bolometric corrections in the absence of UV and/or NIR data. The overall spectral evolution of SN 2005cf is similar to that of a normal SN Ia, but with variety in the strength and profile of the main feature lines. The spectra at early times displayed strong, high-velocity (HV) features in the Ca II H&K doublet and NIR triplet, which were distinctly detached from the photosphere ( $v \approx 10,000$  km s<sup>-1</sup>) at a velocity ranging from 19,000 to 24,000 km s<sup>-1</sup>. One interesting feature is the flat-bottomed absorption observed near 6000 Å in the earliest spectrum, which rapidly evolved into a triangular shape and then became a normal Si II  $\lambda 6355$  absorption profile at about one week before maximum brightness. This pre-maximum spectral evolution is perhaps due to the blending of the Si II  $\lambda 6355$  at photospheric velocity and another HV absorption component (e.g., Si II shell at a velocity  $\sim 18,000$  km s<sup>-1</sup>) in the outer ejecta, and may be common in other normal SNe Ia. The possible origin of the HV absorption features is briefly discussed.

*Subject headings:* supernovae: general – supernovae: individual (SN 2005cf)

<sup>1</sup> Department of Astronomy, University of California, Berkeley, CA 94720-3411; wangxf@astro.berkeley.edu .

<sup>2</sup> Physics Department and Tsinghua Center for Astrophysics (THCA), Tsinghua University, Beijing, 100084, China; wang\_xf@mail.tsinghua.edu.cn .

<sup>3</sup> Harvard-Smithsonian Center for Astrophysics, 60 Garden Street, Cambridge, MA, 02138.

<sup>4</sup> Clay Fellow.

<sup>5</sup> Miller Fellow.

<sup>6</sup> Pennsylvania State University, Department of Astronomy & Astrophysics, University Park, PA 16802.

<sup>7</sup> Astrophysics Research Institute, Liverpool John Moores University, Twelve Quays House, Egerton Wharf, Birkenhead CH41 1LD, UK.

<sup>8</sup> Ben-Ziyo Center for Astrophysics, Weizmann Institute of Science, 76100 Rhovot, Israel.

<sup>9</sup> Department of Physics, Texas A&M University, College Station, Texas, 77843.

<sup>10</sup> Steward Observatory, University of Arizona, 933 North Cherry Avenue, Tucson, AZ 85721.

<sup>11</sup> Department of Physics, University of Pittsburgh, 100 Allen Hall, Pittsburgh, PA 15260.

<sup>12</sup> Space Radiation Laboratory, MS 220-47, California Institute of Technology, Pasadena, CA 91125

<sup>13</sup> Department of Astronomy & Astrophysics, 525 Davey Laboratory, Pennsylvania State University University park, PA 16802

### 1. INTRODUCTION

Type Ia supernovae (SNe Ia) play important roles in diverse areas of astrophysics, from chemical evolution of galaxies to observational cosmology. They, together with the core-collapse SNe, are responsible for most of the heavy elements in the universe. SNe Ia have also been used over the past decade as the most powerful tool probing the expansion history of the universe. Owing to a relatively homogeneous origin — probably an accreting carbon-oxygen white dwarf (WD) with a mass close to the Chandrasekhar limit ( $\sim 1.4 M_{\odot}$ ) in a binary system (for a review see Hillebrandt & Niemeyer 2000) — most SNe Ia show strikingly similar spectral and photometric

<sup>14</sup> CASS 0424, University of California, San Diego, 9500 Gilman Drive, La Jolla, CA 92093-0424.

<sup>15</sup> Department of Physics and Astronomy, University of California, Los Angeles, CA 90095-1547.

<sup>16</sup> CPPM/CNRS Centre de Physique des Particules de Marseille & LAM/CNRS Laboratoire d'Astrophysique de Marseille Université de la Méditerranée, France.

behavior (e.g., Branch & Tammann 1992; Suntzeff 1996; Filippenko 1997). In particular, the observed peak luminosities of SNe Ia have been shown to correlate with the shapes of their light or color curves (e.g., Phillips 1993; Hamuy et al. 1996; Riess et al. 1996; Perlmutter et al. 1997; Wang et al. 2003; Wang et al. 2005; Guy et al. 2005; Prieto et al. 2006; Jha et al. 2007; Guy et al. 2007; Colney et al. 2008), leading to an uncertainty of  $\lesssim 10\%$  in distance measurements from SN Ia.

Based on the observations of SNe Ia at redshifts  $z \approx 0.5$ , Riess et al. (1998) and Perlmutter et al. (1999) first reported the discovery of an accelerating universe. The evidence for the acceleration expansion from SNe Ia improved markedly with follow-up studies (Barris et al. 2004; Tonry et al. 2003; Knop et al. 2003; Riess et al. 2004, 2007; Astier et al. 2006; Wood-Vasey et al. 2007a), suggesting that  $\sim 70\%$  of the universe is composed of a mysterious dark energy (for a review see, e.g., Filippenko 2005a). Elucidating the nature of dark energy would require a large sample of well-observed SNe Ia at even higher redshifts (e.g.,  $z \gtrsim 1.0$ ), and also relies on the improvement of the SN Ia standardization (e.g.,  $\lesssim 0.01$  mag). Progress can be made by searching for additional luminosity-dependent parameters, or by identifying a subsample of SNe Ia with the lowest scatter of the luminosity. This depends on the degree of our understanding of SN Ia physics as well as on the good controlling of various systematic effects such as the photometry itself, the SN luminosity evolution, and the absorption by dust. Clarification of the above issues demands a large sample of SNe Ia with well-observed spectra and light curves, from which we can get better constraints of their physical properties.

Quite a few detailed studies have been conducted of spectroscopically and/or photometrically peculiar SNe Ia such as SNe 1991T (Filippenko et al. 1992a; Phillips et al. 1992), 1991bg (Filippenko et al. 1992b, Leibundgut et al. 1993), 2000cx (Li et al. 2001; Thomas et al. 2003; Candia et al. 2003), 2002cx (Li et al. 2003; Branch et al. 2004; Jha et al. 2006a), and 2006gz (Hicken et al. 2007). A comparable number of relatively normal SNe Ia have also been individually studied, including SNe 1994D (Patat et al. 1996), 1996X (Salvo et al. 2001), 1998aq (Branch et al. 2003; Riess et al. 2005), 1998bu (Jha et al. 1999), 1999ee (Stritzinger et al. 2002; Hamuy et al. 2002), 2001el (Krisciunas et al. 2003), 2002er (Pignata et al. 2004), 2003cg (Elisa-Rosa et al. 2006), 2003du (Stanishev et al. 2007), 2004eo (Pastorello et al. 2007a), 2002bo (Benetti et al. 2004), and 2006X (Wang et al. 2008a), though the last two may differ from other typical SNe Ia due to an unusually high expansion velocity of their photospheres and a relatively flat evolution of their  $B$ -band light curves starting from the early nebular phase (Wang et al. 2008a). However, a much larger sample of SNe Ia must be investigated in order to determine the dispersion among their properties and refine possible systematic effects for precision cosmology. In addition, the sample of “golden standard” SNe Ia having extensive observations from ultraviolet (UV) through near-infrared (NIR) wavelengths is sparse. The UV properties could provide clues to the diversity and evolution of the progenitor system, as they are more sensitive to the metallicity of the ejecta as well as the degree of mixing of the synthesized  $^{56}\text{Ni}$  (Höflich et al. 1998; Blinnikov & Sorokina

2000), while the NIR data are particularly suitable for the study of dust properties and the determination of absorption corrections. The UV and NIR data are also important in helping to determine, by means of the light curves, the bolometric luminosity of SNe Ia.

In this paper, we present extensive observations of the SN Ia 2005cf in UV, optical, and NIR bands, providing a “golden standard” with which to compare other SNe Ia. Pastorello et al. (2007b; hereafter P07) and Garavini et al. (2007; hereafter G07) have previously studied the optical properties of SN 2005cf, but our unique UV data along with an excellent independent optical/NIR dataset allow us to provide better constraints on the properties of SN 2005cf. We compare our results with those of P07 and G07 where appropriate. Our observations and data reduction are described in §2, while §3 presents the UV-optical-NIR (*uvoir*) light curves, the color curves, and the reddening estimate. The spectral evolution is given in §4. In §5 we construct the bolometric light curve of SN 2005cf. Our discussion and conclusions are given in §6.

## 2. OBSERVATIONS AND DATA REDUCTION

SN 2005cf was discovered at an unfiltered magnitude of 16.4 on 2005 May 28.36 (UT dates are used throughout this paper) by Pugh & Li (2005) during the Lick Observatory Supernova Search (LOSS) with the 0.76 m Katzman Automatic Imaging Telescope (KAIT; Filippenko et al. 2001; Filippenko 2005b), with J2000 coordinates  $\alpha = 15^{\text{h}}21^{\text{m}}32^{\text{s}}.21$  and  $\delta = -07^{\circ}24'47''.5$ . It exploded in the vicinity of the tidal bridge connecting the S0 galaxy MCG–01–39–003 with the nearby Sb galaxy MCG–01–39–002 (NGC 5917); see Figure 1. Assuming MCG–01–39–003 is the host galaxy of SN 2005cf, we find that the supernova was  $15.7''$  west and  $123.0''$  north of the galaxy nucleus.

An optical spectrum taken on 2006 May 31.22 revealed that SN 2005cf was a very young SN Ia, at a phase of  $\sim 10$  d before maximum brightness (Modjaz et al. 2005). On this basis, we requested frequent optical and NIR imaging, as well as optical spectroscopy; we collected a total of 634 photometric datapoints and 39 optical spectra. Moreover, *Hubble Space Telescope (HST)* UV and NIR observations were soon triggered (proposal GO-10182; PI A. V. Filippenko) with the Advanced Camera for Surveys (ACS) and the Near-Infrared Camera and Multi-Object Spectrometer (NICMOS) at 12 different epochs. UV and optical photometry was also obtained with the Ultraviolet/Optical Telescope (UVOT) on the space-based *Swift* telescope.

### 2.1. Ground-Based Observations

#### 2.1.1. Optical and NIR Photometry

The ground-based optical photometry of SN 2005cf, spanning from 12 d before to 3 months after the  $B$ -band maximum, was obtained with the following telescopes: (1) the KAIT and the 1.0 m Nickel telescope at Lick Observatory in California; (2) the 1.2 m telescope at the Fred Lawrence Whipple Observatory (FLWO) of the Harvard-Smithsonian Center for Astrophysics (CfA) in Arizona; (3) the 1.3 m and 0.9 m telescopes at Cerro Tololo Inter-American Observatory (CTIO) in Chile; (4) the 1.5 m telescope at Palomar Observatory in Califor-

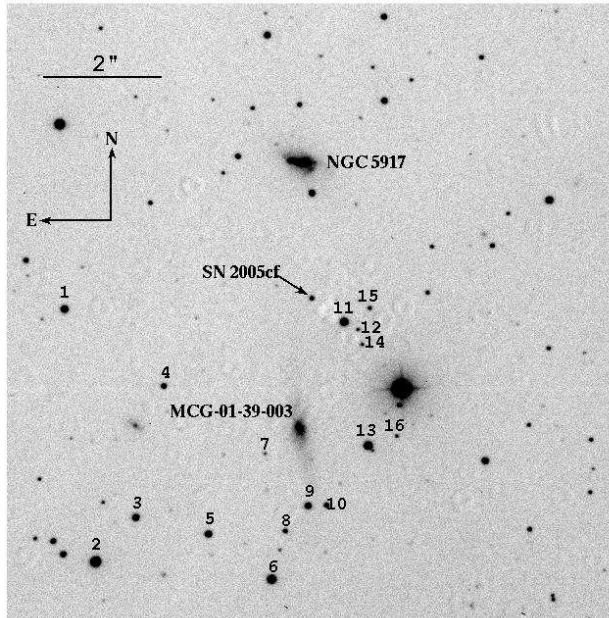


FIG. 1.— SN 2005cf in MCG-01-39-003. This is a  $V$ -band image taken with the 0.8 m TNT on 2005 Sep. 21. The supernova and 16 local reference stars are marked. North is up, and east is to the left.

nia (Cenko et al. 2006); (5) the 2.0 m Liverpool telescope at La Palma in Spain; and (6) the 0.8 m THCA-NAOC Telescope (TNT) at Beijing Xinglong Observatory (BAO) in China. Broad-band  $BVRI$  photometry was obtained with all the above telescopes, except for the FLWO 1.2 m and Liverpool 2.0 m telescopes which followed SN 2005cf in  $BV$  and Sloan  $ri$  filters. Observations made with KAIT, FLWO 1.2 m, the CTIO 0.9 m, and the Nickel 1.0 m also sampled the  $U$  band. Table 1 lists the average color terms for all of the involved telescopes and filters. The NIR ( $JHK_s$ ) photometry was obtained with the 1.3 m Peters Automated Infrared Imaging Telescope (PAIRITEL; Bloom et al. 2006) at FLWO.

As part of routine processing, all CCD images were corrected for bias, flat fielded, and cleaned of cosmic rays. Since SN 2005cf is isolated far away from the host-galaxy center, we omitted the usual step of subtracting the galaxy template from the SN images; instead, the foreground sky was determined locally and subtracted. Instrumental magnitudes of the SN and the local standard stars (labeled in Fig. 1) were measured by the point-spread function (PSF) fitting method, performed using the IRAF<sup>17</sup> DAOPHOT package (Stetson 1987).

The transformation from the instrumental magnitudes to the standard Johnson  $UBV$  (Johnson 1966) and Kron-Cousins  $RI$  (Cousins 1981) systems was established by observing, during a photometric night, a series of Landolt (1992) standards covering a large range of airmasses and colors. The average value of the photometric zero-points determined on 7 photometric nights was used

to calibrate the local standard stars in the field of SN 2005cf. Table 2 lists the standard  $UBVRI$  magnitudes and uncertainties of 16 comparison stars which were used to convert the instrumental magnitudes of the supernova to those of the standard system. Note, however, that our  $U$ -band calibration may have an uncertainty larger than that quoted in Table 2, as it was established on only a single photometric night. The  $UBV$  calibrations of SN 2005cf were also used by Li et al. (2006) to calibrate the *Swift* UVOT optical observations.

A comparison of 9 standard stars in common with P07 reveals that some systematic differences exist between the datasets. With respect to P07, our measurements are fainter by  $0.138 \pm 0.029$  mag in  $U$ ,  $0.023 \pm 0.012$  mag in  $B$ ,  $0.038 \pm 0.016$  mag in  $V$ ,  $0.041 \pm 0.006$  mag in  $R$ , and  $0.029 \pm 0.007$  mag in  $I$ . The discrepancies are non-negligible and worrisome, especially in the  $U$  band. Such differences were also noticed by Stanishev et al. (2007) in studying photometry of the comparison stars of SN 2003du; their measurements of the stars in common were found to be systematically brighter than those given in Leonard et al. (2005) and Anupama et al. (2005) by 0.04–0.06 mag in some wavebands. The origin is unclear, and further studies are needed if systematic errors are to be minimized (to  $\lesssim 0.01$  mag) when using SNe Ia to measure cosmological distances.

To reasonably assemble the optical photometric data for SN 2005cf obtained with different telescopes and place them on the Johnson-Cousins  $UVBRI$  system [e.g., from the Sloan  $ri$  to the broad-band  $RI$ ], we applied additional magnitude corrections ( $S$ -corrections; Stritzinger et al. 2002) to the photometry. This is because the color-term corrections only account for the differences derived from normal stars, whereas the spectra of SNe are quite dissimilar. Properly modeling the instrumental response is essential for deriving reliable  $S$ -corrections. The normalized instrumental response functions, obtained by multiplying the filter transmission functions with the quantum efficiency of the CCD detectors and the atmospheric transmission, are shown in Figure 2. Details of the application of the  $S$ -corrections are given in the Appendix.

Figure 3 shows the time evolution of the  $S$ -corrections and the resulting color variances for different telescopes, computed with the spectra of SN 2005cf presented in this paper and those published by G07, as well as with some late-time spectra of SN 2003du (Stanishev et al. 2007). Note that all of the  $U$ -band filter responses were cut off at  $3300 \text{ \AA}$  in the convolution due to the spectral coverage. The resulting  $S$ -corrections are generally small in  $BVR$  bands, but can be noticeably large in the  $U$  and  $I$  bands (e.g.,  $\sim 0.1$ – $0.2$  mag). It is worth noting that, without applying such a systematic magnitude correction, the  $B - V$  color measured at the CTIO 0.9 m and Palomar 1.5 m (or Lick 1.0 m) telescopes could differ by  $\sim 0.1$  mag in the early nebular phase when the colors are usually used as the reddening indicators.

Applying the  $S$ -corrections to the photometry noticeably improved the consistency of the datasets obtained with different telescopes. This is demonstrated in Fig. 4, where the scatter around the best-fit curve decreases from 0.06 mag to 0.03 mag in the  $I$  band. Improvements are also achieved for the other bands, with the photometric scatter reduced to within 0.02–0.03 mag. Such a

<sup>17</sup> IRAF, the Image Reduction and Analysis Facility, is distributed by the National Optical Astronomy Observatory, which is operated by the Association of Universities for Research in Astronomy (AURA), Inc. under cooperative agreement with the National Science Foundation (NSF).

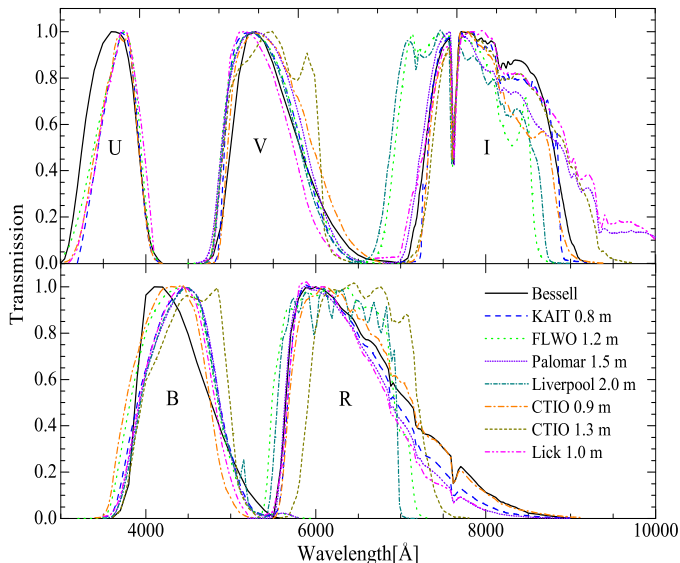


FIG. 2.— Comparison of instrumental responses of the seven telescopes, normalized to the peak transmission, with the standard Bessell Johnson/Kron-Cousins functions.

normalization in the photometry could be potentially important when comparing the properties of SNe measured with different systems. This is because a shift of a few percent in the  $B - V$  color might systematically bias the extinction correction, hence producing an error of  $\sim 10\%$  (a factor of 3–4 larger) in the derived luminosity of the SN.

We further applied  $K$ -corrections to our photometry using the same set of spectra as for the  $S$ -corrections. We note that the  $U$ -band  $K$ -correction could reach  $\sim 0.06$  mag at the earliest phases, perhaps due to a rapid evolution of the spectral shape. The large  $K$ - and  $S$ -corrections required in the  $U$  band, which were usually unavailable due to the insufficient spectral coverage, might partially account for the large scatter seen in the  $U$ -band light curve of SN 2005cf.

The final calibrated  $UBVRI$  magnitudes, after performing the  $K$ - and  $S$ -corrections, are presented in Table 3. The error bars (in parentheses) are dominated by the uncertainty in the calibration of the comparison stars.

Since the NIR observations of SN 2005cf were conducted with PAIRITEL, the instrument that defines the 2MASS photometric system, we use the 2MASS point-source catalog (Cutri et al. 2003) to calibrate the supernova. The calibrated  $JHK_s$  magnitudes of SN 2005cf are given in Table 4, which were corrected for the  $K$ -corrections (Columns (7)–(9)) computed from the NIR spectra of SN 1999ee. No  $S$ -corrections were applied to the NIR photometry because of the similarity of the transmission curves between the 2MASS system and the Persson et al. (1998) system. The filter transmission curves of these two systems are shown in Figure 5.

### 2.1.2. Optical spectroscopy

Low-resolution spectra of SN 2005cf were obtained with the Kast double spectrograph (Miller & Stone 1993) on the 3.0 m Shane telescope at Lick Observatory and the FAST spectrograph (Fabricant et al. 1998) on the Tillingham 1.5 m telescope at FLWO. Two late-time spectra

were also obtained at the W. M. Keck Observatory: one with the Low Resolution Imaging Spectrometer (LRIS; Oke et al. 1995) mounted on the 10 m Keck I telescope, and the other with the Deep Extragalactic Imaging Multi-Object Spectrograph (DEIMOS; Faber et al. 2003) mounted on the 10 m Keck II telescope. A journal of the spectroscopic observations is given in Table 5.

All spectra were reduced using standard IRAF routines (e.g., Foley et al. 2003). For the Lick/Kast observations, flatfields for the red-side spectra were taken at the position of the object to reduce NIR fringing effects. For two Lick/Kast spectra taken on 2005 June 10 and June 11, there was condensation on the red-side camera, producing non-standard and variable absorption features. To compensate for this effect, we created a two-dimensional surface map of a flat field image. We smoothed the surface map to remove any fringing in the flat. We then divided our images by this surface to remove the absorption features from our images. Although this process produced significantly improved spectra, there are still some persistent systematic features in those spectra. The Keck/DEIMOS data were reduced using a modified version of the DEEP pipeline and our own routines as described by Foley et al (2007).

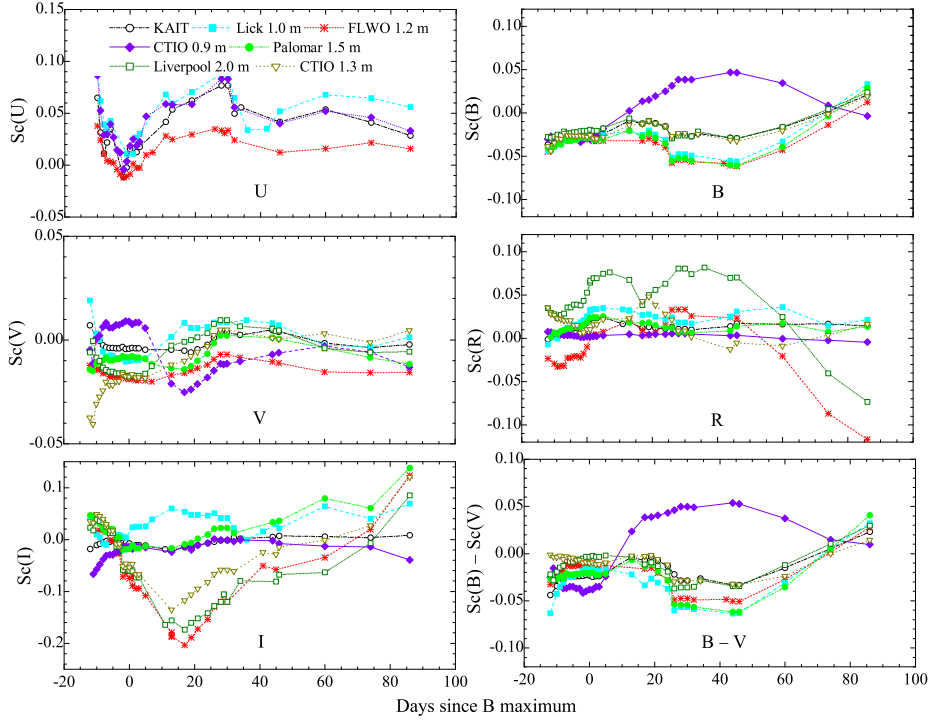
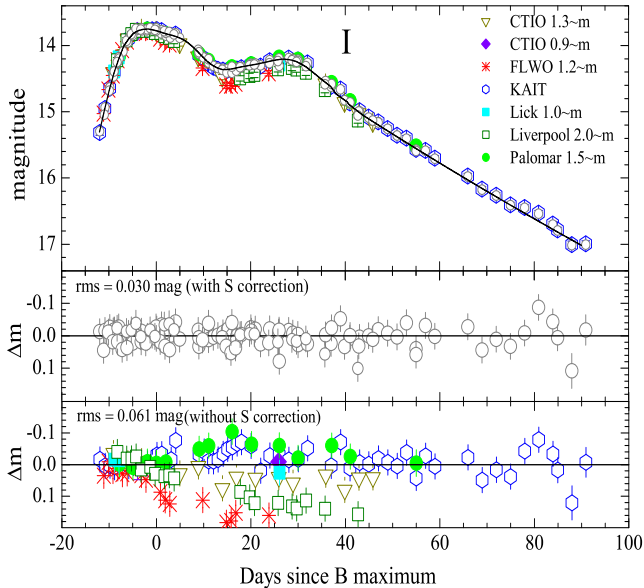
Flux calibration of the spectra was performed by means of spectrophotometric standard stars observed at similar airmass on the same night as the SN. Using our own IDL routines, the extracted, wavelength calibrated spectra were corrected for continuum atmospheric extinction using mean extinction curves for FLWO and Lick Observatory; moreover, telluric lines were removed from the data. For all the spectra observed at Lick and FLWO, the slit was always aligned along the parallactic angle to avoid chromatic effects in the data (Filippenko 1982).

## 2.2. HST UV and NIR Observations

### 2.2.1. ACS UV Photometry

Imaging of SN 2005cf was carried out with the *HST* ACS High Resolution Camera (HRC) during Cycle 13. The field of view of this CCD-based instrument is about  $29'' \times 25''$  with a scale of  $0.028'' \times 0.025'' \text{ pixel}^{-1}$ . The observations were made in the F220W, F250W, and F330W bands, with exposure times of 1040 s, 800 s, and 360 s, respectively. The exposure time was split into several equal segments that were used in the data reduction process to reject cosmic-ray events. The data produced by the STScI reduction pipeline had bias and dark-current frames subtracted and were divided by a flatfield image. In addition, known hot pixels and other defects were masked. Individual exposures were combined using the MultiDrizzle task within STSDAS to reject cosmic rays and perform geometric-distortion corrections.

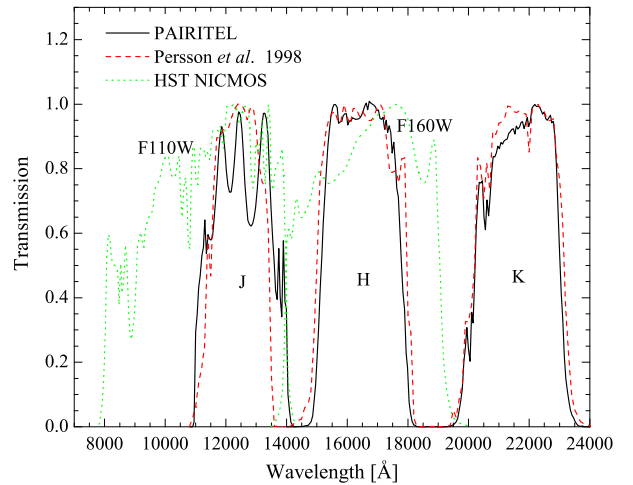
To get the optimal signal-to-noise ratio (S/N), we performed aperture photometry in all of the drizzled images using an aperture radius of 4 pixels ( $\sim 0.1''$ ). The background level was determined from the median counts in an annulus of radius 100–130 pixels. The measured magnitudes were further corrected to an infinite-radius aperture and placed on the Vega magnitude system (Sirianni et al. 2005). The final *HST* ACS UV magnitudes of SN 2005cf are listed in Table 6. Uncertainties were calculated by combining in quadrature the Poisson photon errors, the readout-noise errors from the pixels within

FIG. 3.— Time evolution of the  $S$ -corrections at the various telescopes.FIG. 4.— The  $I$ -band light curve of SN 2005cf with and without applying the  $S$ -corrections. The solid line in the upper panel represents the best fit to the  $S$ -corrected light curve.

the aperture, and errors in the aperture correction.

### 2.2.2. NICMOS NIR Photometry

The infrared observations were obtained with the *HST* NICMOS3, which has a scale of  $0.20'' \text{ pixel}^{-1}$  and a field of view of  $51'' \times 51''$ . Images were acquired through the F110W and F160W filters (see Fig. 5 for the transmission curves) at similar epochs as the optical ones with the ACS. The data were preprocessed using the STSDAS package CALNICA and the latest reference files provided by STScI. Unlike the ACS, the NICMOS cali-

FIG. 5.— Comparison of near-infrared transmission curves of PAIRITEL (ex-2MASS) and *HST* NICMOS3 with that of the Persson et al. (1998) system.

brated data are given in count rate ( $\text{DN s}^{-1}$ , where DN are data-number counts).

Aperture photometry was performed on the calibrated NICMOS3 images. Counts were summed within an aperture of 5.5 pixel radius ( $1.10''$ , the size of the aperture used for the standard-star measurements) centered on the source. To correct for a nominal infinite aperture, the measured count rates in F110W and F160W were, respectively, multiplied by 1.056 and 1.087. The total count rates were then converted into flux using the recently determined photometric scale factors,  $1.59 \times 10^{-6} \text{ Jy s DN}^{-1}$  at  $1.1 \mu\text{m}$  and  $1.93 \times 10^{-6} \text{ Jy s DN}^{-1}$  at  $1.6 \mu\text{m}$ . Corresponding zeropoints were calculated on the Vega system, assuming the zero-magnitude flux den-



sities of 1886 and 1086 Jy and the effective wavelengths of 1.12  $\mu\text{m}$  and 1.60  $\mu\text{m}$  for F110W and F160W, respectively. All of the above parameters involved in the calculations were taken from the website for *HST* NICMOS photometry<sup>18</sup>.

As the NICMOS3 filters do not match ground-based *JHK* well (especially the F110W filter, which is much broader and bluer), it is necessary to apply *S*-corrections as well as color-term corrections to place the photometry on the ground-based *JHK* system. A total of six stars (2 white dwarfs, 2 solar analogs, and 2 red stars) have been observed through both the NICMOS NIR system (F110W, F160W, and F222M filters) and the ground-based *JHK* system (Persson et al. 1998). These stars, along with the Sun, Vega, and Sirius with model IR spectra from the Kurucz web site<sup>19</sup>, allow us to establish a rough transformation between the NICMOS3 and the ground-based NIR systems for normal stars. In computing the NIR *S*-corrections we used data for SN 1999ee (Hamuy et al. 2002), which has relatively good temporal coverage of the NIR spectra and a value of  $\Delta m_{15}$  similar to that of SN 2005cf.

Table 7 gives the color-, *K*- and *S*-corrected NIR photometric results from the *HST* NICMOS3 images, consistent with the ground-based measurements within the error bars. The *S*- and color-corrections that were added to normalize the photometry to the Persson et al. (1998) system are also listed.

### 2.3. *Swift* UVOT Optical/UV Observations

SN 2005cf was also observed with the Ultraviolet/Optical Telescope (UVOT; Roming et al. 2005) onboard the *Swift* observatory (Gehrels et al. 2004), covering from 8 d before to 42 d after the *B*-band maximum. The photometric observations were performed in three UV filters (uvw1, uvm2, and uvw2) and three broadband optical filters (*U*, *B*, and *V*). As shown in Figure 6, the instrumental response curves of the UVOT uvm2 and uvw1 filters are, respectively, very similar to those of the *HST* ACS F220W and F250W filters. The UVOT optical filters are close to the standard Johnson system in *B* and *V* but exhibit noticeable difference in *U*.

Images of SN 2005cf were retrieved from the *Swift* Data Center, and were reprocessed utilizing an improved plate scale for the uvw2 images and corrections to the exposure times in the image headers (Brown et al. 2008). To maximize the S/N, we performed aperture photometry using an optimal aperture of 3.0'' radius suggested by Li et al. (2006), after first subtracting the host-galaxy light using a template image. Since the UVOT is a photon-counting detector and suffers from coincidence losses when observing bright sources, the observed counts of SN 2005cf were corrected for such losses using the empirical relation described by Poole et al. (2008). Finally, aperture corrections were applied to bring the measurements from an aperture of 3.0'' to the 5.0'' aperture with which the photometric zeropoints are calibrated on the Vega magnitude system.

As the instrumental response curves of the UVOT optical filters do not follow exactly those of the Johnson *UBV* system (see also Fig. 6), some color terms are expected.

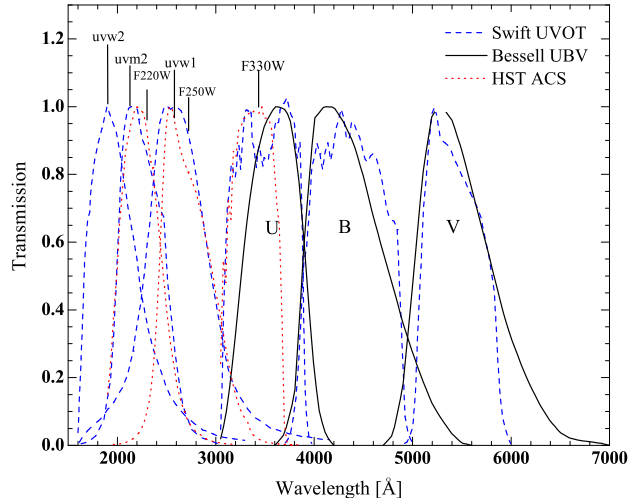


FIG. 6.— Comparison of transmission curves of *Swift* UVOT filters with *HST* ACS in the UV and with the Johnson system in *UBV*.

We calculated the synthetic color terms by convolving the instrumental response of the UVOT in the optical with the 93 spectrophotometric Landolt standard stars published by Stritzinger et al. (2005). These are  $-0.104$ ,  $-0.012$ , and  $-0.030$  in a linear correlation of the parameter pairs (*U*, *U* - *B*), (*B*, *B* - *V*), and (*V*, *B* - *V*), respectively.

The synthetic color terms are small in the *B* and *V* bands but relatively large in the *U* band. Our determinations are consistent with those measured by Poole et al. (2008) who preferred a polynomial expression. The *S*-corrections of the UVOT optical filters were derived using spectra of SN 2005cf; they are given in Table 8 (columns 10–12) and are non-negligible in the *U* band (e.g., 0.1–0.2 mag). Columns 4–9 in Table 8 list the final UVOT UV/optical magnitudes. The magnitudes in optical have been corrected for the color- and *S*-corrections.

## 3. LIGHT CURVES OF SN 2005CF

Figure 7 shows the *uvoir* light curves of SN 2005cf. The *S*- and *K*-corrections have been applied to the light curves in all of the optical and NIR bands. No *S*- or *K*-corrections were applied to the UV data. The optical light curves were sampled nearly daily during the period  $t \approx -12$  to  $+90$  d, making SN 2005cf one of the best-observed SNe Ia. The morphology of the light curves resembles that of a normal SN Ia, having a shoulder in the *R* band and pronounced secondary-maximum features in the NIR bands. The NIR light curves of SN 2005cf reached their peaks slightly earlier than the *B*-band curve. This is also the case for the UV light curves, which are found to have narrower peaks, with the exceptions of the *HST* ACS F220W and the *Swift* UVOT uvm2 filters. Detailed analysis of the light curves is described in the following subsections.

### 3.1. Optical Light Curves

A polynomial fit to the *B*-band light curve around maximum brightness yields  $B_{\text{max}} = 13.63 \pm 0.02$  mag on JD 2,453,533.66  $\pm$  0.28 (2005 June 12.16). The maximum epoch  $t_{\text{max}}(B)$  is consistent with the estimate by

<sup>18</sup> <http://www.stsci.edu/hst/nicmos/performance/photometry/>

<sup>19</sup> <http://kurucz.harvard.edu/>

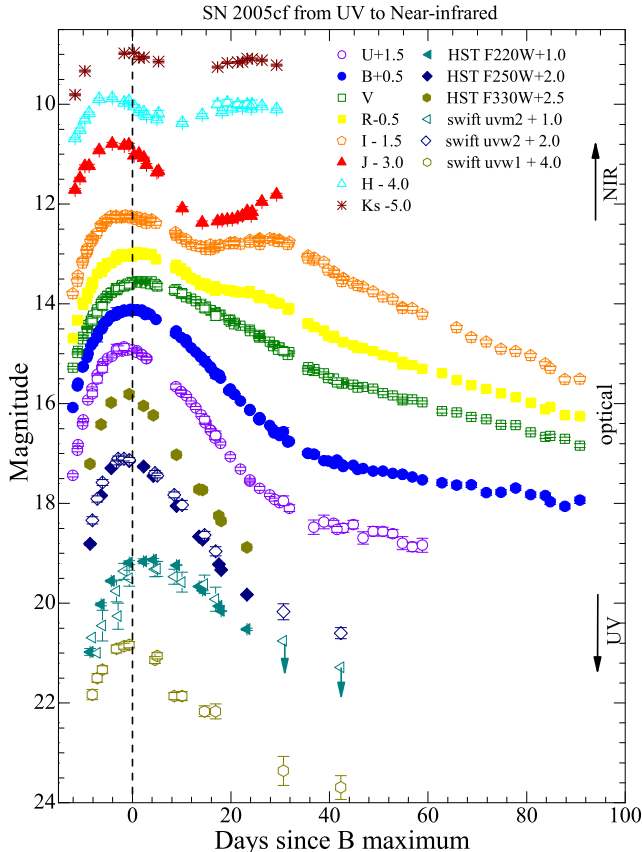


FIG. 7.— The UV, optical, and NIR light curves of SN 2005cf. The UV light curves were obtained from the photometry with *HST* ACS and the *Swift* UVOT; the *UBVRI* optical photometry was collected at eight ground-based telescopes as well as the *Swift* UVOT; and the *JHK<sub>s</sub>* data were taken with the 1.3 m PAIRITEL and with *HST* NICMOS3.

P07 while  $B_{\max}$  itself is fainter than that of P07 by 0.09 mag. The derived value of  $t_{\max}(B)$  indicates that our observations started from  $-11.9$  d and extended to  $+90.3$  d with respect to the  $B$  maximum. Likewise, the  $V$ -band light curve reached a peak magnitude of  $13.55 \pm 0.02$  on JD 2,453,535.54  $\pm 0.33$ , about 1.9 d after  $t_{\max}(B)$ . A comparable measurement was obtained by P07 who gives  $V_{\max} = 13.53 \pm 0.02$  mag. The fitting parameters for the maxima in the other bands are presented in Table 9, together with the initial decline rates within the first 15 d after their maxima (see below).

From the  $B$ - and  $V$ -band light curves, we derive an observed  $\Delta m_{15}(B) = 1.05 \pm 0.03$  mag and  $B_{\max} - V_{\max} = 0.08 \pm 0.03$  mag.<sup>20</sup> These values are slightly smaller and redder than those given by P07 [ $\Delta m_{15} = 1.11 \pm 0.05$  and  $B_{\max} - V_{\max} = 0.01 \pm 0.03$ ]. We also measured the  $B - V$  color at 12 d after the  $B$  maximum (Wang et al. 2005), obtaining  $0.47 \pm 0.04$  mag. After removal of the Galactic reddening, these color indexes are slightly redder than the intrinsic value (see also descriptions in §3.3), suggesting some line-of-sight reddening toward SN 2005cf.

Based on the extremely well-sampled photometry in the optical, we constructed the light-curve templates of

SN 2005cf by using a smoothing spline function. To obtain better sampling in the  $U$  band, the late-phase data from P07 were also included in the fit. We tabulate the template light curves in Table 11. In Figure 8, we compare the best-fit *UBVRI* light-curve templates of SN 2005cf with observations from the *Swift* UVOT and P07. We also compare them with other well-observed, nearby SNe Ia having similar  $\Delta m_{15}$  values, including SNe 2001el ( $\Delta m_{15} = 1.15$  mag; Krisciunas et al. 2003), 2002bo ( $\Delta m_{15} = 1.15$  mag; Benetti et al. 2004; Krisciunas et al. 2004), 2002dj ( $\Delta m_{15} = 1.08$  mag; Pignata et al. 2008), 2003du ( $\Delta m_{15} = 1.02$  mag; Stanishev et al. 2007), and 2004S ( $\Delta m_{15} = 1.10$  mag; Krisciunas et al. 2007; Chornock & Filippenko 2008). These 6 objects include all SNe Ia with  $1 < \Delta m_{15} < 1.15$  and at least 15 epochs per band of published *UBVRIJHK* data. The *BVRI* data for SNe 2002bo, 2002dj, and 2004S obtained with KAIT (Ganeshalingam et al., in prep.) are overplotted. The photometric data for the above comparison SNe Ia were  $S$ -corrected. To be consistent with SN 2005cf, the  $K$ -corrections computed with the spectra of the comparison SNe and/or the spectra of SN 2005cf were also applied to their photometry. All of the light curves of the comparison SNe Ia have been normalized to the epoch of their *UBVRI* maxima and shifted in their peaks to match the templates of SN 2005cf.

The overall comparison with the photometry of P07 reveals some systematic differences, especially at the earlier phases, as shown in Figure 9. The magnitudes in P07 are found to be brighter than ours on average over time by  $0.047 \pm 0.005$  mag in  $B$ ,  $0.009 \pm 0.004$  mag in  $V$ ,  $0.040 \pm 0.004$  mag in  $R$ , and  $0.041 \pm 0.005$  mag in  $I$ , while they are fainter by  $0.050 \pm 0.008$  mag in  $U$  (see the filled circles in Fig. 9). This is primarily due to calibration differences, especially in the *BRI* bands. It is puzzling, however, that a remarkable difference of  $\sim 0.14$  mag in the  $U$  band for the comparison stars (see §2.1.1) is not also seen in the  $U$ -band SN photometry. Additional, uncorrected systematic effects are probably present.

With the constructed light-curve templates of SN 2005cf, one may also examine whether the *Swift* UVOT optical observations are consistent with the ground-based data. The mean values of the computed residuals between these two measurements (see the star symbols in Fig. 9) are  $0.015 \pm 0.024$  mag in  $U$ ,  $-0.045 \pm 0.019$  mag in  $B$ , and  $0.009 \pm 0.011$  mag in  $V$ . There appears to be a small systematic shift in  $B$ , but the consistency in the  $U$  and  $V$  bands is satisfactory. This demonstrates the great improvements recently achieved in *Swift* UVOT calibrations (Li et al. 2006; Poole et al. 2008).

Although the light curves of the comparison SNe Ia are similar to each other near maximum brightness, they diverge at earlier (rising) phases. SNe 2001el and 2003du displayed a slower rise rate in each of the *UBVRI* bands. In contrast, the brightness of SNe 2002bo and 2002dj rose at a faster pace than that of SN 2005cf (see also Pignata et al. 2008). This indicates that the rise time might slightly vary among SNe Ia having similar  $\Delta m_{15}$  values, though a larger sample having early-epoch observations is needed to verify this trend.

Differences in the light curves also emerge at late phases, especially in the  $B$  band. We measured a late-time decline rate  $\beta = 1.62 \pm 0.05$  mag  $(100 \text{ d})^{-1}$  in  $B$  for SN 2005cf during the interval  $t = 40\text{--}90$  d, which is

<sup>20</sup> The true  $\Delta m_{15}(B)$  for SN 2005cf is  $1.07 \pm 0.03$  mag, taking into account the reddening effect on the light-curve shape (Phillips et al. 1999).

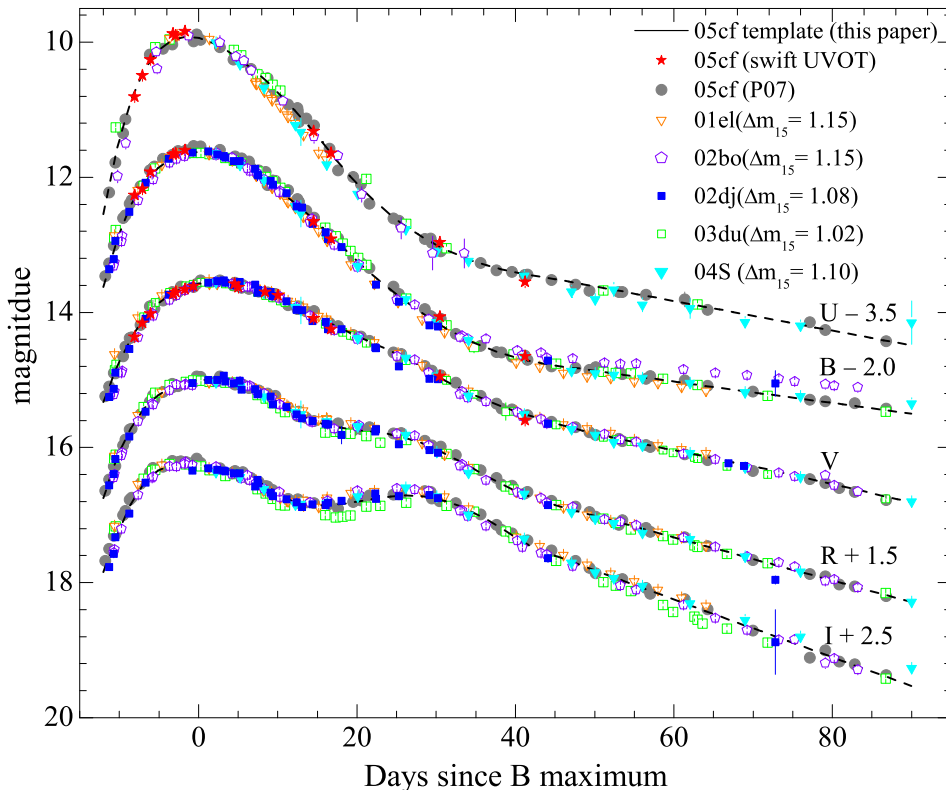


FIG. 8.— Comparison of  $UBVR$  light curves of SN 2005cf with those published by Pastorello et al. (2007) and other well-observed SNe Ia: SNe 2001el, 2002bo, 2002dj, 2003du, and 2004S. See text for the references.

comparable to that of SNe 2001el, 2003du, and 2004S at similar phase. While SNe 2002bo and 2002dj showed much slower decay rates, e.g.,  $\beta \approx 1.2 \text{ mag } (100 \text{ d})^{-1}$ , and they happened to be events with high expansion velocity of the photosphere. These fast-expanding SNe may generally have flatter photometric evolution in  $B$  at late times, similar to that of SN 2006X (Wang et al. 2008a).<sup>21</sup>

In contrast to the  $V$ - and  $R$ -band evolution, the light curves in the  $U$  and  $I$  bands appear more heterogeneous. The largest dispersion is in the premaximum  $U$ -band evolution and in the  $I$ -band secondary-maximum phase. Systematic effects due to filter mismatches might not be fully removed by the  $S$ -corrections because of the incomplete wavelength and/or temporal coverage for the SN spectra. Nevertheless, part of the dispersion is likely to be intrinsic. Significant spectral variations at the wavelengths of the broad-band  $U$  were also found in SNe Ia at redshift  $z \sim 0.5$  (Ellis et al. 2008). The  $U$ -band brightness has also been proposed to depend sensitively on the metallicity of the progenitor (e.g., Höflich et al. 1998; Lentz et al. 2000; Sauer et al. 2008), which may vary from one supernova to another; while emission in the  $I$  band is heavily affected by the Ca II NIR triplet absorption, which is found to vary substantially among SNe Ia at early phases (see Fig. 17 in §4.1).

<sup>21</sup> Measurements of the late-time decline rate in the  $U$  band are usually difficult due to the lack of reliable photometry at this phase. High-quality data are needed to test whether the  $U$ -band data follow the same trend as shown in  $B$ .

### 3.2. The UV Light Curves

UV observations are important for understanding SN Ia physics as well as possible differences among the progenitors in a range of environments. Due to the requirement of space-based observations, however, UV data for SNe Ia have been sparse; see Panagia (2003) and Foley, Filippenko, & Jha (2008) for summaries of *International Ultraviolet Explorer (IUE)* and *HST* spectra. In *HST* Cycle 13, extensive UV observations of SNe Ia were conducted (program GO-10182; PI Filippenko); unfortunately, the Space Telescope Imaging Spectrometer (STIS) failed just before the program began, so the UV prism in ACS was used instead, yielding spectra far inferior to those anticipated with STIS. Recently, *Swift* has obtained UV photometry of SNe Ia (Brown et al. 2008; Milne et al. 2008, in prep.), as well as some low-quality UV ugrism spectra (Bufano et al., in prep.).

Figure 10 shows the UV light curves of SN 2005cf obtained with the *Swift* UVOT and the *uvw1*, *uvw2*, and *uvm2* filters, as well as with the *HST* ACS and the F220W, F250W, and F330W filters. These two UV data sets span the periods from  $t = -8.1 \text{ d}$  to  $t = 41.8 \text{ d}$  and from  $t = -8.6 \text{ d}$  to  $t = 23.4 \text{ d}$ , respectively. Overlaid are the  $U$ -band templates of SN 2005cf, shifted to match the peak of the UV bands. With respect to  $U$ , the F330W-band light curve has a noticeably narrower peak. The UVOT *uvw1* light curve closely resembles that in the *HST* F250W band, with the former being slightly brighter by  $-0.09 \pm 0.02 \text{ mag}$ . Despite the similarity of



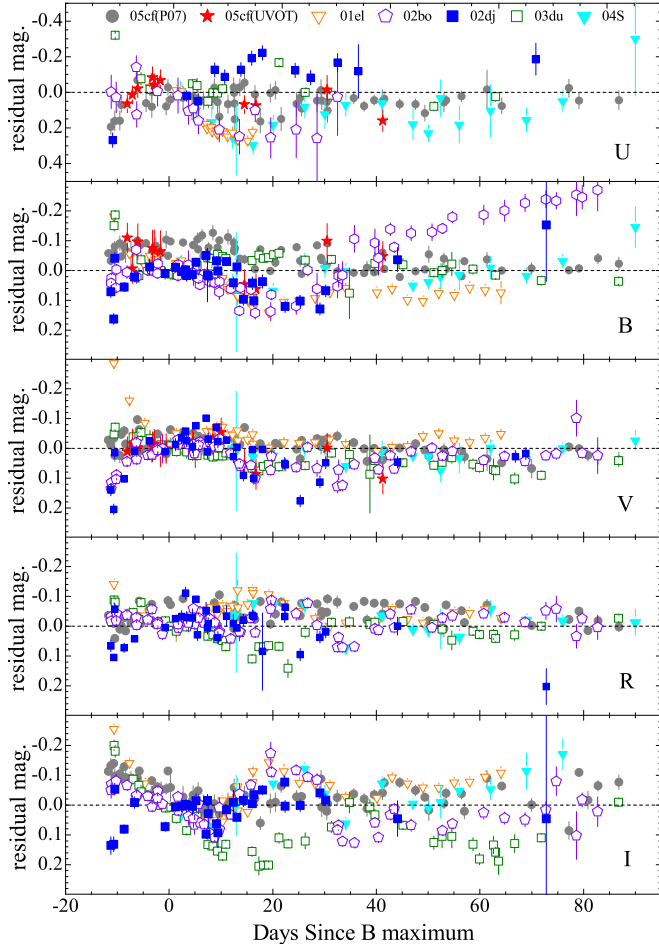


FIG. 9.— The residual magnitudes of the comparison SNe Ia with respect to the light-curve templates derived from our observations of SN 2005cf.

the filter responses, the UVOT *uvm2* light curve appears to be systematically dimmer than that of *HST* F220W by  $\sim 0.2$  mag at comparable phases. This is perhaps due to the calibration uncertainty or reduction errors, but more data are obviously needed to clarify this difference.

The temporal behavior of the UV photometry of SN 2005cf is similar to the optical behavior, but with different epochs for the maximum brightness. As in the *U* band, most of the UV light curves reached their maximum slightly before the optical, with the exception of the *uvm2*/F220W-band photometry, which peaks  $\sim 3$ – $4$  d after the *B* maximum. Another interesting feature is that the light-curve peak in these two filters appears to be much fainter and broader than that of the other UV filters on both sides. A similar feature was seen in SN 2005am (Brown et al. 2005), a normal SN Ia resembling SN 1992A (Kirshner et al. 1993). Brown et al. (2005) suggested that the faintness in *uvm2* could be explained in terms of a bump of the extinction curve near 2200 Å (Cardelli et al. 1989). Assuming a total reddening of  $E(B - V) \approx 0.2$  mag (see §3.6), however, we find that the change of  $R_V$  could only result in a larger extinction in *uvm2*/F220W by  $\sim 0.5$  mag. This is far below the flux drop of  $\sim 1.5$  mag with respect to the neighboring bands, as seen in SN 2005cf. The red leak in the UV fil-

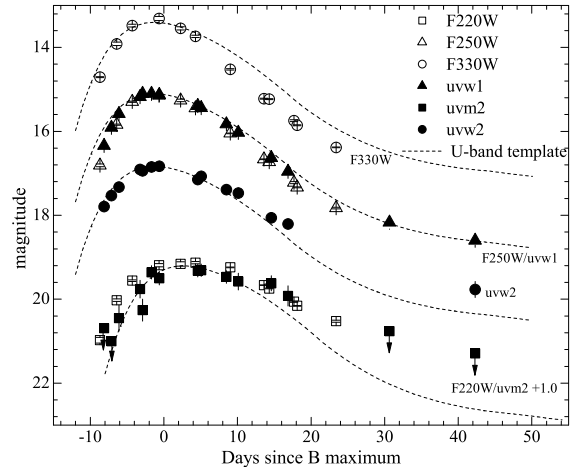


FIG. 10.— UV light curves of SN 2005cf, obtained with the *HST* ACS (F220W, F250W, and F330W) and the *Swift* UVOT (*uvw1*, *uvm2*, *uvw2*). The first two and the last two data points in the *uvm2* band are  $3\text{-}\sigma$  upper limits of the detection. Overlaid are the *U*-band template of SN 2005cf (dashed line).

ters might cause the abnormal behavior in the UV light curves by including some optical light, due to the red tail. However, the report from the most recent check of the *HST* ACS CCDs shows that such an effect is small in the *HST* UV filters<sup>22</sup>. Moreover, the off-band contamination in the F220W filter is found to be larger than that in F250W. This shows that the UV leak may not be responsible for the faint brightness in F220W or *uvm2* filters.

As in the optical, the light-curve parameters in the UV were obtained by using a polynomial fit to the observations (see Table 9). One can see that the luminosity in the F330W band is the brightest, but it declines at the fastest pace after the initial peak. The *uvm2*-band luminosity is the faintest, and has a post-maximum decay rate much slower than the other UV filters.

### 3.3. The NIR Light Curves

The NIR photometry of SN 2005cf was obtained with PAIRITEL (Wood-Vasey et al. 2007b) and the *HST* NICMOS3, spanning from  $-11.4$  d to  $+29.1$  d with respect to  $t_{\max}(B)$ . Due to significant differences between these two photometric systems, we applied both color- and *S*-corrections to the *HST* photometry to normalize it to the PAIRITEL system. As shown in Figure 11, the corrected F110W- and F160W-band magnitudes (smaller filled circles) are consistent with the ground-based results.

In Figure 11, the NIR data of the comparison SNe Ia are overlaid. Although the light curves of all these SNe are similar near maximum, they diverge after the peak phase. As in the optical, SNe 2002dj and 2002bo rise at a faster pace than SN 2005cf and 2003du in the NIR. Scatter is also present near the secondary-maximum phase; the fast-expanding events tend to exhibit more prominent peaks. The secondary-peak feature in the *J* band appears somewhat less pronounced in SN 2001el.

The peak magnitudes in the NIR, estimated by fitting

<sup>22</sup> <http://www.stsci.edu/hst/acs/documents/handbooks/cycle17>

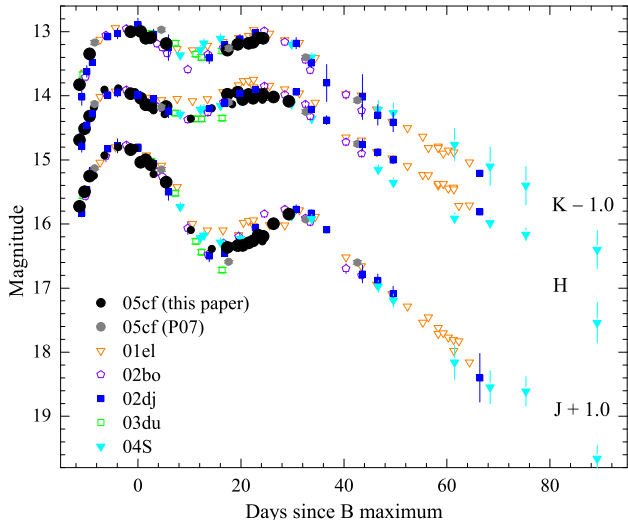


FIG. 11.— Comparison of the NIR light curves of SN 2005cf with those of SNe 2001el, 2002bo, 2002dj, 2003du, and 2004S. All light curves are shifted in time and magnitude to fit the peak values of SN 2005cf. The data sources are cited in the text.

the data with the Krisciunas et al. (2004a) templates, are reported in Table 9. In contrast with the rapid decline in  $J$  after the primary maximum, the  $H$ - and  $K$ -band light curves show much slower decay at comparable phases.

#### 3.4. The Spectral Energy Distribution Evolution

The evolution of the spectral energy distribution (SED) can be best studied through spectroscopy; however, only the optical spectra of SN 2005cf were involved in our study. As an alternative, a rough SED can be constructed from the observed fluxes in various passbands at the same or similar epochs. Since we have photometry in the UV, optical, and NIR bands, covering the 1600–24,000 Å region, we can study the SED evolution of SN 2005cf by means of photometry. Because of the numerous instruments involved in the observations of SN 2005cf, it was not always possible to observe all bands at exactly the same time, and our definition of the “same epoch” refers to a reference date  $\pm 1$  d. The observed apparent magnitudes in each passband were converted to fluxes using the reddening derived in §3.6.

Figure 12 shows SEDs at five selected epochs,  $t \approx -7$ ,  $-1$ ,  $+5$ ,  $+17$ , and  $+42$  d after the  $B$ -band maximum. The SN 2005cf SED went through dramatic changes in going from epochs near  $B$  maximum to the nebular phase. The SEDs at  $t \approx -7$ ,  $-1$  and  $+5$  d are very similar, peaking in  $B$  but showing a flux deficit in F220W/uvm2 ( $\sim 2000$ – $2500$  Å). At these early phases, the emission from the supernova dominated in the blue. By  $t \approx 17$  d the SED showed a significant deficit at short wavelengths compared with earlier epochs, whereas the NIR remained fairly constant (with the exception of the  $J$  band). The flux peak shifted to the  $V$  band by  $t \approx 42$  d, and the deficit in F220W/uvm2 might become less noticeable, though the measurement from the *swift* UVOT is around the detection limit.

To better understand the evolution of the 2000–2500 Å region, we overplot the *HST* FOS spectra of SN 1992A (Kirshner et al. 1993) in Figure 12. One sees that the

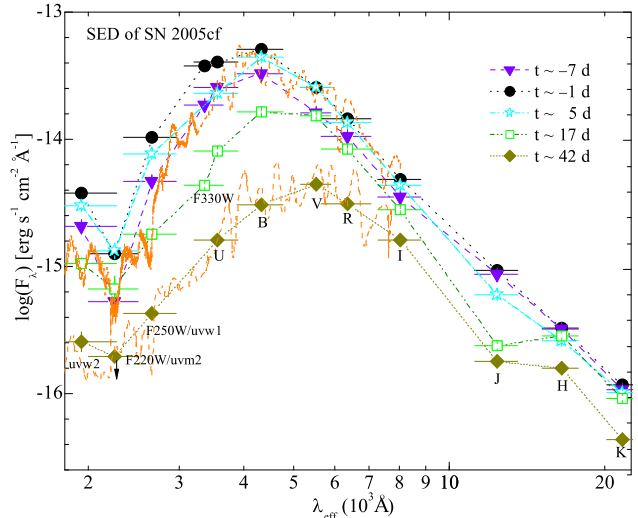


FIG. 12.— The spectral energy distribution evolution of SN 2005cf at  $t = -7$ ,  $-1$ ,  $+5$ ,  $+18$ , and  $+42$  d after the  $B$ -band maximum. The photometric points are shown with error bars (vertical ones for uncertainties and horizontal ones for the FWHM of the filters). Overlaid are the *HST* FOS spectra of SN 1992A (dotted curves) from Kirshner et al. (1993), obtained at  $t \approx +5$  d and  $+45$  d, respectively. Note that the error bar of the flux is in most cases smaller than the size of the symbol.

F220W/uvm2-band flux deficit in SN 2005cf at  $t \approx 5$  d is consistent with the strong absorption trough present in the UV spectrum of SN 1992A at similar epochs, although the UV brightness of the latter seems relatively fainter with respect to their optical emission. This absorption feature could arise from multiplets of the iron-peak elements at ejection velocities above  $\sim 16,000$  km  $s^{-1}$ , such as Fe II  $\lambda\lambda 2346$ ,  $2357$ ,  $2365$ , and  $2395$ , according to the synthetic-spectrum fit by Kirshner et al. (1993). The complex of iron-peak element line blending might also explain the less prominent, absorption-like feature in the SED blueward of  $2500$  Å at days 42 and 45. As SN 1992A suffers negligible reddening from interstellar material in both the Milky Way and the host galaxy (e.g., Wang et al. 2006; Jha et al. 2007), the observed absorption feature around  $2300$  Å is not caused by novel dust extinction. We suggest that the flux deficit in the F220W/uvm2 filter is likely an indication of the spectral evolution common to normal SNe Ia.

#### 3.5. The Color Curves

Figure 13 shows the optical color curves of SN 2005cf ( $U-B$ ,  $B-V$ ,  $V-R$ , and  $V-I$ ), corrected for the reddening derived in §3.6. Also overplotted are the color curves of the Type Ia SNe 2001el, 2002bo, 2002dj, 2003du, and 2004S, all corrected for reddening in both the Milky Way and the host galaxies.

After a rapid decline at early phases, the  $U-B$  color of SN 2005cf reached a minimum at  $t \approx -5$  d and then became progressively redder in a linear fashion until  $t \approx +23$  d, when the color curves entered a plateau phase (Fig. 13a). SN 2003du exhibited similar behavior. The overall color of SN 2005cf is redder than that of SNe 2001el and 2003du but bluer than that of SN 2004S. The scatter in  $U-B$  at maximum can reach  $\pm 0.2$  mag between SNe Ia having similar values of  $\Delta m_{15}$ , suggesting that a large uncertainty might be introduced when using

this color index to estimate the reddening of SNe Ia.

The  $B - V$  colors of the selected SNe (Fig. 13b) show similar evolution, except for SN 2001el near maximum and SN 2002bo at early nebular phases. We note that SN 2001el reached the bluest color slightly later, and it is also bluer than other comparison SNe Ia at this point, as with  $U - B$ . The  $B - V$  color of SN 2002bo after  $t = +40$  d evolves at a faster pace than the Lira-Phillips relation because of the flatter photometric evolution in the  $B$  band. This serves as a reminder that the Lira-Phillips relation does not hold for all SNe Ia, specifically the fast-expanding events (Wang et al. 2008a) and the SN 2000cx-like objects (Li et al. 2001).

The  $V - R$  and  $V - I$  color curves of SN 2005cf (Fig. 13c and 13d) exhibit a behavior that is quite similar to that of the normal SNe Ia. By contrasting with other normal SNe, SNe 2002bo and 2002dj are very blue in  $V - I$  (and possibly in  $V - R$ ), and they also reach their blue peak in  $V - I$  about 4 d earlier.

Figure 14 shows the observed  $V - JHK$  colors of SN 2005cf, together with the comparison SNe Ia corrected for reddening. The  $V - J$  and  $V - H$  colors are redder than the average values of the comparison SNe Ia by  $\sim 0.2$  mag, but the  $V - K$  color shows little difference. As with  $V - I$ , SNe 2002bo and 2002dj are bluer in all of the  $V - JHK$  colors. We notice, however, that most of the color difference would disappear, were a smaller total-to-selective absorption ratio applied to their extinction corrections ( $R_V = 2.0$  rather than 3.1). This suggests that either the NIR luminosities of the fast-expanding events were relatively faint with respect to the optical luminosities, or a lower  $R_V$  value is required for their dust extinction (Wang et al., in prep.).

The overall color evolution of SN 2005cf closely resembles the selected normal SNe Ia with similar  $\Delta m_{15}$ . We notice that SNe 2002bo and 2002dj exhibit a distinguished bluer  $V - IJHK$  colors with  $R_V = 3.1$ .

### 3.6. Interstellar Extinction

The Galactic extinction toward SN 2005cf is  $A_V^{\text{Gal}} = 0.32$  mag (Schlegel, Finkbeiner, & Davis 1998), corresponding to a color excess of  $E(B - V) = 0.097$  mag adopting the standard reddening law of Cardelli, Clayton, & Mathis (1989). In this section, we use several empirical methods to derive the host-galaxy reddening of SN 2005cf. All methods assume that SN 2005cf has intrinsic colors similar to those of normal SNe Ia, with either similar evolution in some colors or comparable  $\Delta m_{15}$  values.

Phillips et al. (1999) proposed correlations between the light-curve width parameter  $\Delta m_{15}$  and the intrinsic  $B_{\text{max}} - V_{\text{max}}$  or  $V_{\text{max}} - I_{\text{max}}$  values (or  $C_{\text{max}}$ ). The  $B - V$  color at early nebular phases (e.g.,  $30 \text{ d} \lesssim t \lesssim 90 \text{ d}$ ) was found to evolve in a similar fashion for most SNe Ia (dubbed the ‘‘Lira-Phillips relation’’; Phillips et al. 1999), allowing one to statistically separate the reddening from the intrinsic color component. In addition, Wang et al. (2005) suggested using the  $B - V$  color at 12 d after  $B$  maximum [ $(B - V)_{12}$ , or  $C_{12}$ ] as a reddening indicator because the intrinsic value of this post-maximum color was found to be a tight function of  $\Delta m_{15}$ . Based on the Lira-Phillips relation, Jha et al. (2007) also proposed to use the color at  $t = 35$  d to

measure the host-galaxy reddening of SNe Ia.

As shown in Figure 15, the empirical relations between the observed colors and  $\Delta m_{15}$  were recalibrated using 28 well-observed, low-reddening SNe Ia<sup>23</sup>, of which 15 are from the literature and 13 are from the new KAIT photometric database (Ganeshalingam et al., in prep.). The selected SN sample closely follows the Lira-Phillips relation [e.g., with a mean slope of  $-0.011 \pm 0.001$  mag  $\text{d}^{-1}$  and with the measured  $E(B - V)_{\text{host}} \lesssim 0.05$  mag]. With the above sample, the coefficients for the  $C_{\text{max}} - \Delta m_{15}$  relation were determined and are reported in Table 11.

Our determinations are generally comparable to the earlier results by Phillips et al. (1999), but with slightly steeper slope in  $B_{\text{max}} - V_{\text{max}}$  and bluer unreddened zeropoints. Note that the  $(B_{\text{max}} - V_{\text{max}}) - \Delta m_{15}$  correlation break down at large  $\Delta m_{15}$  values; a much steeper slope is required for very fast decliners. The  $V_{\text{max}} - I_{\text{max}}$  color does not show a great correlation with the decline rate, with a root-mean square (rms) scatter of  $\sim 0.06$  mag. Applying the  $C_{\text{max}} - \Delta m_{15}$  relation to SN 2005cf, we obtain  $E(B - V)_{\text{max}} = 0.07 \pm 0.04$  mag and  $E(V - I)_{\text{max}} = -0.08 \pm 0.06$  mag. From the  $B - V$  color of SN 2005cf in the nebular phase, we measured  $E(B - V)_{\text{tail}} = 0.15 \pm 0.04$  mag.

The  $C_{12} - \Delta m_{15}$  relation was also reexamined with the new sample. The zeropoint of the intrinsic color at the nominal decline rate is bluer than in previous reports (Wang et al. 2006) by 0.08 mag. This difference is perhaps due to the stricter criteria of selecting the training sample and also indicates the difficulty of separating reddening from the intrinsic color. This post-maximum color index gives  $E(B - V)_{12} = 0.12 \pm 0.04$  mag.

In comparison with the sample observed with other systems, the KAIT sample of 13 SNe Ia seems to be slightly bluer by  $\sim 0.05$  mag at  $t = 35$  d (see the bottom panel in Fig. 15), while this difference does not hold for the other color indices shown in the same plot. Such a discrepancy may arise from systematic effects, such as the  $S$ -corrections, which were found to show noticeable divergence in the nebular phase (see Fig. 3). In addition, we point out that the  $(B - V)_{35}$  color may not be a constant for the fast decliners; a larger  $\Delta m_{15}$  corresponds to a redder  $(B - V)_{35}$ . With the new unreddened loci, we measured  $E(B - V)_{35} = 0.13 \pm 0.05$  mag for SN 2005cf.

Krisciunas et al. (2000, 2004a) have shown that the intrinsic  $V - JHK$  colors of SNe Ia are uniform and can be used as reddening indicators. Based on Krisciunas unreddened loci (see Fig. 14), for SN 2005cf we obtain  $E(V - J) = 0.28 \pm 0.08$  mag,  $E(V - H) = 0.25 \pm 0.06$  mag, and  $E(V - K) = 0.16 \pm 0.06$  mag. This corresponds to an  $E(B - V)$  reddening of  $0.13 \pm 0.08$  mag,  $0.10 \pm 0.06$  mag, and  $0.06 \pm 0.06$  mag, respectively.

The color excesses of SN 2005cf derived from various empirical methods are summarized in Table 12. They are consistent with each other within the uncertainties, except the  $V - I$  color which shows larger scatter and may be not a reliable reddening color index. The mean value gives  $E(B - V)_{\text{host}} = 0.09 \pm 0.03$  mag, indicating that

<sup>23</sup> SNe 1992A, 1992al, 1992bc, 1992bl, 1992bo, 1993H, 1993O, 1994D, 1994S, 1996X, 1998aq, 1998bp, 1998de, 1999by, 1999ej, 2000ca, 2000dk, 2000dr, 2001ba, 2002dl, 2002ha, 2002fk, 2003gs, 2003hv, 2003du, 2004at, 2005el, and 2005ki.

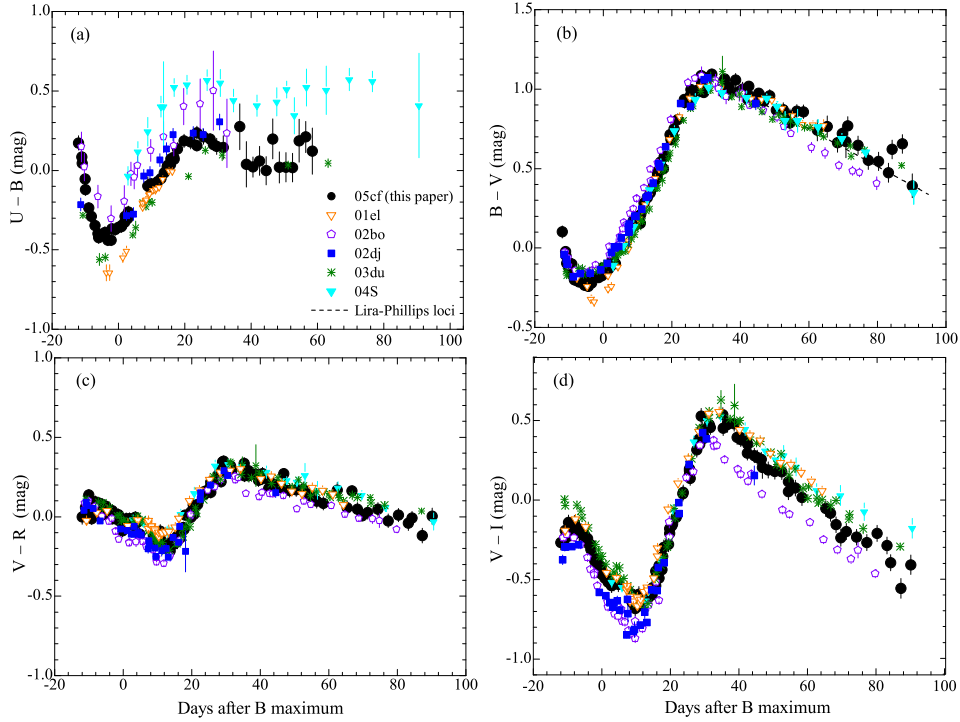


FIG. 13.—  $U - B$ ,  $B - V$ ,  $V - R$ , and  $V - I$  color curves of SN 2005cf compared with those of SNe 2001el, 2002bo, 2002dj, 2003du, and 2004S. All of the comparison SNe have been dereddened. The dash-dotted line shows the unreddened Lira-Phillips loci. The data sources are cited in the text.

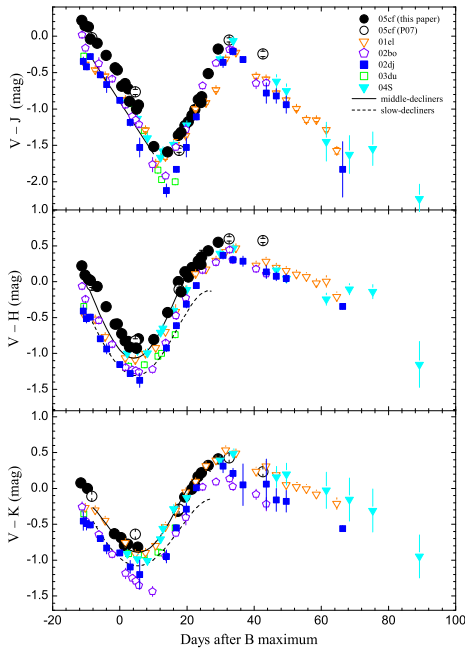


FIG. 14.— The  $V - JHK$  color curves of SN 2005cf, together with those of SNe 2001el, 2002bo, 2002dj, 2003du, and 2004S. The dashed lines represent the mean loci of the unreddened SNe Ia with  $\Delta m_{15} = 0.8\text{--}1.0$  mag; the solid lines denote those with  $\Delta m_{15} = 1.0\text{--}1.3$  mag (Krisciunas et al. 2004a).

SN 2005cf suffers a small but non-negligible reddening in the host galaxy.

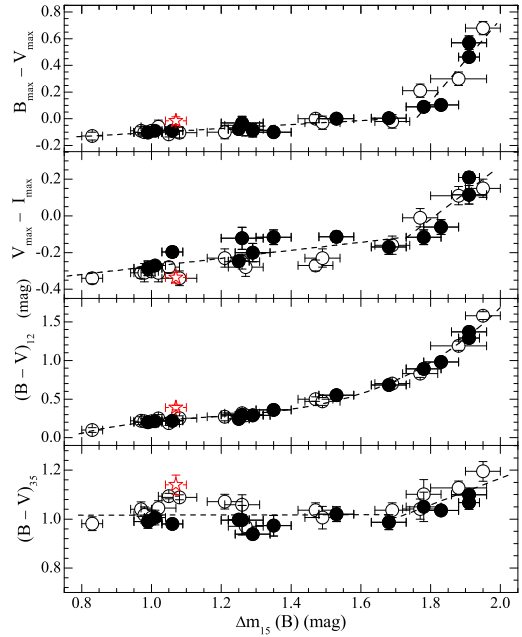


FIG. 15.— Correlation between the decline rate  $\Delta m_{15}$  and the observed colors for low-reddening SNe Ia. Open circles represent the sample collected from the literature (Hamuy et al. 1996; Riess et al. 1999; Riess et al. 2005; Jha et al. 2006b; Garnavich et al. 2004; Patat et al. 1996; Salvo et al. 2001; Krisciunas et al. 2004a); filled circles show those from the KAIT photometry (Ganeshalingam et al. in prep.). The observed colors of SN 2005cf, corrected for the Galactic reddening, were also overplotted (star symbol).

#### 4. OPTICAL SPECTRA



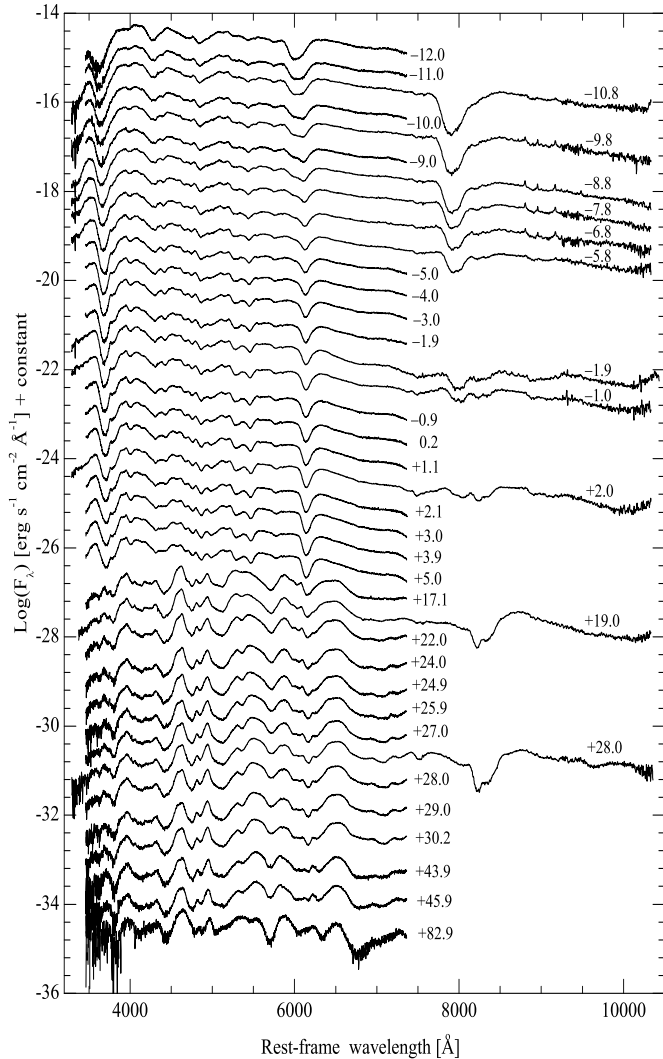


FIG. 16.— Optical spectral evolution of SN 2005cf. The spectra have been corrected for the redshift of the host galaxy ( $v_{\text{hel}} = 1967 \text{ km s}^{-1}$ ) but not reddening, and they have been shifted vertically by arbitrary amounts for clarity. The numbers on the right-hand side mark the epochs of the spectra in days after  $B$  maximum.

There are a total of 38 optical spectra of SN 2005cf obtained at Lick Observatory and FLWO, spanning from  $t = -12.0$  to  $t = +83.0$  d with respect to the  $B$  maximum. The complete spectral evolution is displayed in Figure 16, and two late-time nebular spectra are presented in Figure 18. The earliest spectra show very broad and highly blueshifted absorption features at  $3700 \text{ \AA}$  (Ca II H&K),  $6020 \text{ \AA}$  (Si II  $\lambda 6355$ ), and  $7900 \text{ \AA}$  (Ca II NIR triplet). In particular, a flat-bottomed feature is distinctly seen in Si II  $\lambda 6355$ . The spectral evolution near maximum generally follows that of a normal SN Ia, with the distinctive “W”-shaped S II lines near  $5400 \text{ \AA}$  and the blended lines of Fe II and Si II near  $4500 \text{ \AA}$ . We discuss in detail the spectral evolution of SN 2005cf in the following subsections.

#### 4.1. Temporal Evolution of the Spectra

In Figure 17, we compare the spectra of SN 2005cf with those of SNe Ia having similar  $\Delta m_{15}$  at four different epochs ( $t \approx -11$  d,  $-7$  d,  $0$  d, and  $18$  d past  $B$

maximum). All spectra have been corrected for reddening and redshift. For SN 2001el,  $R_V = 2.1$  is assumed according to the analysis by Krisciunas et al. (2007). For the other SNe, the host-galaxy reddening is measured using the empirical correlations presented in Table 11 and the extinctions are corrected using the standard value  $R_V = 3.1$ . The line identifications adopted here are taken from Branch et al. (2005, 2006).

Figure 17a shows the comparison of the spectra at  $t \approx -11$  d. As in the comparison SNe Ia, the absorption near  $3700 \text{ \AA}$  due to the blending of Ca II H&K and Si II  $\lambda 3858$  is prominent in the earliest spectrum of SN 2005cf. The Si II  $\lambda 4130$  absorption feature appears common in the early spectra, except in the spectrum of SN 1990N. In the  $4000\text{--}4500 \text{ \AA}$  wavelength range, all of the SNe show a strong absorption feature at  $\sim 4300 \text{ \AA}$ , probably owing to a blend of Mg II  $\lambda 4481$  and Fe III  $\lambda 4404$ . The weak Si III  $\lambda\lambda 4553, 4568$  blend can be identified in the comparison SNe, though its absence in SN 2002bo may indicate a cooler temperature in the photosphere. The “W”-shaped feature of the two S II lines appears at this phase. The lines of Si II  $\lambda 6355$  and the Ca II NIR triplet of SN 2005cf are very broad and deep, comparable to those in SNe 2001el and 2002bo. One interesting feature is the flat-bottomed profile of Si II  $\lambda 6355$ , which was previously only observed in SN 1990N at  $t = -14$  d and in SN 2001el at  $t = -9$  d. In contrast, SNe 2003du and 2005cg displayed a triangular-shape feature at similar phases.

Figure 17b shows the comparison at  $t \approx -7$  d. A second minimum begins to develop on the red side of the Ca II H&K absorption, as in SN 2003du. The weak features (e.g., Si II  $\lambda 4130$ , Si III  $\lambda 4560$ , and the S II “W”) strengthen with time. The flat-bottomed feature associated with Si II  $\lambda 6355$  is barely visible in the SN 2005cf spectrum, with only a small notch on the blue side of the absorption minimum. The Ca II NIR triplet now weakens and shows a double minimum on the red side of the main absorption.

In Figure 17c, we compare the spectrum of SN 2005cf near maximum with those of SNe 2001el, 2002bo, 2003du, and 2004S. At  $t \approx -1$  d, the spectrum of SN 2005cf has evolved while maintaining most of its characteristics shown at earlier epochs. The second absorption minimum in Ca II H&K now becomes noticeable in SNe 2005cf and 2003du, while it is still barely observed in SN 2004S. (The spectrum of SN 2001el did not cover this wavelength range.) The Si II  $\lambda 6355$  absorption in SN 2005cf now appears quite similar to that of the other normal SNe Ia. The O I  $\lambda 7773$  line strengthens in all cases in our sample. The two absorption components of the Ca II NIR triplet evolve rapidly, with the blue component becoming weak and the red one gaining strength in the minimum, similar to SNe 2001el and 2004S. SN 2002bo still shows broader and deeper absorptions of Si II  $\lambda 6355$  and the Ca II NIR triplet with less substructure. We measured the line-strength ratio of Si II  $\lambda\lambda 5958, 5979$  to Si II  $\lambda 6355$ , known as  $R(\text{Si II})$  (Nugent et al. 1995), to be  $0.28 \pm 0.04$  for SN 2005cf near maximum, in good agreement with the measurement reported by G07.

In Figure 17d, we compare the spectra at  $t \approx 18$  d. SN 2005cf exhibits spectral evolution quite similar to that of the other SNe Ia. The Fe II and Si II features are fairly developed in the range  $4700\text{--}5000 \text{ \AA}$ . The stronger Fe II

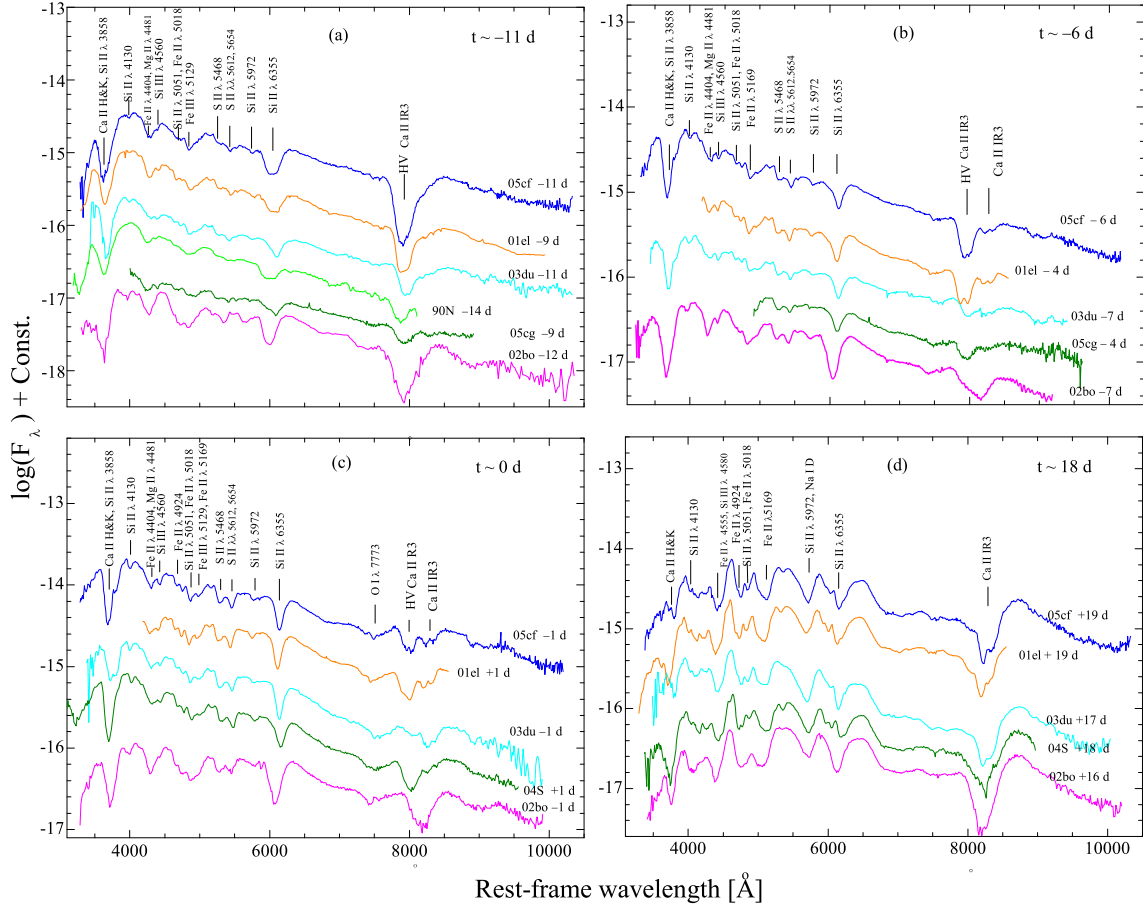


FIG. 17.— The spectrum of SN 2005cf at  $-11$  d,  $-6$  d,  $0$  d, and  $+18$  d after  $B$  maximum, overlotted with the comparable-phase spectra of SNe 1990N (Leibundgut et al. 1991), 1994D (Filippenko et al. 1997), 2001el (Wang et al. 2003; Mattila et al. 2005), 2002bo (Benetti et al. 2004), 2003du (Stanishev et al. 2007), 2004S (Krisciunas et al. 2007), and 2005cg (Quimby et al. 2006). All spectra shown here have been corrected for the reddening and redshift of the host galaxy. For clarity of display, the spectra were arbitrarily shifted in the vertical direction.

lines dominate around  $5000\text{\AA}$ , and Na I D appears in the region overlapping with Si II  $\lambda 5972$ . The Si II  $\lambda 6355$  trough becomes affected by Fe II  $\lambda\lambda 6238, 6248$  and Fe II  $\lambda\lambda 6456, 6518$ . Although the Ca II NIR triplet shows the most diverse features at the earlier epochs, they develop into a rather smooth absorption profile by 2 weeks after  $B$  maximum.

Comparison of the spectra of SNe Ia having similar  $\Delta m_{15}$  values reveals that they show the most diversity at the earliest epochs, with significantly different strengths and profiles of the main features (e.g., Si II  $\lambda 6355$  and the Ca II NIR triplet). In general, the overall spectral evolution of SN 2005cf at early phases closely resembles that of SN 2001el.

Two late-time nebular Keck spectra, obtained with LRIS on day  $+319$  and with DEIMOS on day  $+614$ , are shown in Figure 18. They do not exhibit any detectable signature of a low-velocity hydrogen emission, though the S/N is low, especially in the case of the day  $+614$  spectrum. (See also the deep observations of SN 2005cf performed by Leonard 2007.) The spectrum on day  $+319$  is dominated by the forbidden lines of singly and doubly ionized Fe and Co lines; its overall shape is very similar to that of SN 2003du at a similar phase. The nebular

spectrum of SN 2002dj at this phase is also quite normal, without showing extra flux (or an evidence for presence of an echo) at shorter wavelengths as in the extreme HV event SN 2006X (Wang et al. 2008b). We note, however, that SN 2002dj is a slightly fast-expanding object with less significant reddening (Pignata et al. 2008).

#### 4.2. The Photospheric Expansion Velocity

In this paper, we examine the photospheric expansion velocity  $v_{\text{exp}}$  from the velocity evolution of the Si II  $\lambda 6355$  and S II  $\lambda 5640$  lines. The derived  $v_{\text{exp}}$  values of SN 2005cf from Si II  $\lambda 6355$  and S II  $\lambda 5640$  as a function of time are shown in Figure 19, together with those of the comparison SNe Ia. The measurements from the spectra published by G07 are also overlotted (small filled circles). All velocities have been corrected for the redshifts of the host galaxies.

At the earliest phases, the photospheric expansion velocity implied from Si II  $\lambda 6355$  for SN 2005cf is higher than that for SNe 1990N (Leibundgut et al. 1992), 1998aq (Branch et al. 2003), and 2003du (Stanishev et al. 2007) by  $\sim 2000 \text{ km s}^{-1}$ , and comparable to that for SNe 1994D (Filippenko 1997, Patat et al. 1996) and 2001el (Wang et al. 2003; Mattila et al. 2005). This expansion

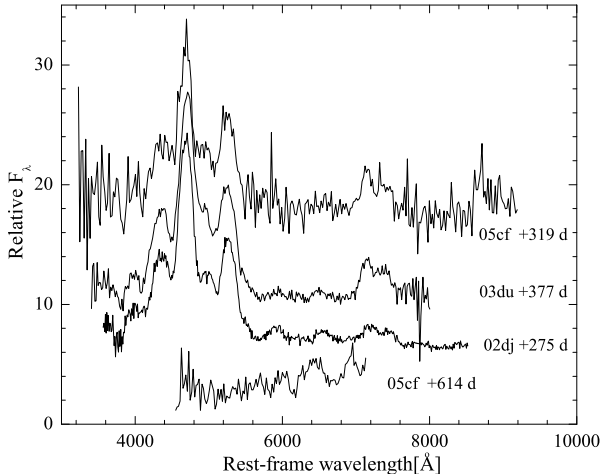


FIG. 18.— Late-time nebular spectra of SN 2005cf, slightly smoothed. The nebular spectra of SN 2003du (Stanishev et al. 2007) and SN 2002dj (Pignata et al. 2008) at about the same phase as the earlier SN 2005cf spectrum are shown for comparison. Both reddening and redshift corrections have been applied to the spectra.

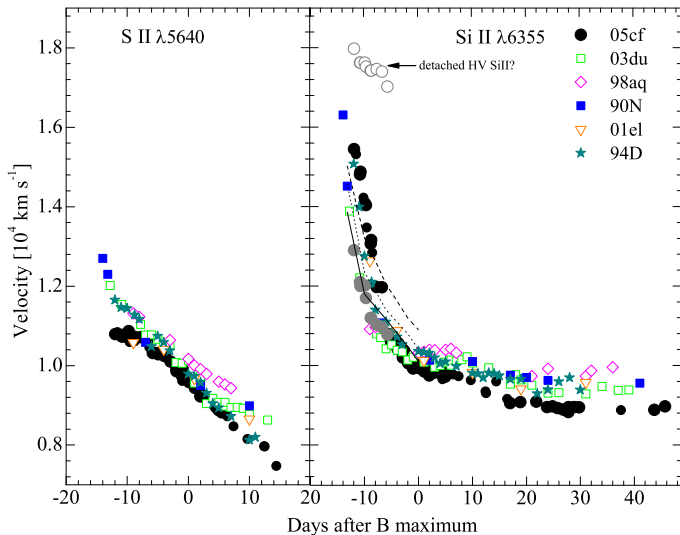


FIG. 19.— Evolution of the expansion velocity of SN 2005cf as measured from the minimum of Si II  $\lambda 6355$  and S II  $\lambda 5640$ , compared with the values of SNe 1990N, 1994D, 1998aq, 2001el, and 2003du (see text for the references). The grey dots show the low-velocity component decomposed from the Si II  $\lambda 6355$  absorption of SN 2005cf by using the double-Gaussian model (see §4.3.1 and Fig.20); the open circles represent the detached high-velocity component. Overplotted are velocities predicted by the Lentz et al. (2000) model for cases of  $\times 10$  (dashed line),  $\times 3$  (dotted line), and  $\times 1/3$  (solid line) solar C + O layer metallicity.

velocity declines very rapidly within the first two weeks before  $B$  maximum and then maintains a plateau phase for about a month. Such evolution may be related to the fact that the Si II absorption region is close to the photosphere at earlier phases but becomes more detached at later times (Patat et al. 1996). In contrast, the velocity yielded from the S II  $\lambda 5640$  line is slightly lower than that of the other SNe Ia and shows a flat evolution from  $t \approx -12$  d to  $-5$  d. SN 2001el may show a similar

plateau feature, though the data are sparse.

Following Benetti et al. (2005), we calculate the velocity gradient  $\dot{v}$  of Si II  $\lambda 6355$  for SN 2005cf as  $31 \pm 5$  km s $^{-1}$  d $^{-1}$  during the period  $t \approx 0$ –30 d, which puts SN 2005cf in the group of normal SNe Ia having low velocity gradients (LVGs).

#### 4.3. The High-Velocity Features

In addition to the evolution of the photospheric expansion, the well-sampled spectra of SN 2005cf (especially those at earlier phases) provide a good opportunity to study the high-velocity (HV) features that were only seen in the earliest spectra. The HV material is usually located in the outermost layers of the ejecta where SNe Ia show the highest degree of heterogeneity.

##### 4.3.1. The High-Velocity Si II

Figure 20 (see the left panel) shows the pre-maximum evolution of the velocity-space distribution of Si II  $\lambda 6355$  in the spectra of SN 2005cf. In the  $-12$  d spectrum, this absorption profile is broad and asymmetric with a stronger minimum on the blue side. At  $t = -11$  d, the Si II line exhibits a flat-bottomed feature with comparable absorption minima on both red and blue sides. As the spectrum evolves, the red-side minimum gradually dominates. By  $t = -6$  d, the Si II absorption feature gradually develops into a single minimum with a typical velocity of  $\sim 10,500$  km s $^{-1}$ , though the line profile may still be affected by the blue component until around maximum light (G07).

The observed line profiles of Si II  $\lambda 6355$  at earlier phases can be well fit by a double-Gaussian function with separate central wavelengths, probably suggesting the presence of another HV absorption component. The HV component could be a thin pure Si shell or a mixed layer of Si II and C II  $\lambda 6580$  (Fisher et al. 1997; Mazzali et al. 2001, 2005). Assuming that the blue-side absorption component is primarily produced by the HV Si II detached from the photosphere, the mean absorption-minimum velocity is estimated to be  $17,500 \pm 500$  km s $^{-1}$  during the period from  $t = -12$  d to  $t = -7$  d (see also the open circles in Fig.19). This velocity is much higher than the value inferred from the absorption minimum on the red side.

The presence of HV Si II in SN 2005cf was also proposed by G07 by modeling the observed spectra with the use of the parameterized code for supernova synthetic spectroscopy, SYNOW (Fisher 2000). Their analysis suggested that the HV feature of Si II  $\lambda 6355$  in SN 2005cf is detached at  $19,500$  km s $^{-1}$ . Given the contamination by such a HV Si II feature, the photospheric velocity measured directly from the overall line profile was overestimated. The recomputed  $v_{\text{exp}}$  values from the Si II line (see the gray dots in Fig. 19), after removing the HV component, closely match the velocity evolution predicted from the  $1/3$  solar metallicity models by Lentz et al (2000).

In the right panels of Figure 20, we also compare the Si II absorption features in the earliest spectra. The presence of the HV feature of Si II has also been suggested in SNe 1990N, 1999ee, 2001el, and SN 2005cg (Mazzali et al. 2001; Mattila et al. 2005; Quimby et al. 2006), but none of them could be securely established due to

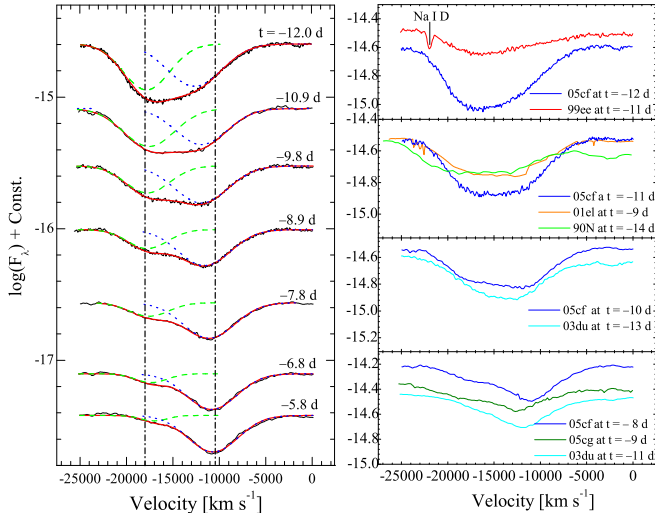


FIG. 20.— *Left Panel*: The evolution in velocity space of Si II  $\lambda 6355$  in SN 2005cf compared with the double-Gaussian fit. Dashed green lines show the velocity distribution on the blue side, and dotted blue lines show the component on the red side. The red solid lines represent the best-fit curve to the observed profile. *Right Panels*: Comparison of pre-maximum evolution of the Si II  $\lambda 6355$  profile of SN 2005cf with that of SNe 1999N, 1999ee, 2001el, 2003du, and 2005cg at four selected epochs (see text for the references).

the sparse coverage of the pre-maximum spectra. Of the above SNe Ia, the flat-bottomed profile of the Si II line is seen only in SN 1990N at  $t = -14$  d and SN 2001el at  $t = -9$  d. Inspection of the  $t = -13$  d spectrum of SN 2003du reveals a Si II absorption reminiscent of the feature seen in SN 2005cf at  $t = -10$  d. A triangular-shaped profile is present in the spectra of all the other events. It is therefore likely that such a “peculiar” line profile is just a snapshot of the common evolutionary pattern (see similar arguments by Stanishev et al. 2007).

In addition to the absorption by the HV material, alternative interpretations have also been proposed for the formation of the broad profile of Si II absorption. Mattila et al. (2005) suggest that the flat-bottomed line shape in SN 2001el can be produced by pure scattering within a thin region moving at the continuum photospheric velocity; it disappears as the photosphere recedes and the scattering region widens. The ejecta slowly extending to the HV part, typical for delayed-detonation models (Khokhlov 1991), may also account for the triangular feature of the Si II profile in SN 2005cg (Quimby et al. 2006). However, neither of these two models can explain the asymmetric line profile with a stronger HV component, as observed in SN 2005cf at  $t = -12$  d and in SN 1999ee at  $t \approx -11$  d (Hamuy et al. 2002) (see the top right panel of Fig. 20).

#### 4.3.2. The High-Velocity Ca II

Figure 21 presents the detailed evolution of the Ca II NIR triplet and Ca II H&K of SN 2005cf. In comparison with the Si II line, the HV features in the Ca II NIR triplet are more frequently observed in SNe Ia (e.g., Mazzali et al. 2005), as they are more pronounced and may have a longer duration. The HV component dominates in the Ca II NIR lines at earlier phases, but it gradually loses its strengths with time. In the Ca II NIR triplet, the HV components are more separated from the photo-

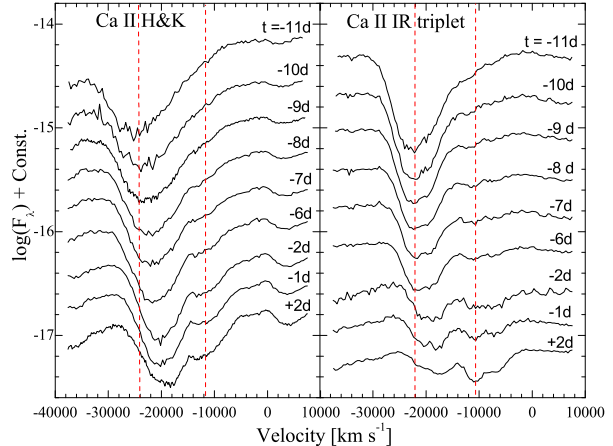


FIG. 21.— Premaximum evolution in velocity space for the Ca II H&K and NIR triplet of SN 2005cf. Vertical dashed lines indicate, respectively, the highest velocity in the earliest phase ( $\sim 23000$  km  $s^{-1}$ ) and the photospheric velocity (at  $\sim 11000$  km  $s^{-1}$ ).

spheric components than in the Si II line. At  $t = -11$  d, the HV component shows an expansion velocity at about  $22,000$  km  $s^{-1}$ . By  $t = +2$  d, the velocity is around  $19,000$  km  $s^{-1}$  and the absorption minimum is beginning to be dominated by the photospheric component at  $\sim 10,000$  km  $s^{-1}$ .

The Ca II H&K lines may show similar HV features, but they overlap with the Si II  $\lambda 3858$  line at earlier phases. Due to the severe line blending, it is difficult to disentangle the HV component and quantify its strength. Assuming a double-Gaussian model, we measure the velocity of the HV component at  $\sim 24,500$  km  $s^{-1}$  and  $20,000$  km  $s^{-1}$  in the  $t = -11$  d and  $-1$  d spectra, respectively, similar to those measured for the Ca II NIR triplet. The higher velocity of the HV component in the Ca II lines with respect to the Si II line perhaps suggests a different abundance distribution in the ejecta.

#### 4.3.3. Origin for the HV features

Currently, the origin of the HV features is still debated. In principle, their formation can be due to an abundance and/or a density enhancement in the ejecta at outer layers. According to Mazzali et al. (2005), the single abundance enhancement may not account for the observed HV features, as the nuclear burning cannot produce enough Si and Ca required in the outer region. In contrast, an enhancement in the local density could lead to a good reproduction of the HV spectral evolution, as demonstrated by the three-dimensional (3D) explosion models (e.g., Ropke et al. 2006). One possible scenario for the density enhancement is the interaction of the outermost ejecta with the circumstellar matter (CSM) produced in the vicinity of the SN (e.g., Gerardy et al. 2005). On the other hand, an aspherical ejecta model could also cause the HV density enhancement. Variations of the strength of the HV features may be explained by different viewing angles if they result from aspherical structures like a torus or clumps (Tanaka et al. 2006).

Inspection of the early-time spectra presented in Figure 17 reveals that the strength of the HV features from Si II and Ca II may be correlated in a given SN, though their strength varies from SN to SN. This holds true for



SN 2005cf and all the comparison objects, perhaps favoring the origin of the observed HV features from either CSM interaction or aspherical structure of the ejecta produced by the explosion itself. Note that the detached HV features discussed here seem different from those observed in SN 2006X or even in SN 2002bo; however, the same configuration with a much larger photospheric velocity may explain the difference (Tanaka et al. 2008).

## 5. THE DISTANCE AND LUMINOSITY OF SN 2005CF

The extensive photometric observations of SN 2005cf, from the UV to the NIR bands, enable us to construct the *uvoir* “bolometric” light curve within 0.2–2.4  $\mu\text{m}$ . For this calculation, we used the normalized passband transmission curves given by Bessell (1990). The integrated flux in each filter was approximated by the mean flux multiplied by the effective width of the passband, and was corrected for the reddening. Since the filter transmission curves do not continuously cover the spectrum and some also overlap, we corrected for these gaps and overlaps by adjusting the effective wavelengths of the filters in the UV, optical, and NIR passbands.

### 5.1. The Distance to SN 2005cf

The distance to SN 2005cf is important for deriving the bolometric luminosity. Direct measurements were unavailable in the literature, so we used several methods to estimate the distance. According to Wang et al. (2006), a nominal standard SNe Ia with Cepheid-based calibration has an absolute magnitude of  $-19.27 \pm 0.05$  mag in the *V* band. Combining this value with the fully corrected apparent magnitude of SN 2005cf, we obtain a distance modulus  $\mu = 32.29 \pm 0.12$  mag. We also determine the distance using the latest version of the MLCS2k2 fitting technique (Jha et al. 2007), which yields  $\mu = 32.43 \pm 0.13$  mag.

Krisciunas et al. (2004b) propose that SNe Ia are more uniform in the NIR bands than in the optical; their NIR peak luminosities are found to be nearly independent of the light-curve shape. The absolute NIR peak magnitudes for SNe Ia with  $\Delta m_{15} < 1.7$  are reported as  $-18.61$  in *J*,  $-18.28$  in *H*, and  $-18.44$  mag in *K*, respectively. Assuming the same NIR magnitudes for SN 2005cf, we derive a mean distance modulus  $\mu = 32.20 \pm 0.10$  mag.

Averaging the above three distances, we obtain a weighted mean of  $\mu = 32.31 \pm 0.11$  mag for SN 2005cf. Note that this estimate may still suffer from an additional uncertainty of 0.12–0.15 mag, due to the intrinsic luminosity dispersion of SNe Ia in both optical and NIR bands (Krisciunas et al. 2004; Wang et al. 2006; Wood-Vasey et al. 2007b).

### 5.2. The Missing Flux Below the Optical Window

The filled circles in Figure 22 show the temporal evolution of the ratio of the NIR-band emission (9000–24,000  $\text{\AA}$ ) to the optical (3200–9000  $\text{\AA}$ ),  $F_{\text{IR}}/F_{\text{opt}}$ . The flux ratios obtained from SNe 2001el and 2004S are overplotted. The dashed curve in the plot represents the best fit to the data of SN 2005cf. In the fit, the NIR contribution at  $t > 40$  d is assumed to be the same as that of SN 2001el and SN 2004S. This assumption is reasonable because the  $F_{\text{IR}}/F_{\text{opt}}$  ratio of SN 2005cf agrees well with the corresponding values of these two SNe Ia from the

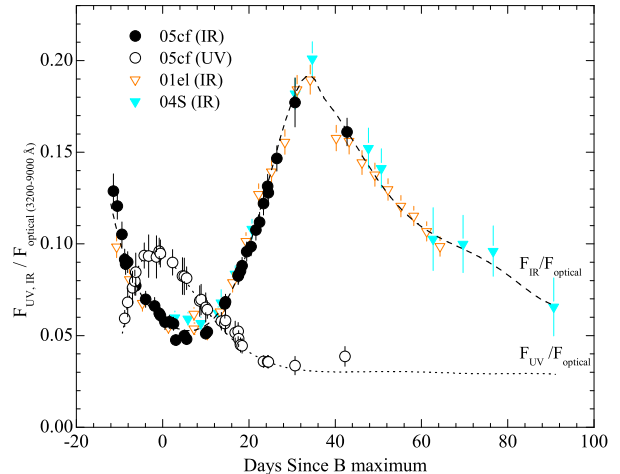


FIG. 22.— The ratio of the UV and NIR fluxes to the optical for SN 2005cf. Overplotted are the NIR flux ratios of SNe 2001el and 2004S.

very beginning to  $t \approx +40$  d. Initially, the ratio shows a sharp decline with a minimum  $\sim 4$  d after the *B* maximum. Then it rises rapidly in a linear fashion and reaches a peak ( $\sim 20\%$ ) at  $t \approx +30$  d, when the secondary maximum appears in the NIR. At nebular phases, the NIR contribution gradually declines and becomes  $< 10\%$  at  $t \approx +80$  d, similar to that found by Suntzeff in studying SN 1992A (1996).

The contribution of the UV flux in the 1600–3200  $\text{\AA}$  range to the optical is shown with the open circles in Fig. 22. The dotted line indicates the best fit to the observed data points, assuming that the UV flux remains constant at  $t > +30$  d. A flat contribution at late times was evidenced by the UV data of SN 2001el from the *HST* archive (see Fig. 14 in Stanishev et al. 2007). The UV contribution is found to be generally a few percent of the optical in SN 2005cf, with a peak ( $\sim 10\%$ ) at around the *B* maximum. Three weeks after the maximum, the ratio remains at a level of 3–4%.

It is also interesting to estimate the ratios of the optical fluxes to the bolometric fluxes, as most SNe Ia were not observed in the UV or the NIR bands. These ratios are useful for correcting the observed optical luminosity to the bolometric luminosity. Figure 23 shows the correction factors (defined as the missing fraction of the observed flux relative to the generic *uvoir* bolometric luminosity) obtained from SN 2005cf; one can see that the bolometric luminosity is dominated by the optical fluxes. The missing flux beyond the optical window is about 20%, with a slightly larger fraction at  $t \approx +30$  d due to the appearance of the secondary maximum in the NIR. The corrections, based on the fluxes in the *UBVRI*, *BVRI*, *BVI*, *BV*, and *V* bands, are also shown in the plot. We note that the bolometric correction for the *V* filter exhibits the least variation with time: the overall variation is less than 4% before  $t \approx +30$  d, and at later phases the correction stays nearly constant. This validates previous assumptions that the *V*-band photometry can well represent the bolometric light curve, in particular at later phases, at a constant fraction of about 20%.

### 5.3. The Bolometric Light Curve

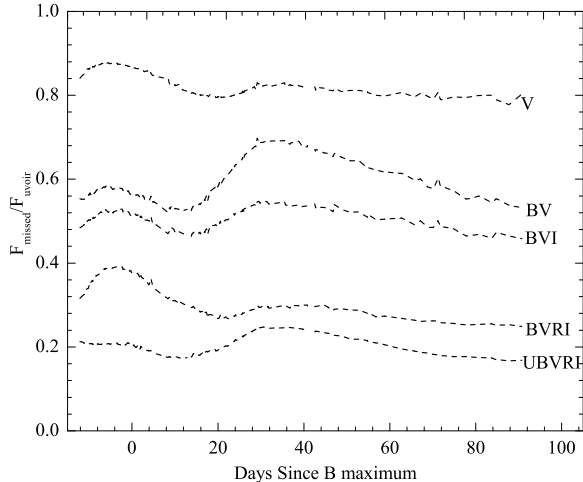


FIG. 23.— Correction factors for missing passbands. The correction factors are obtained by comparing the fluxes in the passbands with the total *uvoir* flux.

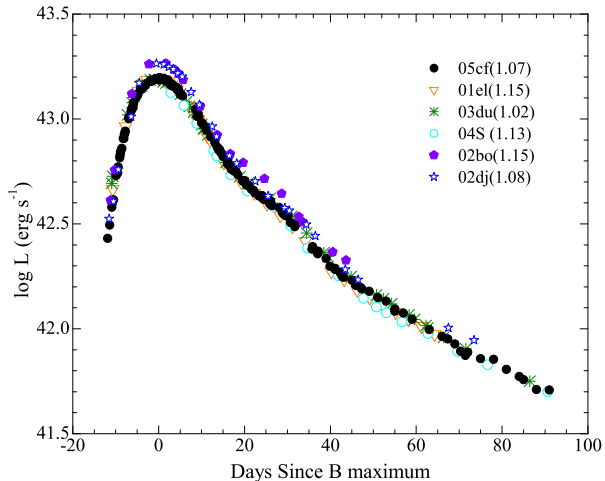


FIG. 24.— The *uvoir* bolometric light curve of SN 2005cf. Overplotted are the corresponding light curves of the comparison SNe Ia. The number in parentheses represent the  $\Delta m_{15}$  values for the SNe Ia.

Figure 24 shows the “*uvoir*” bolometric light curves of SN 2005cf and several other SNe Ia. The UV emission of all the comparison SNe was corrected on the basis of SN 2005cf. Similar corrections were applied to their light curves when the NIR observations are missing. The distances to the comparison SNe Ia were derived using the methods adopted in §5.1. The *uvoir* bolometric light curves of our SN Ia are overall very similar in shape, with the exceptions of SN 2002bo and SN 2002dj, which seem to rise at a faster pace. The maximum bolometric luminosity of SN 2005cf is estimated to be  $(1.54 \pm 0.20) \times 10^{43}$  erg s<sup>-1</sup> around the *B*-band maximum, which is similar to that of SNe 2001el and 2003du but less than that of SNe 2002bo and 2002dj. However, differences in the bolometric luminosity at maximum may be due to errors in the absorption corrections and/or the distance modulus.

With the derived bolometric luminosity, we can estimate the synthesized <sup>56</sup>Ni mass — one of the primary physical parameters determining the peak luminosity,

the light curve width, and the spectroscopic evolution of SNe Ia (e.g., Kasen et al. 2006). Assuming the Arnett law (Arnett 1982; Arnett et al. 1985; Branch 1992), the maximum luminosity produced by the radioactive <sup>56</sup>Ni can be written as (Stritzinger & Leibundgut 2005)

$$L_{\max} = (6.45e^{\frac{-t_r}{(8.8 \text{ d})}} + 1.45e^{\frac{-t_r}{(111.3 \text{ d})}}) \left( \frac{M_{\text{Ni}}}{M_{\odot}} \right) \times 10^{43} \text{ erg s}^{-1}, \quad (1)$$

where  $t_r$  is the rise time of the bolometric light curve, and  $M_{\text{Ni}}$  is the <sup>56</sup>Ni mass (in units of solar masses,  $M_{\odot}$ ). With the photometric data in the *R* band and our earliest unfiltered data from the database of the KAIT survey, we estimate the rise time to the *B* maximum as  $18.4 \pm 0.5$  d. Inserting this value and the maximum bolometric luminosity into the above equation, we derive a nickel mass of  $0.77 \pm 0.11 M_{\odot}$  for SN 2005cf. This is within the reasonable range of <sup>56</sup>Ni masses for a normal SN Ia. The quoted error bar includes uncertainties in the rise time and in the peak luminosity.

The lower bolometric luminosity and smaller nickel mass obtained by P07 is primarily due to the neglected host-galaxy extinction for SN 2005cf in their analysis. Table 13 lists all of the important parameters for SN 2005cf and its host galaxy, as we derived in the previous sections.

## 6. DISCUSSION AND CONCLUSIONS

In this paper we present extensive optical, UV, and NIR photometry as well as optical spectroscopy of SN 2005cf. In particular, the photometric observations in the optical bands were extremely well-sampled with numerous telescopes. To minimize systematic deviations from the standard system, we carefully computed the *S*-corrections and applied them to SN 2005cf. Photometry without such corrections may potentially lead to a noticeably inconsistent measurement of the reddening, which makes precise extinction corrections difficult.

The *Swift* UVOT optical photometry is found to be consistent with the ground-based observations to within  $\lesssim 0.05$  mag, after applying the *S*-corrections. The *Swift* UVOT UV uvm2 and uvw2 photometry is relatively close to that of *HST* ACS F220W and F250W, respectively, with a small shift of up to 0.1–0.2 mag.

Our observations show that SN 2005cf is a normal SN Ia with a typical luminosity decline rate  $\Delta m_{15}(\text{true}) = 1.07 \pm 0.03$  mag. Based on the *V* – *JHK* colors and the refurbished Color- $\Delta m_{15}$  relations, we estimated the host-galaxy reddening of  $E(B-V)_{\text{host}} = 0.09 \pm 0.03$  mag, which is small but non-negligible. The NIR light curves closely resemble those of normal SNe Ia, with a prominent secondary maximum. One distinguishing feature is the UV luminosity in the 2000–2500 Å range which appears much fainter and peaks later than that of the neighboring bands. This is likely caused by intrinsic spectral features in the UV, an explanation favored by the evolution of the SED.

The comprehensive data, from UV to NIR bands, allow us to establish the *uvoir* bolometric light curve of SN 2005cf in the 1600–24,000 Å range. The maximum bolometric luminosity is found to be  $(1.54 \pm 0.20) \times 10^{43}$  erg s<sup>-1</sup>, corresponding to a synthesized nickel mass of  $0.77 \pm 0.11 M_{\odot}$ . The bolometric luminosity is dominated by the optical emission; the UV contribution is

found to be a few percent of the optical, and the peak value ( $\sim 10\%$ ) occurs at around maximum light. The NIR flux contribution shows more complicated temporal evolution: the ratio decreases from the beginning of the explosion and reaches a minimum of  $\sim 5\%$  at  $t \approx +5$  d; it then rises up to a peak value of  $\sim 20\%$  at  $t \approx 35$  d, and finally declines in a linear fashion.

In general, the optical spectra of SN 2005cf are similar to those of normal SNe Ia. Strong HV features are distinctly present in the Ca II NIR triplet and the Ca II H&K lines; these are detached from the photosphere at a velocity  $\sim 19,000$ - $24,000$  km s $^{-1}$ . A HV Ca II feature is commonly seen in other SNe Ia, while the flat-bottomed shape of the Si II  $\lambda 6355$  line is relatively rare perhaps due to the paucity of the very early spectra. The excellent temporal coverage of the spectra of SN 2005cf reveals that either the flat-bottomed feature or the triangular-shaped feature associated with Si II  $\lambda 6355$  in some SNe Ia might be due to contamination by another HV absorption component, such as the pure Si II shell.

Although HV absorptions of Ca II and Si II are observed in many SNe Ia, they diverge in strength and duration. For instance, the HV features are very strong in SN 2005cf and SN 2001el, remaining until a few days after  $B$  maximum, whereas they are relatively weak in SN 2003du and SN 2005cg and becomes marginally detectable around  $B$  maximum. Given a common origin of the HV absorption from the aspherical ejecta (e.g., a torus or clumps), the diversity in strength of the HV features could be interpreted by a line-of-sight effect (see also Tanaka et al. 2006). Aspherical structure of the ejecta is favored by the evidence that the degree of polarization for the line features in SN 2001el is much higher than that for the continuum (Wang et al. 2003; Kasen et al. 2003; see also Chornock & Filippenko 2008 for SN 2004S). It is thus interesting to examine whether the strength of the HV line features correlates, at least for a subset of SNe Ia, with that of the line polarization. Unfortunately, similar high-quality polarimetric measurements at early phases are sparse for SNe Ia (but see Wang et al. 2007). Obviously, polarization spectra obtained from the very beginning would allow us to penetrate the layered geometrical structure of the SN ejecta as well as the immediate environment surrounding the explosion site.

The well-observed, multi-wavelength data presented in this paper makes SN 2005cf a rare "golden standard" sample of normal type Ia supernova, which could be used as a testbed either for the theoretical models of SN Ia, or for the studies of the systematic errors in SN Ia cosmology.

We thank Ryan Chornock and Stefanie Blondin for useful discussions. Some of the data presented herein

were obtained at the W. M. Keck Observatory, which is operated as a scientific partnership among the California Institute of Technology, the University of California, and the National Aeronautics and Space Administration (NASA). The Observatory was made possible by the generous financial support of the W. M. Keck Foundation. We thank the the Lick Observatory, Palomar Observatory, NAOC, and CTIO staffs for their assistance with the observations. The research of A.V.F.'s supernova group at UC Berkeley is supported by NSF grant AST-0607485, the TABASGO Foundation, Gary and Cynthia Bengier, and Department of Energy grant DE-FG02-08ER41563. Additional support was provided by NASA grant GO-10182 from the Space Telescope Science Institute (STScI), which is operated by AURA, Inc., under NASA contract NAS5-26555. We are also grateful to the National Natural Science Foundation of China (NSFC grant 10673007), the 973 Key Program of China (2009CB824800), and the Basic Research Funding at Tsinghua University (JCqn2005036). Supernova research at Harvard University is supported by NSF grant AST06-06772. M.M. is supported by a fellowship from the Miller Institute for Basic Research. The work of AG is supported by grants from the Israeli Science Foundation and the EU Marie Curie IRG program, and by the Benozziyo Center for Astrophysics, a research grant from the Peter and Patricia Gruber Awards, and the William Z. and Eda Bess Novick New Scientists Fund at the Weizmann Institute. KAIT and its ongoing operation were made possible by donations from Sun Microsystems, Inc., the Hewlett-Packard Company, AutoScope Corporation, Lick Observatory, the NSF, the University of California, the Sylvia & Jim Katzman Foundation, and the TABASGO Foundation. The PAIRITEL project is operated by the Smithsonian Astrophysical Observatory (SAO) and was made possible by a grant from the Harvard University Milton Fund, a camera loan from the University of Virginia and continued support of the SAO and UC Berkeley. PAIRITEL is further supported by the NASA/*Swift* Guest Investigator grant NNG06GH50G. The CTIO 1.3 m telescope is operated by the Smart and Moderate Aperture Research Telescope System (SMARTS) Consortium. We are particularly grateful for the scheduling flexibility of SMARTS. The Liverpool Telescope is operated on the island of La Palma by Liverpool John Moores University in the Spanish Observatorio del Roque de los Muchachos of the Instituto de Astrofísica de Canarias with financial support from the UK Science and Technology Facilities Council. We made use of the NASA/IPAC Extragalactic Database (NED), which is operated by the Jet Propulsion Laboratory, California Institute of Technology, under contract with NASA.

#### REFERENCES

- Aunupama, G. C., Sahu, D. K., & Jose, J. 2005, *A&A*, 429, 667  
 Arnett, W. D., 1982, *ApJ*, 253, 785  
 Arnett, W. D., Branch D., & Wheeler J. C., 1985, *Nature*, 314, 337  
 Astier, P., et al. 2006, *A&A*, 447, 31  
 Barbon, B., Rosino L., & Iijima, T. 1989, *A&A*, 220, 83  
 Barris, B. J., et al. 2004, *ApJ*, 602, 571  
 Benetti, S., et al. 2004, *MNRAS*, 348, 261  
 Benetti, S., et al. 2005, *ApJ*, 623, 1011  
 Bessell, M. S. 1990, *PASP*, 102, 1181  
 Blinnikov, S. I., & Sorokina, E. I. 2000, *A&A*, 356, 30  
 Bloom, J. S., Starr, D. L., Blake, C. H., Skrutskie, M. F., & Falco, E. E. 2006, in *ASP Conf. Ser.351: Astronomical Data Analysis Software and Systems XV*, ed. C. Gabriel, et al., 751  
 Branch D., & Tammann, G. A. 1992, *ARA&A*, 30, 359  
 Branch, D., et al. 2003, *AJ*, 126, 1489

- Branch, D., Baron, E., Thomas, R. C., Kasen, D., Li, W., & Filippenko, A. V. 2004, *PASP*, 116, 903
- Branch D., et al. 2005, *PASP*, 117, 545
- Branch D., et al. 2006, *PASP*, 118, 560
- Brown, P. J., et al. 2008, arXiv:0803.1265
- Brown, P. J., et al. 2005, *ApJ*, 635, 1192
- Candia, P., et al. 2003, *PASP*, 115, 277
- Cardelli, J. A., Clayton, G. C., & Mathis, J. S. 1989, *ApJ*, 345, 245
- cenko, S. B., et al. 2006, *PASP*, 118, 1396
- Chornock, R., & Filippenko, A. V. 2008, *AJ*, 136, 2227
- Conley, A., et al. 2008, *ApJ*, 681, 482
- Cousins, A. W. J. 1981, *South African Astron. Obs. Circ.* 6, 4
- Cutri, R. M., et al. The IRSA 2MASS All-Sky Point Source Catalog, NASA/IPAC Infrared Science Archive
- Elias-Rosa, N., et al. 2006, *MNRAS*, 369, 1880
- Ellis, R. S., et al. 2008, *ApJ*, 674, 51
- Faber, S. M., et al. 2003, *Proc. SPIE*, 4841, 1657
- Fabricant, D., Cheimets, P., Caldwell, N., & Geary, J. 1998, *PASP*, 110, 79
- Filippenko, A. V. 1982, *PASP*, 94, 715
- Filippenko, A. V. 1997, *ARA&A*, 35, 309
- Filippenko, A. V. 2005a, in *White Dwarfs: Cosmological and Galactic Probes*, ed. E. M. Sion, S. Vennes, & H. L. Shipman (Dordrecht: Springer), 97
- Filippenko, A. V. 2005b, in *The Fate of the Most Massive Stars*, ed. R. Humphreys & K. Stanek (San Francisco: ASP), 33
- Filippenko, A. V., Li, W., Treffers, R. R., & Modjaz, M. 2001, in *Small Telescope Astronomy on Global Scales*, ed. B. Paczyński, W.-P. Chen, & C. Lemme (San Francisco: ASP), 121
- Filippenko, A. V., et al. 1992a, *ApJ*, 384, L15
- Filippenko, A. V., et al. 1992b, *AJ*, 104, 1543
- Fisher, A., Branch, D., Nugent, P., & Baron, E. 1997, *ApJ*, 481, 89
- Fisher, A. K. 2000, Ph.D. Thesis, University of Oklahoma
- Foley, R. J., et al. 2003, *PASP*, 115, 1220
- Foley, R. J., Smith, N., Ganeshalingam, M., Li, W. D., Chornock, R., Filippenko, A. V. 2007, *ApJ*, 657, L105
- Foley, R. J., Filippenko, A. V., & Jha, S. W. 2008, *ApJ*, 686, 117
- Garnavich, P., et al. 2004, *ApJ*, 613, 1120
- Garavini, G., et al. 2007, *A&A*, 471, 527 (G07)
- Gehrels, N., et al. 2004, *ApJ*, 611, 1005
- Gerardy, C., et al. 2004, *ApJ*, 607, 391
- Guy, J., Astier, P., Nobili, S., Regnault, N., & Pain, P. 2005, *A&A*, 443, 781
- Guy, J., et al. 2007, *A&A*, 466, 11
- Hamuy, M., et al. 1996a, *AJ*, 112, 2391
- Hamuy, M., et al. 1996b, *AJ*, 112, 2408
- Hamuy, M., et al. 2002, *AJ*, 124, 417
- Hicken, M., Garnavich, P. M., Prieto, J. L., Blondin, S., DePoy, D. L., Kirshner, R. P., & Parrent, J. 2007, *ApJ*, 669, 17
- Hillebrandt, W., & Niemeyer, J. C. 2000, *ARA&A*, 38, 191
- Höflich, P., Wheeler, J. C., & Thielemann, F.-K. 1998, *ApJ*, 495, 617
- Jha, S., Riess, A. G., & Kirshner, R. P. 2007, *ApJ*, 659, 122
- Jha, S., et al. 1999, *ApJS*, 125, 73
- Jha, S., et al. 2006, *AJ*, 131, 527
- Jha, S., Branch, D., Chornock, R., Foley, R. J., Li, W., Swift, B. J., Casebeer, D., & Filippenko, A. V. 2006, *AJ*, 132, 189
- Johnson, H. L., Iriarte, B., Mitchell, R. I., & Wisniewski, W. Z. 1966, *Commun. Lunar Planet. Lab.*, 4, 99
- Kasen, D., et al. 2003, *ApJ*, 593, 788
- Knop, R. A., et al. 2003, *ApJ*, 598, 102
- Kirshner, R. P., et al. 1993, *ApJ*, 415, 589
- Kowalski, M., et al. 2008, *ApJ*, 686, 749
- Krisciunas, K., et al. 2000, *ApJ*, 539, 658
- Krisciunas, K., et al. 2003, *AJ*, 125, 166
- Krisciunas, K., et al. 2004a, *AJ*, 128, 3034
- Krisciunas, K., et al. 2004b, *AJ*, 127, 1664
- Krisciunas, K., et al. 2007, *AJ*, 133, 58
- Leibundgut, B., Kirshner, R. P., Filippenko, A. V., Shields, J. C., Foltz, C. B., Phillips, M. M., & Sonneborn, G. 1991, *ApJ*, 371, L23
- Leibundgut, B., et al. 1993, *AJ*, 105, 301
- Lentz, E. J., Baron, E., Branch, D., Hauschildt, P. H., & Nugent, P. E. 2000, *ApJ*, 530, 966
- Leonard, D. C., Li, W., Filippenko, A. V., Foley, R. J., & Chronock, R. 2005, *ApJ*, 632, 450
- Leonard, D. C. 2007, *ApJ*, 670, 1275
- Lira, P. 1995, Masters thesis, University of Chile
- Li, W., et al. 2001, *PASP*, 113, 1178
- Li, W., et al. 2003, *PASP*, 115, 453
- Li, W., et al. 2006, *PASP*, 118, 37
- Mattila, S., Lundqvist, P., Sollerman, J., Kozma, C., Baron, E., Fransson, C., Leibundgut, B., & Nomoto, K. 2005, *A&A*, 443, 649
- Modjaz M., Kirshner R., Challis P. 2005, Circular No. 8534
- Mazzali, P. A., Lucy, L. B., Danziger, I. J., Couffes C., Cappellaro, E., & Turatto, M. 1993, *A&A*, 269, 423
- Mazzali, P. A., et al. 2001, *ApJ*, 547, 988
- Mazzali, P. A., et al. 2005, *ApJ*, 623, L37
- Miller, J. S., & Stone, R. P. S. 1993, *Lick Obs. Tech. Rep. No. 66*
- Modjaz, M., Kirshner, R., Challis, P., & Berlind, P. 2005, *IAUC*, 8534
- Nugent, P., et al. 1995, *ApJ*, 455, L147
- Oke, J. B., et al. 1995, *PASP*, 107, 375
- Panagia, N., et al. 2003, in *Supernovae and Gamma-Ray Bursters*, ed. K. Weiler (Berlin: Springer), 113
- Pastorello, A., et al. 2007a, *MNRAS*, 377, 1531
- Pastorello, A., et al. 2007b, *MNRAS*, 376, 1301 (P07)
- Patat, F., et al. 2007, *Science*, 317, 924
- Patat, F., Benetti, S., Cappellaro, E., Danziger, I. J., Della Valle, M., Mazzali, P. A., & Turatto, M. 1996, *MNRAS*, 278, 111
- Peebles, P. J. & Ratra, B. et al. 2003, *Reviews of Modern Physics*, 75, 559
- Perlmutter, S. et al. 1997, *ApJ*, 483, 565
- Perlmutter, S., et al. 1999, *ApJ*, 517, 565
- Persson, S. E., Murphy, D. C., Krzeminski, W., Roth, M., & Rieke, M. J. 1998, *AJ*, 116, 2475
- Phillips, M. M. 1993, *ApJ*, 413, L105
- Phillips, M. M., et al. 1992, *AJ*, 103, 1632
- Phillips, M. M., et al. 1999, *AJ*, 118, 1766 (P99)
- Pignata, G., et al. 2004, *MNRAS*, 355, 178
- Pignata, G., et al. 2008, *MNRAS*, 388, 971
- Poole, T. S., et al. 2008, *MNRAS*, 383, 627
- Prieto, J. L., Rest, A., & Suntzeff, N. B. 2006, *ApJ*, 647, 501
- Pugh, H., & Li, W. 2005, *CBET*, 158
- Quimby, R., Höflich, P., Kannappan, S. J., Rykoff, E., Rujopakarn, W., Akerlof, C. W., Gerardy, C. L., & Wheeler, J. C. 2006, *ApJ*, 636, 400
- Riess, A. G., Press, W. H., & Kirshner, R. P. 1996, *ApJ*, 473, 588
- Riess, A. G., et al. 1998, *AJ*, 116, 1009
- Riess, A. G., et al. 1999, *AJ*, 117, 707
- Riess, A. G., et al. 2004, *ApJ*, 607, 665
- Riess, A. G., et al. 2005, *ApJ*, 627, 579
- Riess, A. G., et al. 2007, *ApJ*, 659, 98
- Roming, P. W. A., et al. 2005, *Space Science Reviews*, 120, 95
- Ropke, F. K., Gieseler, M., Reinecker, M., Travaglio, C., & Hillebrandt, W. 2006, *A&A*, 453, 203
- Sauer, D., et al. 2008, *MNRAS*, in press
- Schlegel, D. J., Finkbeiner, D. P., & Davis, M. 1998, *ApJ*, 500, 525
- Salvo, M. E., Cappellaro, E., Mazzali, P. A., Benetti, S., Danziger, I. J., Patat, F., & Turatto, M. 2001, *MNRAS*, 321, 254
- Sirianni, M., et al. 2005, *PASP*, 117, 1049
- Stanishev, V., et al. 2007, *A&A*, 469, 645
- Stetson, P. B. 1987, *PASP*, 99, 191
- Stritzinger, M., & Leibundgut, B. 2005, *A&A*, 431, 423
- Stritzinger, M., et al. 2002, *AJ*, 124, 2100
- Stritzinger, M., et al. 2005, *PASP*, 117, 810
- Suntzeff, N. B. 1996, in *Supernova and Supernova Remnants (IAU Colloquium 145)*, ed. R. McCray & Z. R. Wang (Cambridge: Cambridge Univ. Press), 41
- Tanaka, M., Mazzali, P. A., Maeda, K., & Nomoto, K. 2006, *ApJ*, 645, 470
- Tanaka, M., et al. 2008, *ApJ*, 677, 448
- Thomas, R. C., Branch, D., Baron, E., Nomoto, K., Li, W., & Filippenko, A. V. 2004, *ApJ*, 601, 1019
- Tonry, J. L., et al. 2003, *ApJ*, 594, 1
- Walker G. 1987, *Astronomical Observations*. Cambridge University Press, Cambridge, p47
- Wang, L., et al. 2003b, *ApJ*, 591, 1110



- Wang, L., Goldhaber, G., Aldering, G., & Perlmutter, S. 2003a, ApJ, 590, 944.
- Wang, L., Baade D., & Patat, F. 2007, Science, 315, 212
- Wang, X., Wang, L., Zhou, X., Lou, Y., & Li, Z. 2005, ApJ, 620, L87
- Wang, X., et al. 2006, ApJ, 645, 488
- Wang, X., et al. 2008a, ApJ, 672, 626
- Wang, X., Li, W., Filippenko, A. V., Foley, R. J., Smith, N., & Wang, L. 2008b, ApJ, 676, 1067
- Wood-Vasey, W. M., et al. 2007a, ApJ, 666, 694
- Wood-Vasey, W. M., et al. 2007b, arXiv:0711.2068

TABLE 1  
INSTRUMENTAL COLOR TERMS FOR DIFFERENT TELESCOPES

Telescope	$U$	$B$	$V$	$R$	$I$
KAIT 0.76 m	-0.085(017)	-0.043(011)	0.035(007)	0.070(012)	-0.010(006)
FLWO 1.2 m	-0.037(003)	-0.080(003)	0.039(002)	0.207(010)	0.109(008)
CTIO 1.3 m	...	-0.035(001)	0.049(005)	0.029(009)	0.070(006)
CTIO 0.9 m	-0.100(004)	0.096(011)	-0.016(001)	0.006(001)	-0.006(001)
Palomar 1.5 m	...	-0.100(011)	0.020(007)	0.070(012)	0.040(006)
Lick 1.0 m	-0.080(010)	-0.080(011)	0.060(007)	0.100(012)	-0.035(006)
Liverpool 2.0 m	...	-0.045(004)	0.054(005)	0.200(008)	0.100(004)
TNT 0.8 m	...	-0.132(004)	0.080(004)	0.106(006)	-0.037(003)

Note: Uncertainties, in units of 0.001 mag, are  $1\sigma$ .

TABLE 2  
MAGNITUDES OF PHOTOMETRIC STANDARDS IN THE SN 2005CF FIELD<sup>a</sup>

Star	$U$	$B$	$V$	$R$	$I$
1	...	15.265(010)	14.380(007)	13.877(006)	13.493(093)
2	13.650(030)	13.486(012)	12.799(013)	12.417(076)	12.035(017)
3	16.370(030)	15.625(008)	14.676(012)	14.086(002)	13.560(008)
4	16.582(030)	16.466(008)	15.756(007)	15.349(008)	14.947(014)
5	15.311(030)	15.328(011)	14.820(011)	14.519(005)	14.199(002)
6	14.014(030)	14.059(027)	13.604(014)	13.329(005)	13.037(019)
7	18.297(030)	18.434(017)	17.786(001)	17.518(020)	17.156(025)
8	18.926(030)	17.810(020)	16.264(007)	15.236(007)	14.048(007)
9	15.831(030)	15.660(023)	14.986(010)	14.597(007)	14.248(023)
10	18.294(030)	17.124(016)	15.947(011)	15.155(012)	14.488(018)
11	14.956(030)	14.747(008)	14.022(005)	13.594(001)	13.201(017)
12	19.353(030)	18.338(012)	17.327(017)	16.708(009)	16.205(025)
13	15.340(030)	14.760(006)	13.883(006)	13.337(005)	12.823(015)
14	18.558(030)	18.139(025)	17.393(027)	16.925(030)	16.451(019)
15	18.297(030)	17.591(011)	16.715(007)	16.187(005)	15.756(011)
16	17.933(030)	17.981(020)	17.450(015)	17.107(039)	16.724(074)

<sup>a</sup> See Fig. 1 for a chart of SN 2005cf and the comparison stars.  
Note: Uncertainties, in units of 0.001 mag, are  $1\sigma$ .

TABLE 3  
THE  $K$ - AND  $S$ -CORRECTED OPTICAL PHOTOMETRY OF SN 2005CF.

UT Date	JD-2,450,000	Phase <sup>a</sup>	$U$	$B$	$V$	$R$	$I$	Instrument <sup>b</sup>
2005 May 31	3521.75	-11.91	15.862(0.038)	15.600(0.022)	15.346(0.022)	15.189(0.032)	15.360(0.041)	2
2005 May 31	3521.77	-11.89	15.850(0.038)	15.579(0.029)	15.293(0.024)	15.206(0.041)	15.312(0.041)	1
2005 Jun 1	3522.74	-10.92	15.360(0.035)	15.151(0.022)	15.000(0.022)	14.838(0.032)	15.062(0.041)	2
2005 Jun 1	3522.87	-10.79	15.254(0.035)	15.096(0.022)	14.955(0.022)	14.846(0.032)	14.953(0.041)	1
2005 Jun 1	3523.15	-10.51	...	15.054(0.041)	14.954(0.032)	14.793(0.032)	14.896(0.041)	3
2005 Jun 2	3523.77	-9.89	14.851(0.035)	14.774(0.022)	14.721(0.022)	14.474(0.032)	14.701(0.041)	2
2005 Jun 2	3523.87	-9.79	14.768(0.035)	14.765(0.022)	14.670(0.022)	14.536(0.032)	14.651(0.041)	1
2005 Jun 2	3524.13	-9.53	...	14.751(0.022)	14.654(0.022)	14.488(0.032)	14.573(0.041)	3
2005 Jun 3	3524.63	-9.03	...	14.587(0.022)	14.497(0.022)	14.411(0.032)	14.464(0.041)	4
2005 Jun 3	3524.68	-8.98	...	14.543(0.022)	14.502(0.022)	14.291(0.032)	14.487(0.041)	2
2005 Jun 3	3524.79	-8.87	...	14.512(0.022)	14.489(0.022)	14.326(0.032)	14.409(0.041)	5
2005 Jun 3	3524.85	-8.81	14.380(0.035)	14.494(0.022)	14.438(0.022)	14.298(0.032)	14.407(0.041)	1
2005 Jun 3	3525.42	-8.24	...	14.343(0.024)	14.344(0.022)	14.190(0.032)	14.269(0.041)	6
2005 Jun 4	3525.69	-7.97	14.154(0.035)	14.304(0.022)	14.293(0.022)	14.079(0.032)	14.259(0.041)	2
2005 Jun 4	3525.76	-7.90	...	14.293(0.022)	14.299(0.022)	14.128(0.032)	14.199(0.041)	5
2005 Jun 4	3525.87	-7.79	...	14.274(0.022)	14.247(0.022)	14.095(0.032)	14.217(0.041)	7
2005 Jun 5	3526.68	-6.98	...	14.127(0.022)	14.122(0.022)	13.916(0.032)	14.108(0.041)	2
2005 Jun 5	3526.75	-6.91	13.883(0.035)	14.101(0.022)	14.118(0.022)	...	...	5
2005 Jun 5	3527.44	-6.22	...	14.007(0.022)	14.003(0.022)	13.875(0.032)	13.948(0.041)	6
2005 Jun 6	3527.64	-6.02	...	14.014(0.022)	13.992(0.022)	13.884(0.032)	13.948(0.041)	4
2005 Jun 6	3527.69	-5.97	13.734(0.035)	13.979(0.022)	13.981(0.022)	13.785(0.032)	13.970(0.041)	2
2005 Jun 6	3527.85	-5.81	13.655(0.035)	13.950(0.022)	13.942(0.022)	13.796(0.032)	13.915(0.041)	1
2005 Jun 6	3528.43	-5.23	...	13.863(0.022)	13.896(0.022)	13.781(0.032)	13.845(0.041)	6
2005 Jun 7	3528.75	-4.91	...	13.861(0.022)	13.852(0.022)	13.708(0.032)	13.863(0.041)	7
2005 Jun 7	3528.84	-4.82	13.564(0.035)	13.843(0.022)	13.843(0.022)	13.697(0.032)	13.828(0.041)	1
2005 Jun 8	3529.43	-4.23	...	13.755(0.025)	13.795(0.022)	13.704(0.032)	13.765(0.041)	6
2005 Jun 8	3529.71	-3.95	13.527(0.035)	13.768(0.022)	13.783(0.022)	13.683(0.032)	13.778(0.041)	8
2005 Jun 8	3530.42	-3.24	...	13.716(0.022)	13.736(0.022)	13.629(0.032)	13.774(0.041)	6
2005 Jun 8	3530.59	-3.07	...	13.741(0.022)	13.712(0.022)	13.644(0.032)	13.755(0.041)	4
2005 Jun 9	3530.68	-2.98	13.433(0.035)	13.718(0.022)	13.713(0.022)	13.558(0.032)	13.786(0.041)	2
2005 Jun 10	3531.67	-1.99	13.395(0.035)	13.677(0.022)	13.655(0.022)	13.523(0.032)	13.783(0.041)	2
2005 Jun 10	3531.79	-1.87	...	13.666(0.022)	13.630(0.022)	13.551(0.032)	13.767(0.041)	7
2005 Jun 10	3531.83	-1.83	13.422(0.035)	13.664(0.022)	13.639(0.025)	13.577(0.032)	13.767(0.041)	1
2005 Jun 10	3532.42	-1.24	...	13.654(0.022)	13.638(0.022)	13.550(0.032)	13.745(0.041)	6
2005 Jun 11	3532.87	-0.79	13.403(0.035)	13.643(0.022)	13.600(0.022)	13.548(0.032)	13.766(0.041)	1
2005 Jun 11	3533.42	-0.24	...	13.621(0.021)	13.595(0.022)	13.559(0.032)	13.772(0.041)	6
2005 Jun 12	3533.66	0	...	13.650(0.022)	13.592(0.022)	13.578(0.032)	13.748(0.041)	4
2005 Jun 12	3533.72	0.06	...	13.623(0.022)	13.570(0.022)	13.515(0.032)	13.785(0.041)	7
2005 Jun 12	3533.84	0.18	13.393(0.035)	13.619(0.022)	13.568(0.022)	13.517(0.032)	13.761(0.041)	1
2005 Jun 13	3534.73	1.07	13.444(0.035)	13.637(0.022)	13.574(0.022)	13.485(0.032)	13.821(0.041)	2
2005 Jun 13	3534.84	1.18	13.412(0.035)	13.622(0.022)	13.549(0.022)	13.525(0.032)	13.773(0.041)	1
2005 Jun 13	3535.43	1.77	...	13.649(0.022)	13.581(0.022)	13.540(0.032)	13.787(0.041)	6
2005 Jun 14	3535.72	2.06	...	13.641(0.022)	13.564(0.022)	13.505(0.032)	13.812(0.041)	7
2005 Jun 14	3535.74	2.08	13.489(0.035)	13.654(0.022)	13.574(0.022)	13.496(0.032)	13.858(0.041)	2
2005 Jun 14	3535.83	2.17	13.487(0.035)	13.631(0.022)	13.556(0.032)	13.509(0.032)	...	1
2005 Jun 14	3536.44	2.78	...	13.719(0.021)	13.591(0.022)	13.539(0.032)	13.800(0.041)	6
2005 Jun 15	3536.70	3.04	13.564(0.035)	13.702(0.022)	13.581(0.022)	13.519(0.032)	13.884(0.041)	2
2005 Jun 15	3536.83	3.17	13.563(0.035)	13.681(0.022)	13.558(0.022)	13.545(0.032)	13.840(0.041)	1
2005 Jun 15	3537.47	3.81	...	13.717(0.022)	13.616(0.022)	13.551(0.032)	13.833(0.041)	6
2005 Jun 16	3537.82	4.16	...	...	13.554(0.022)	13.527(0.032)	13.814(0.041)	1
2005 Jun 17	3538.68	5.02	...	13.815(0.022)	13.624(0.022)	13.638(0.032)	13.884(0.041)	4
2005 Jun 21	3542.61	8.95	...	14.093(0.045)	13.733(0.022)	13.813(0.032)	14.059(0.041)	4
2005 Jun 21	3542.72	9.06	14.117(0.054)	14.090(0.022)	13.740(0.022)	13.789(0.032)	14.117(0.041)	1
2005 Jun 21	3542.76	9.10	...	14.040(0.035)	13.709(0.033)	13.742(0.032)	14.093(0.041)	7
2005 Jun 21	3543.06	9.40	...	...	13.717(0.031)	13.795(0.032)	14.143(0.053)	3
2005 Jun 22	3543.68	10.02	14.216(0.035)	14.171(0.022)	13.797(0.022)	13.814(0.032)	14.171(0.041)	2
2005 Jun 22	3543.82	10.16	14.219(0.035)	14.182(0.022)	13.808(0.022)	13.868(0.032)	14.168(0.041)	1
2005 Jun 23	3544.77	11.11	...	14.217(0.021)	13.867(0.027)	13.888(0.032)	14.197(0.041)	7
2005 Jun 23	3544.80	11.14	14.299(0.035)	14.278(0.023)	13.866(0.032)	13.941(0.035)	14.248(0.041)	1
2005 Jun 24	3545.82	12.16	14.429(0.035)	14.377(0.022)	13.894(0.029)	14.013(0.032)	14.297(0.041)	1
2005 Jun 25	3546.75	13.09	14.539(0.035)	14.465(0.026)	13.946(0.034)	14.054(0.034)	14.328(0.041)	1
2005 Jun 26	3547.67	14.01	...	14.553(0.022)	14.015(0.022)	14.141(0.032)	14.336(0.041)	4
2005 Jun 26	3547.82	14.16	14.682(0.035)	14.570(0.022)	14.002(0.022)	14.103(0.032)	14.343(0.041)	1
2005 Jun 27	3548.66	15.00	14.841(0.037)	14.647(0.022)	14.071(0.022)	14.117(0.032)	14.400(0.041)	2
2005 Jun 27	3548.79	15.13	14.828(0.036)	14.670(0.037)	14.053(0.027)	14.154(0.032)	14.347(0.041)	1
2005 Jun 28	3549.71	16.05	14.99(0.035)	14.778(0.022)	14.134(0.022)	14.161(0.032)	14.402(0.041)	2
2005 Jun 28	3549.74	16.08	...	14.755(0.022)	14.118(0.023)	14.168(0.032)	14.309(0.041)	7
2005 Jun 28	3549.79	16.13	14.983(0.035)	14.781(0.022)	14.119(0.029)	14.200(0.039)	14.349(0.041)	1
2005 Jun 29	3550.66	17.00	15.141(0.035)	14.879(0.022)	14.178(0.022)	14.161(0.032)	14.371(0.041)	2
2005 Jun 29	3550.67	17.01	...	14.911(0.022)	14.195(0.022)	14.251(0.032)	14.340(0.041)	4
2005 Jun 29	3550.79	17.13	15.082(0.035)	14.879(0.021)	14.162(0.022)	14.196(0.032)	14.332(0.041)	1
2005 Jun 29	3551.49	17.83	...	14.913(0.032)	14.222(0.022)	14.217(0.032)	14.317(0.041)	6
2005 Jun 30	3551.73	18.07	15.251(0.035)	14.984(0.025)	14.210(0.026)	14.216(0.032)	14.314(0.041)	1
2005 Jun 30	3552.07	18.41	...	15.045(0.032)	14.279(0.022)	14.206(0.032)	14.316(0.041)	3

TABLE 3 — *Continued*

UT Date	JD-2,450,000	Phase <sup>a</sup>	<i>U</i>	<i>B</i>	<i>V</i>	<i>R</i>	<i>I</i>	Instrument <sup>b</sup>
2005 Jul 1	3553.44	19.78	...	15.229(0.031)	14.323(0.022)	14.244(0.032)	14.290(0.041)	6
2005 Jul 2	3553.73	20.07	15.513(0.039)	15.193(0.021)	14.308(0.022)	14.242(0.032)	14.270(0.041)	7
2005 Jul 2	3553.83	20.17	...	15.224(0.022)	14.351(0.022)	14.250(0.032)	14.279(0.041)	1
2005 Jul 2	3554.45	20.79	...	15.298(0.021)	14.405(0.022)	14.260(0.032)	14.280(0.041)	6
2005 Jul 3	3554.66	21.00	...	15.308(0.022)	14.369(0.022)	14.280(0.032)	14.263(0.041)	4
2005 Jul 4	3555.77	22.11	15.761(0.038)	15.439(0.025)	14.430(0.026)	14.288(0.031)	14.294(0.041)	1
2005 Jul 6	3557.68	24.02	15.977(0.035)	15.604(0.022)	14.535(0.022)	14.261(0.032)	14.260(0.041)	2
2005 Jul 6	3557.73	24.07	16.008(0.034)	15.621(0.026)	14.506(0.024)	14.302(0.032)	14.217(0.041)	1
2005 Jul 7	3559.48	25.82	...	15.791(0.022)	14.636(0.022)	14.381(0.032)	14.230(0.041)	6
2005 Jul 8	3559.59	25.93	...	15.801(0.022)	14.663(0.022)	14.383(0.032)	14.223(0.041)	8
2005 Jul 8	3559.61	25.95	...	15.811(0.022)	14.645(0.022)	14.401(0.032)	14.201(0.041)	4
2005 Jul 8	3559.70	26.04	16.149(0.044)	15.778(0.022)	14.626(0.021)	14.345(0.032)	14.197(0.041)	1
2005 Jul 8	3559.73	26.07	...	15.765(0.021)	14.610(0.027)	14.357(0.032)	14.192(0.041)	7
2005 Jul 8	3559.76	26.10	...	15.799(0.022)	14.662(0.022)	14.391(0.032)	14.304(0.041)	5
2005 Jul 10	3561.73	28.07	16.280(0.035)	15.925(0.022)	14.738(0.024)	14.417(0.032)	14.186(0.041)	1
2005 Jul 10	3562.42	28.76	...	16.010(0.022)	14.829(0.022)	14.470(0.032)	14.220(0.041)	6
2005 Jul 11	3562.63	28.97	...	16.071(0.022)	14.813(0.022)	14.497(0.032)	14.203(0.041)	4
2005 Jul 11	3562.72	29.06	16.373(0.035)	16.057(0.022)	14.817(0.022)	14.496(0.032)	...	5
2005 Jul 11	3563.03	29.37	...	16.101(0.025)	14.811(0.026)	14.482(0.032)	14.196(0.041)	3
2005 Jul 11	3563.42	29.76	...	16.081(0.023)	14.904(0.022)	14.497(0.032)	14.245(0.041)	6
2005 Jul 12	3563.70	30.04	...	16.101(0.025)	14.859(0.022)	14.513(0.032)	14.232(0.041)	7
2005 Jul 12	3563.73	30.07	16.433(0.045)	16.127(0.024)	14.854(0.023)	14.515(0.032)	14.214(0.041)	1
2005 Jul 13	3565.39	31.73	...	16.256(0.022)	15.004(0.022)	14.632(0.032)	14.311(0.041)	6
2005 Jul 14	3565.71	32.05	16.544(0.071)	16.244(0.025)	14.943(0.022)	14.609(0.032)	14.263(0.041)	1
2005 Jul 17	3569.40	35.74	...	16.479(0.031)	15.302(0.022)	14.914(0.032)	14.587(0.041)	6
2005 Jul 18	3569.54	35.88	...	16.483(0.022)	15.244(0.022)	14.902(0.032)	14.536(0.041)	4
2005 Jul 19	3570.70	37.04	16.926(0.141)	16.501(0.033)	15.323(0.027)	14.986(0.035)	14.624(0.041)	1
2005 Jul 19	3570.80	37.14	...	16.508(0.054)	15.285(0.027)	14.979(0.032)	14.583(0.041)	7
2005 Jul 21	3572.70	39.04	16.818(0.138)	16.632(0.037)	15.368(0.022)	15.052(0.032)	14.665(0.041)	1
2005 Jul 22	3573.60	39.94	...	16.638(0.026)	15.473(0.022)	15.166(0.032)	14.829(0.041)	4
2005 Jul 23	3574.70	41.04	16.845(0.059)	16.674(0.023)	15.482(0.022)	15.195(0.032)	14.878(0.041)	1
2005 Jul 23	3574.76	41.10	...	16.690(0.036)	15.480(0.024)	15.161(0.032)	14.865(0.041)	7
2005 Jul 24	3576.40	42.74	...	16.710(0.022)	15.580(0.022)	...	15.061(0.041)	6
2005 Jul 25	3576.61	42.95	...	16.744(0.022)	15.554(0.022)	15.287(0.032)	15.002(0.041)	4
2005 Jul 25	3576.73	43.07	16.945(0.088)	16.735(0.025)	15.574(0.022)	15.292(0.032)	14.997(0.041)	1
2005 Jul 27	3578.69	45.03	16.873(0.086)	16.723(0.022)	15.601(0.022)	15.348(0.032)	15.096(0.041)	1
2005 Jul 28	3579.55	45.89	...	16.805(0.022)	15.661(0.022)	15.396(0.032)	15.140(0.041)	4
2005 Jul 29	3580.69	47.03	17.141(0.123)	16.789(0.026)	15.649(0.022)	15.415(0.032)	15.169(0.041)	1
2005 Jul 29	3581.00	47.34	...	16.828(0.055)	15.691(0.022)	15.451(0.032)	15.236(0.065)	3
2005 Jul 31	3582.69	49.03	17.011(0.095)	16.839(0.025)	15.683(0.032)	15.466(0.032)	15.270(0.041)	1
2005 Aug 2	3584.69	51.03	17.014(0.088)	16.841(0.028)	15.775(0.032)	15.550(0.032)	15.373(0.041)	1
2005 Aug 4	3586.69	53.03	17.056(0.084)	16.885(0.033)	15.820(0.032)	15.591(0.032)	15.419(0.041)	1
2005 Aug 6	3588.69	55.03	17.248(0.132)	16.906(0.026)	15.924(0.032)	15.735(0.032)	15.589(0.041)	1
2005 Aug 6	3588.71	55.05	...	16.905(0.033)	15.886(0.032)	15.684(0.032)	15.606(0.042)	7
2005 Aug 8	3590.69	57.03	17.323(0.094)	16.957(0.027)	15.901(0.032)	15.746(0.032)	15.605(0.041)	1
2005 Aug 10	3592.69	59.03	17.291(0.142)	17.013(0.031)	15.963(0.032)	15.819(0.032)	15.727(0.041)	1
2005 Aug 14	3596.68	63.02	...	17.070(0.055)	16.140(0.037)	15.910(0.032)	...	1
2005 Aug 17	3599.68	66.02	...	17.121(0.059)	16.164(0.032)	16.047(0.032)	16.002(0.041)	1
2005 Aug 18	3601.01	67.35	...	...	16.240(0.032)	16.094(0.025)	16.074(0.041)	3
2005 Aug 19	3602.67	69.01	...	17.115(0.051)	16.259(0.032)	16.150(0.032)	16.201(0.041)	1
2005 Aug 20	3604.01	70.35	...	17.225(0.038)	16.309(0.032)	16.201(0.027)	16.297(0.041)	3
2005 Aug 21	3605.11	71.35	...	17.263(0.078)	16.350(0.064)	...	...	3
2005 Aug 22	3605.67	72.01	...	17.270(0.051)	16.310(0.032)	16.219(0.032)	16.295(0.041)	1
2005 Aug 25	3608.67	75.01	...	17.261(0.051)	16.421(0.032)	16.308(0.032)	16.443(0.041)	1
2005 Aug 28	3611.67	78.01	...	17.175(0.051)	16.429(0.032)	16.385(0.032)	16.487(0.041)	1
2005 Aug 31	3614.66	81.00	...	17.309(0.051)	16.573(0.032)	16.489(0.032)	16.575(0.041)	1
2005 Sept 3	3617.66	84.00	...	17.325(0.051)	16.663(0.034)	16.625(0.032)	16.744(0.041)	1
2005 Sept 4	3618.65	84.99	...	17.453(0.051)	16.646(0.032)	16.572(0.032)	16.836(0.041)	1
2005 Sept 7	3621.66	88.00	...	17.545(0.051)	16.706(0.031)	16.739(0.034)	17.061(0.054)	1
2005 Sept 10	3624.65	90.99	...	17.422(0.064)	16.844(0.039)	16.756(0.032)	17.054(0.047)	1

<sup>a</sup> Relative to the epoch of *B*-band maximum (JD = 2,453,533.66).

<sup>b</sup> 1 = KAIT 0.76 m; 2 = FLWO 1.2 m; 3 = TNT 0.8 m; 4 = CTIO 1.3 m; 5 = Lick 1.0 m; 6 = Liverpool 2.0 m; 7 = Palomar 1.5 m; 8 = CTIO 0.9 m

\* Note: Uncertainties, in units of 0.001 mag, are  $1\sigma$ .

TABLE 4  
*JHK<sub>s</sub>* MAGNITUDES OF SN 2005CF FROM PAIRITEL

UT Date	JD - 2,450,000	Phase <sup>a</sup>	<i>J</i>	<i>H</i>	<i>K<sub>s</sub></i>	<i>K<sub>J</sub></i>	<i>K<sub>H</sub></i>	<i>K<sub>K<sub>s</sub></sub></i>
31/05/05	3522.24	-11.42	14.724(0.023)	14.689(0.019)	14.825(0.021)	0.015	0.010	0.016
01/06/05	3523.25	-10.41	14.495(0.015)	14.514(0.031)	...	0.015	0.010	...
02/06/05	3524.24	-9.42	14.254(0.028)	14.316(0.031)	14.347(0.021)	0.015	0.010	0.016
10/06/05	3532.23	-1.43	13.841(0.039)	13.969(0.023)	14.002(0.023)	0.011	0.006	0.026
12/06/05	3534.23	0.57	14.035(0.044)	14.040(0.036)	13.995(0.015)	0.010	0.004	0.030
13/06/05	3535.22	1.56	13.997(0.013)	14.142(0.014)	14.102(0.034)	0.009	-0.003	0.034
14/06/05	3536.21	2.55	14.076(0.014)	14.154(0.034)	14.093(0.019)	0.008	-0.006	0.038
17/06/05	3539.21	5.55	14.346(0.023)	14.169(0.056)	14.184(0.029)	0.006	-0.010	0.046
29/06/05	3551.16	17.50	15.365(0.025)	13.974(0.064)	14.288(0.019)	0.022	-0.021	0.037
01/07/05	3553.17	19.51	15.339(0.028)	13.943(0.063)	14.196(0.017)	0.025	-0.021	0.032
02/07/05	3554.17	20.51	15.333(0.023)	14.060(0.033)	...	0.027	-0.022	...
03/07/05	3555.28	21.62	15.294(0.018)	13.979(0.060)	14.181(0.017)	0.029	-0.023	0.026
04/07/05	3556.17	22.51	15.261(0.023)	14.040(0.017)	14.167(0.021)	0.030	-0.024	0.023
05/07/05	3557.15	23.49	15.174(0.023)	13.984(0.081)	14.101(0.011)	0.033	-0.022	0.019
06/07/05	3558.15	24.49	15.191(0.036)	13.983(0.089)	14.105(0.023)	0.036	-0.021	0.016
08/07/05	3560.16	26.50	14.995(0.026)	14.017(0.018)	14.123(0.021)	0.041	-0.017	0.008
11/07/05	3563.15	29.49	14.846(0.024)	14.087(0.021)	14.219(0.019)	0.041	-0.008	0.005

<sup>a</sup> Relative to the epoch of *B*-band maximum (JD = 2,453,533.66).

Note: The *K* corrections listed in columns (7)-(9) were added to the *JHK<sub>s</sub>* magnitudes.

TABLE 5  
 JOURNAL OF SPECTROSCOPIC OBSERVATIONS OF SN 2005CF

UT Date	JD-2,450,000	Phase <sup>a</sup>	Range(Å)	Res. <sup>b</sup> (Å)	Airmass	Exposure(s)	Inst. <sup>c</sup>	Observers
31/05/2005	3521.7	-12.0	3480-7500	7	1.3	1200	Fast	PB
01/06/2005	3522.7	-11.0	3480-7500	7	1.3	960	Fast	PB
01/06/2005	3522.9	-10.8	3300-10400	5-12	1.8	600	Kast	MG;DW;BS
02/06/2005	3523.7	-10.0	3480-7500	7	1.3	600	Fast	PB
02/06/2005	3523.9	-9.8	3300-10400	5-12	1.3	300	Kast	DR
03/06/2005	3524.7	-9.0	3480-7500	7	1.3	900	Fast	MC
03/06/2005	3524.9	-8.8	3300-10400	5-12	1.4	300	Kast	DR
04/06/2005	3525.9	-7.8	3300-10400	5-12	1.4	600	Kast	DR
05/06/2005	3526.9	-6.8	3300-10400	5-12	1.4	600	Kast	DR
06/06/2005	3527.9	-5.8	3300-10400	5-12	1.4	600	Kast	MAM
07/06/2005	3528.7	-5.0	3480-7500	7	1.3	900	Fast	PB
08/06/2005	3529.7	-4.0	3480-7500	7	1.3	900	Fast	PB
09/06/2005	3530.7	-3.0	3480-7500	7	1.3	900	Fast	PB
10/06/2005	3531.8	-1.9	3480-7500	7	1.7	900	Fast	PB
10/06/2005	3531.8	-1.9	3300-10400	5-12	1.4	300	Kast	MG;FS
11/06/2005	3532.7	-1.0	3300-10400	5-12	1.5	600	Kast	FS
11/06/2005	3532.8	-0.9	3480-7500	7	1.5	600	Fast	MC
12/06/2005	3533.8	0.2	3480-7500	7	2.1	600	Fast	MC
13/06/2005	3534.7	1.1	3480-7500	7	1.4	600	Fast	PB
14/06/2005	3535.7	2.0	3300-10400	5-12	1.4	600	Kast	AF;MG;BS
14/06/2005	3535.8	2.1	3480-7500	7	1.5	600	Fast	PB
15/06/2005	3536.7	3.0	3480-7500	7	1.3	600	Fast	PB
16/06/2005	3537.6	3.9	3480-7500	7	1.3	780	Fast	MC
17/06/2005	3538.7	5.0	3480-7500	7	1.3	660	Fast	MC
29/06/2005	3550.8	17.1	3480-7500	7	2.0	900	Fast	RH
01/07/2005	3552.7	19.0	3300-10400	5-12	1.4	300	Kast	MG;DW
04/07/2005	3555.7	22.0	3480-7500	7	1.4	600	Fast	JG
06/07/2005	3557.7	24.0	3480-7500	7	1.4	900	Fast	JG
07/07/2005	3558.6	24.9	3480-7500	7	1.3	900	Fast	EF
08/07/2005	3559.6	25.9	3480-7500	7	1.3	900	Fast	PB
09/07/2005	3560.7	27.0	3480-7500	7	1.5	900	Fast	PB
10/07/2005	3561.7	28.0	3480-7500	7	1.4	900	Fast	PB
10/07/2005	3561.7	28.0	3300-10400	5-12	1.5	500	Kast	AF;FS
11/07/2005	3562.7	29.0	3480-7500	7	1.4	900	Fast	MC
12/07/2005	3563.9	30.2	3480-7500	7	1.3	1800	Fast	MC
26/07/2005	3577.6	43.9	3480-7500	7	1.4	1800	Fast	PB
28/07/2005	3579.6	45.9	3480-7500	7	1.5	1200	Fast	PB
03/09/2005	3616.6	82.9	3480-7500	7	2.2	1200	Fast	MC
26/04/2006	3853.1	319.4	3250-9250	6	1.5	1200	LRISB	AF;RF
16/02/2007	4148.1	614.4	4585-7230	1.3	1.3	6300	DEIMOS	AF;JS;RF;RC



TABLE 5 — *Continued*

UT Date	JD−2,450,000	Phase <sup>a</sup>	Range(Å)	Res. <sup>b</sup> (Å)	Airmass	Exposure(s)	Inst. <sup>c</sup>	Observers
---------	--------------	--------------------	----------	-----------------------	---------	-------------	--------------------	-----------

<sup>a</sup> Relative to the *B* maximum (JD=2,453,533.66).

<sup>b</sup> Approximate spectral resolution.

\* Fast = FLWO 1.5 m FAST; Kast = Lick Shane 3 m KAST; LIRSB = Keck I 10 m LRISBLUE; DEIMOS = Keck II 10 m DEIMOS.

\* AF = Alex Filippenko; RH = Robert Hutchins; EF = Emilio Falco; JG = Joseph Gallagher; PB = Perry Berlind; MC = Mike Calkins; MG = Mohan Ganeshalingam; DW = Diane Wong; BS = Brandont Swift; DR = David Reitzel; JS = Jeffrey Silverman; MAM = Matthew A. Malkan; FS = Frank Serduke; RC = Ryan Chronock; RF = Ryan Floey

TABLE 6  
*HST* ACS ULTRAVIOLET PHOTOMETRY OF SN 2005CF

UT Date	JD	Phase <sup>a</sup>	F220W	F250W	F330W
03/06/05	3524.99	-8.67	19.978(070)	16.624(015)	14.675(005)
05/06/05	3527.26	-6.40	19.024(030)	15.638(005)	13.766(004)
07/06/05	3529.36	-4.30	18.557(019)	15.341(005)	13.439(005)
11/06/05	3532.96	-0.70	18.189(038)	14.972(004)	13.272(004)
14/06/05	3535.95	2.28	18.160(051)	15.026(004)	13.395(004)
16/06/05	3537.95	4.29	18.131(027)	15.243(005)	13.719(006)
21/06/05	3542.61	9.02	18.240(009)	15.941(005)	14.424(004)
25/06/05	3547.28	13.62	18.665(011)	16.589(005)	15.051(004)
26/06/05	3547.98	14.32	18.745(007)	16.745(008)	15.259(005)
29/06/05	3551.28	17.68	19.060(013)	17.068(005)	15.677(004)
30/06/05	3551.77	18.11	19.158(009)	17.162(005)	15.797(005)
05/07/05	3557.07	23.41	19.524(023)	17.766(008)	16.369(005)

<sup>a</sup> Relative to the epoch of *B*-band maximum (JD = 2,453,533.66)

Note: Uncertainties, in units of 0.001 mag, are  $1\sigma$ .

TABLE 7  
*HST* NICMOS3 NIR PHOTOMETRY OF SN 2005CF

UT Date	JD −2,450,000	Phase <sup>a</sup>	<i>J</i> <sup>b</sup>	<i>H</i> <sup>b</sup>	Color F110W→ <i>J</i>	Correction F160W→ <i>H</i>	S F110W→ <i>J</i>	Correction F160W→ <i>H</i>
2005 June 3	3525.08	−8.58	14.246(0.030)	14.185(0.025)	0.126	0	−0.162	−0.120
2005 June 7	3527.15	−6.51	13.932(0.029)	13.905(0.023)	0.116	0	−0.190	−0.110
2005 June 10	3529.81	−3.85	13.803(0.029)	13.885(0.023)	0.207	−0.002	−0.220	−0.095
2005 June 13	3533.14	−0.52	13.821(0.029)	13.945(0.023)	0.222	−0.002	−0.235	−0.078
2005 June 16	3536.74	3.08	14.222(0.030)	14.229(0.025)	0.168	−0.001	−0.143	−0.056
2005 June 18	3538.87	5.21	14.370(0.030)	14.285(0.025)	0.175	−0.001	−0.040	−0.047
2005 June 23	3544.01	10.35	15.093(0.032)	14.357(0.027)	0.119	0	0.410	−0.195
2005 June 27	3548.08	14.42	15.389(0.032)	14.197(0.026)	0.021	0.002	0.730	−0.275
2005 July 1	3552.08	18.42	15.350(0.032)	14.132(0.025)	−0.045	0.003	0.710	−0.250
2005 July 7	3558.00	24.34	15.271(0.032)	14.063(0.025)	−0.042	0.003	0.720	−0.210

<sup>a</sup> Relative to the epoch of *B*-band maximum (JD = 2,453,533.66)

<sup>b</sup> The *J*- and *H*-band magnitudes were converted, respectively, from the F110W- and F160W-band magnitudes using the color- and S-corrections listed in columns 6–9.

TABLE 8  
SWIFT UVOT ULTRAVIOLET/OPTICAL PHOTOMETRY OF SN 2005CF.

UT Date	JD <sup>a</sup>	Phase <sup>b</sup>	<i>uvw2</i>	<i>uvm2</i>	<i>uvw1</i>	<i>U</i>	<i>B</i>	<i>V</i>	<i>Sc<sub>U</sub></i>	<i>Sc<sub>B</sub></i>	<i>Sc<sub>V</sub></i>
2005 June 4	3525.55	-8.11	17.79(0.09)	>19.69	16.34(0.07)	14.31(0.05)	14.26(0.05)	14.36(0.05)	-0.17	-0.02	0.01
2005 June 5	3526.55	-7.11	17.53(0.08)	>20.00	15.91(0.06)	13.99(0.05)	14.17(0.09)	14.16(0.05)	-0.13	-0.01	0.01
2005 June 6	3527.55	-6.11	17.33(0.08)	19.45(0.31)	15.58(0.06)	13.76(0.05)	13.92(0.06)	14.02(0.04)	-0.11	-0.01	0.01
2005 June 8	3530.43	-3.23	16.91(0.07)	18.76(0.31)	15.18(0.05)	13.37(0.06)	13.66(0.06)	13.73(0.05)	-0.12	-0.01	0.01
2005 June 9	3530.77	-2.89	16.94(0.06)	19.26(0.26)	15.10(0.05)	13.40(0.06)	13.65(0.07)	13.70(0.05)	-0.12	-0.01	0.01
2005 June 10	3531.97	-1.69	16.85(0.06)	18.36(0.16)	15.10(0.05)	13.34(0.06)	13.60(0.07)	13.66(0.05)	-0.12	-0.01	0.01
2005 June 11	3533.05	-0.61	16.83(0.06)	18.50(0.16)	15.13(0.05)	...	...	13.61(0.06)	...	...	0.01
2005 June 16	3538.26	4.60	17.15(0.07)	18.32(0.15)	15.39(0.05)	...	...	13.58(0.06)	...	...	0.02
2005 June 17	3538.74	5.08	17.07(0.07)	18.31(0.15)	15.44(0.05)	...	...	13.63(0.06)	...	...	0.02
2005 June 20	3542.15	8.49	17.39(0.07)	18.47(0.15)	15.83(0.06)	...	...	13.70(0.06)	...	...	0.03
2005 June 22	3543.70	10.04	17.47(0.08)	18.58(0.20)	16.03(0.09)	...	...	13.75(0.07)	...	...	0.03
2005 June 26	3548.26	14.60	18.06(0.10)	18.62(0.18)	16.63(0.07)	14.82(0.05)	14.65(0.05)	14.09(0.05)	-0.21	0	0.04
2005 June 29	3550.51	16.85	18.21(0.11)	18.92(0.24)	16.96(0.09)	15.14(0.05)	14.91(0.05)	14.25(0.05)	-0.22	0	0.04
2005 July 12	3564.32	30.66	19.36(0.29)	>19.76	18.17(0.16)	16.46(0.08)	16.07(0.06)	14.94(0.05)	-0.17	0	0.06
2005 July 23	3575.16	41.50	...	...	...	17.05(0.06)	16.65(0.05)	15.60(0.05)	-0.18	0	0.05
2005 July 24	3575.97	42.31	19.77(0.19)	>20.29	18.60(0.11)	...	...	...	...	...	...

<sup>a</sup> Julian Date  $-2,450,000$

<sup>b</sup> Relative to the epoch of *B*-band maximum (JD = 2,453,533.66).

TABLE 9  
LIGHT-CURVE PARAMETERS OF SN 2005CF

Band	$\lambda_{\text{central}}$ (Å)	$t_{\text{max}}$ $-2,450,000$	$m_{\text{peak}}$ (mag)	$\Delta m_{15}^{\text{a}}$ (mag)
<i>uvw2</i>	1928	3533.05±0.50	16.84±0.05	1.11±0.06
<i>uvm2</i>	2246	3537.86±0.71	18.30±0.13	0.75±0.08
<i>uvw1</i>	2600	3532.35±0.44	15.10±0.04	1.44±0.05
F220W	2228	3537.17±0.48	18.14±0.05	1.00±0.06
F250W	2696	3532.49±0.42	15.13±0.04	1.54±0.05
F330W	3354	3532.30±0.40	13.31±0.04	1.91±0.05
<i>U</i>	3650	3532.42±0.30	13.40±0.03	1.26±0.04
<i>B</i>	4450	3533.66±0.28	13.63±0.02	1.05±0.03
<i>V</i>	5500	3535.54±0.33	13.55±0.02	0.62±0.03
<i>R</i>	6450	3534.80±0.26	13.53±0.03	0.67±0.03
<i>I</i>	7870	3532.56±0.34	13.76±0.04	0.59±0.03
<i>J</i>	12700	3530.54±0.44	13.78±0.05	1.45±0.05
<i>H</i>	16700	3529.48±0.42	13.84±0.04	0.42±0.05
<i>K</i>	22200	3530.32±0.59	13.94±0.05	0.40±0.06

<sup>a</sup> The magnitude decline in 15 days after the initial maximum of the light curve.

TABLE 10  
THE *UBVRI* TEMPLATE LIGHT CURVES OF SN 2005CF<sup>a</sup>

Days	<i>U</i>	<i>B</i>	<i>V</i>	<i>R</i>	<i>I</i>
-12	2.58	2.00	1.78	1.75	1.61
-11	1.97	1.55	1.45	1.37	1.28
-10	1.48	1.20	1.17	1.05	0.97
-9	1.08	0.91	0.93	0.80	0.70
-8	0.76	0.68	0.72	0.60	0.48
-7	0.51	0.49	0.56	0.44	0.31
-6	0.33	0.35	0.41	0.32	0.18
-5	0.19	0.23	0.30	0.22	0.09
-4	0.09	0.14	0.21	0.14	0.04
-3	0.04	0.08	0.14	0.09	0.01
-2	0.01	0.03	0.08	0.05	0
-1	0	0.01	0.04	0.02	0.01
0	0.02	0	0.02	0.01	0.02
1	0.05	0.01	0	0	0.04
2	0.10	0.03	0	0	0.05
3	0.16	0.06	0.01	0.02	0.08
4	0.22	0.11	0.02	0.04	0.10
5	0.30	0.16	0.04	0.07	0.13
6	0.39	0.23	0.07	0.11	0.16
7	0.48	0.30	0.11	0.16	0.21
8	0.58	0.37	0.15	0.21	0.27
9	0.69	0.46	0.19	0.27	0.33
10	0.80	0.55	0.24	0.34	0.41
11	0.92	0.64	0.29	0.40	0.48
12	1.04	0.73	0.34	0.47	0.54
13	1.17	0.84	0.39	0.53	0.57
14	1.31	0.94	0.45	0.59	0.59
15	1.45	1.05	0.50	0.63	0.59
16	1.59	1.15	0.56	0.66	0.59
17	1.74	1.27	0.61	0.68	0.59
18	1.89	1.38	0.67	0.70	0.57
19	2.02	1.49	0.72	0.72	0.56
20	2.15	1.60	0.78	0.74	0.54
21	2.27	1.71	0.83	0.75	0.52
22	2.38	1.81	0.88	0.76	0.50
23	2.49	1.91	0.93	0.78	0.48
24	2.59	2.00	0.98	0.80	0.47
25	2.68	2.10	1.04	0.82	0.46
26	2.77	2.19	1.09	0.85	0.45
27	2.85	2.27	1.14	0.89	0.45
28	2.92	2.36	1.21	0.93	0.46
29	2.99	2.44	1.29	0.97	0.47
30	3.06	2.51	1.35	1.02	0.50
31	3.12	2.58	1.42	1.08	0.53
34	3.27	2.77	1.60	1.27	0.66
37	3.38	2.92	1.75	1.47	0.86
40	3.46	3.03	1.88	1.64	1.08
43	3.53	3.11	1.99	1.77	1.28
46	3.58	3.16	2.09	1.89	1.40
49	3.65	3.21	2.18	1.98	1.53
52	3.72	3.26	2.26	2.08	1.66
57	3.83	3.34	2.39	2.23	1.88
62	3.94	3.42	2.51	2.39	2.10
65	4.00	3.46	2.58	2.49	2.23
70	4.11	3.54	2.71	2.64	2.45
75	4.22	3.62	2.84	2.80	2.67
80	4.33	3.70	2.98	2.96	2.89
85	4.44	3.78	3.12	3.12	3.10
90	4.55	3.86	3.25	3.28	3.32

<sup>a</sup> All of the light curves have been normalized to the *B*-band maximum epoch and their peak values listed in Table 9.

TABLE 11  
THE INTRINSIC COLOR –  $\Delta m_{15}(B)$  RELATION

Color	$a$	$b_1$	$b_2$	$b_3$	$\sigma$
$B_{\max} - V_{\max}^a$	-0.09(04)	0.15(03)	...	...	0.03
$B_{\max} - V_{\max}^b$	-1.61(35)	2.60(47)	...	...	0.11
$V_{\max} - I_{\max}^a$	-0.27(01)	0.22(03)	...	...	0.06
$V_{\max} - I_{\max}^b$	-1.03(10)	1.45(14)	...	...	0.06
$(B - V)_{12}$	0.25(01)	0.34(05)	-0.38(21)	1.98(23)	0.04
$(B - V)_{35}^a$	1.02(01)	...	...	...	0.04
$(B - V)_{35}^b$	0.72(07)	0.46(10)	...	...	0.04

$$Color = a + b_1(\Delta m_{15} - 1.1) + b_2(\Delta m_{15} - 1.1)^2 + b_3(\Delta m_{15} - 1.1)^3.$$

<sup>a</sup> The correlation holds for SNe Ia with  $0.8 < \Delta m_{15} < 1.7$ .

<sup>b</sup> The correlation applies to SNe Ia with  $\Delta m_{15} \gtrsim 1.7$ .

TABLE 12  
HOST-GALAXY REDDENING OF SN 2005CF

Method	$E(B - V)_{\text{host}}$	References
$B_{\max} - V_{\max}$	$0.07 \pm 0.04$	1,2
$V_{\max} - I_{\max}$	$-0.06 \pm 0.06$	1,2
$(B - V)_{12}$	$0.12 \pm 0.04$	3,2
$(B - V)_{35}$	$0.13 \pm 0.05$	4,2
$(B - V)_{\text{tail}}$	$0.15 \pm 0.04$	1
$V - J$	$0.13 \pm 0.08$	5
$V - H$	$0.10 \pm 0.06$	5
$V - K$	$0.06 \pm 0.06$	5
Mean	$0.09 \pm 0.03$	...

REFERENCES. — (1) Phillips et al. (1999); (2) this paper; (3) Wang et al. (2005); (4) Jha et al. (2007); (5) Krisciunas et al. (2004).

TABLE 13  
RELEVANT PARAMETERS FOR SN 2005CF AND ITS HOST.

Parameter	Value	Source
Photometric parameters		
Discovery date	28.26 May 2005	1
Epoch of $B$ maximum	$2453533.66 \pm 0.28$	2
$B_{\max}$	$13.63 \pm 0.02$ mag	2
$B_{\max} - V_{\max}$	$0.08 \pm 0.03$ mag	2
$E(B - V)_{\text{host}}$	$0.10 \pm 0.03$ mag	2
$\Delta m_{15}(\text{true})$	$1.07 \pm 0.03$ mag	2
$\Delta C_{12}(\text{true})$	$0.27 \pm 0.03$	2
Late-time $B$ decline rate	$1.62 \pm 0.05$ mag (100 d) <sup>-1</sup>	2
$L_{\text{bol}}^{\text{max}}$	$(1.54 \pm 0.20) \times 10^{43}$ erg s <sup>-1</sup>	2
$t_r$	$18.4 \pm 0.5$ d	2
$^{56}\text{Ni}$	$0.77 \pm 0.11 M_{\odot}$	2
Spectroscopic parameters		
$v_{\max}(\text{Si II } \lambda 6355)$	$\sim 10,100$ km s <sup>-1</sup>	2
$v_{\max}(\text{S II } \lambda 5460)$	$\sim 9600$ km s <sup>-1</sup>	2
$\dot{v}(\text{Si II } \lambda 6355)$	$30 \pm 5$ km s <sup>-1</sup>	2
$R(\text{Si II})_{\max}$	$0.28 \pm 0.04$	2
Parameters for MCG-01-39-003		
Galaxy type	S0 pec	3
$E(B - V)_{\text{Gal}}$	0.097	3
$(m - M)$	$32.31 \pm 0.11$	2
$v_{\text{hel}}$	$1937$ km s <sup>-1</sup>	3

References: (1) Hugh & Li 2005; (2) this paper; (3) NASA Extragalactic Database.

## APPENDIX

THE  $S$ - AND  $K$ -CORRECTIONS

It is always tricky to transform photometric observations from one filter system to another, requiring many response parameters characterizing the instruments. According to the description in Stritzinger et al. (2002), the instrumental response  $S(\lambda)$  can be simply defined as

$$S(\lambda) = F(\lambda) \times A(\lambda) \times QE(\lambda), \quad (\text{A1})$$

where  $F(\lambda)$  is the filter transmission function,  $A(\lambda)$  is the transparency of the Earth’s atmosphere, and  $QE(\lambda)$  is the detector quantum efficiency. The atmospheric transmission at the sites where it is not directly available was obtained by modifying the standard atmospheric model (Walker 1987) to be consistent with the average broadband absorption coefficients. Here we did not include the mirror reflectivities, dichroic transmission, or dewar window transmissions due to the absence of this information. Various instrumental responses, normalized to the peak transmission, are shown in Figure 2.

To check whether the instrumental response curves match those actually used at the telescopes, we computed the synthetic magnitudes and hence the color terms by convolving the model curves with a large sample of spectrophotometric standard stars from Stritzinger et al. (2005). The resulting synthetic color terms are generally consistent with the values listed in Table 1 of the main text, but small differences are present. The differences are probably due to the mirror reflectivities, dichroic mirror transmission, or other unknown transmissivity of the optical elements. Following the method proposed by Stritzinger et al. (2002), we shifted the wavelength of the model response curves in order to reproduce exactly the measured color terms. The wavelength shifts of different instrumental responses are given in Table A1. They are usually  $\lesssim 100$  Å, except in the  $R$  and  $I$  filters at the CTIO 1.3 m telescope where the required shifts are 128 Å and 377 Å, respectively.

TABLE 14  
WAVELENGTH SHIFTS TO INSTRUMENTAL RESPONSE CURVES<sup>a</sup>

Telescope	$U$	$B$	$V$	$R$	$I$
KAIT 0.8 m	29 blue	20 blue	9 red	38 blue	29 blue
CfA 1.2 m	29 blue	58 red	9 red	0	0
CTIO 1.3 m	...	70 blue	58 blue	128 blue	377 blue
CTIO 0.9 m	6 blue	0	0	46 blue	41 red
Palomar 1.5 m	...	0	17 red	15 red	107 blue
Lick 1.0 m	38 blue	38 red	46 red	15 blue	58 red
Liverpool 2.0 m	...	35 blue	9 red	0	29 red

<sup>a</sup> All values are measured in Angstrom units.

With proper model response curves and better spectral coverage for SN 2005cf, we are able to compute the  $S$ -corrections using

$$Sc_{\lambda_1} = M_{\lambda_1} - m_{\lambda_1} - CT_{\lambda_1}(m_{\lambda_1} - m_{\lambda_2}) - ZP_{\lambda_1}, \quad (\text{A2})$$

where  $M_{\lambda_1}$  is the  $\lambda_1$ -band SN magnitude synthesized with the Bessell function, and  $m_{\lambda_1}$  and  $m_{\lambda_2}$  are (respectively) the  $\lambda_1$ -band and  $\lambda_2$ -band magnitudes synthesized with the instrumental response function. The color term is  $CT_{\lambda_1}$ , and  $ZP_{\lambda_1}$  is the zeropoint, which can be determined from the spectrophotometric standards with a precision close to 0.01 mag. However, since the spectra of SN 2005cf taken 1–3 months after  $B$ -band maximum did not have adequate wavelength coverage and were sparsely sampled, we also used the spectra of SN 2003du (Stanishev et al. 2007) to compute the  $S$ -corrections during that phase.

In order to estimate the corresponding  $S$ -corrections at any epochs without photometry, a polynomial function was used to fit the data points shown in Figure 3. The resulting  $S$ -corrections are listed in Table A2 (columns 4–8).

Owing to a redshift effect on the spectral energy distribution, we further computed the  $K$ -corrections for SN 2005cf in the optical bands. The  $K$ -corrections, based on the response curves of the Bessell filter band and the observed spectra of SNe 2005cf and 2003du, are listed in Table A2 (columns 9–13). Except in the  $U$  band, the  $K$ -corrections are generally small, 0.02–0.03 mag around maximum brightness, and they depend on the supernova phase.



TABLE 15  
 THE  $K$ - AND  $S$ -CORRECTIONS ADDED TO THE  $UBVRI$  MAGNITUDES OF SN  
 2005CF.

UT Date	JD	Phase <sup>a</sup>	$Sc_U$	$Sc_B$	$Sc_V$	$Sc_R$	$Sc_I$	$K_U$	$K_B$	$K_V$	$K_R$	$K_I$	Inst. <sup>b</sup>
2005 May 31	3521.75	-11.91	0.038	-0.042	-0.012	-0.022	0.015	-0.087	0.004	0.014	0.016	0.017	2
2005 May 31	3521.77	-11.89	0.075	-0.036	0.009	0	-0.020	-0.087	0.004	0.014	0.016	0.017	1
2005 Jun 1	3522.74	-10.92	0.032	-0.043	-0.014	-0.025	0.018	-0.073	0.006	0.013	0.016	0.018	2
2005 Jun 1	3522.87	-10.79	0.071	-0.034	0.005	1E-3	-0.015	-0.071	0.007	0.013	0.016	0.019	1
2005 Jun 1	3523.15	-10.51	...	...	...	...	...	-0.069	0.007	0.013	0.016	0.019	3
2005 Jun 2	3523.77	-9.89	0.021	-0.040	-0.015	-0.027	0.017	-0.060	0.008	0.013	0.016	0.019	2
2005 Jun 2	3523.87	-9.79	0.063	-0.033	0.003	0.002	-0.011	-0.059	0.009	0.013	0.016	0.019	1
2005 Jun 2	3524.13	-9.53	...	...	...	...	...	-0.057	0.009	0.013	0.016	0.019	3
2005 Jun 3	3524.63	-9.03	...	-0.033	-0.028	0.025	0.037	...	0.010	0.013	0.016	0.020	4
2005 Jun 3	3524.68	-8.98	...	-0.037	-0.015	-0.029	0.017	...	0.010	0.013	0.016	0.020	2
2005 Jun 3	3524.79	-8.87	...	-0.034	0.002	0.002	0.004	...	0.010	0.013	0.016	0.020	5
2005 Jun 3	3524.85	-8.81	0.047	-0.031	0	0.003	-0.010	-0.049	0.010	0.013	0.016	0.020	1
2005 Jun 3	3525.42	-8.24	...	-0.024	-0.013	0.026	0.027	...	0.011	0.013	0.016	0.020	6
2005 Jun 4	3525.69	-7.97	0.007	-0.035	-0.016	-0.03	0.018	-0.043	0.011	0.012	0.016	0.020	2
2005 Jun 4	3525.76	-7.90	...	-0.032	-0.003	0.006	-0.003	...	0.011	0.012	0.016	0.020	5
2005 Jun 4	3525.87	-7.79	...	-0.031	-0.009	0.007	0.026	...	0.011	0.012	0.016	0.020	7
2005 Jun 5	3526.68	-6.98	...	-0.032	-0.017	-0.027	0.020	...	0.012	0.012	0.017	0.019	2
2005 Jun 5	3526.75	-6.91	0.042	-0.031	-0.004	...	...	-0.036	0.012	0.012	...	...	5
2005 Jun 5	3527.44	-6.22	...	-0.023	-0.015	0.032	0.010	...	0.012	0.012	0.018	0.019	6
2005 Jun 6	3527.64	-6.02	...	-0.028	-0.021	0.020	0.018	...	0.012	0.012	0.018	0.019	4
2005 Jun 6	3527.69	-5.97	0.003	-0.031	-0.018	-0.026	0.012	-0.032	0.012	0.012	0.018	0.019	2
2005 Jun 6	3527.85	-5.81	0.018	-0.028	-0.004	0.007	-0.002	-0.031	0.012	0.012	0.018	0.018	1
2005 Jun 6	3528.43	-5.23	...	-0.023	-0.016	0.036	1E-3	...	0.012	0.012	0.018	0.018	6
2005 Jun 7	3528.75	-4.91	...	-0.029	-0.008	0.012	0.013	...	0.012	0.011	0.019	0.018	7
2005 Jun 7	3528.84	-4.82	0.012	-0.028	-0.004	0.009	-0.002	-0.028	0.012	0.011	0.019	0.017	1
2005 Jun 8	3529.43	-4.23	...	-0.022	-0.016	0.038	-0.016	...	0.012	0.011	0.019	0.017	6
2005 Jun 8	3529.71	-3.95	0.022	-0.017	0.007	0.003	-0.025	-0.026	0.012	0.011	0.020	0.016	8
2005 Jun 8	3530.42	-3.24	...	-0.021	-0.017	0.041	-0.021	...	0.012	0.011	0.020	0.015	6
2005 Jun 8	3530.59	-3.07	...	-0.028	-0.020	0.017	-0.012	...	0.012	0.011	0.021	0.015	4
2005 Jun 9	3530.68	-2.98	-0.011	-0.03	-0.019	-0.022	-0.024	-0.025	0.012	0.011	0.021	0.015	2
2005 Jun 10	3531.67	-1.99	-0.012	-0.03	-0.019	-0.021	-0.04	-0.024	0.011	0.010	0.022	0.013	2
2005 Jun 10	3531.79	-1.87	...	-0.028	-0.007	0.017	0	...	0.011	0.010	0.022	0.013	7
2005 Jun 10	3531.83	-1.83	-0.005	-0.027	-0.004	0.014	-0.006	-0.024	0.011	0.010	0.022	0.013	1
2005 Jun 10	3532.42	-1.24	...	-0.020	-0.017	0.045	-0.042	...	0.011	0.010	0.022	0.012	6
2005 Jun 11	3532.87	-0.79	0	-0.027	-0.004	0.016	-0.007	-0.025	0.011	0.010	0.023	0.011	1
2005 Jun 11	3533.42	-0.24	...	-0.019	-0.017	0.054	-0.050	...	0.010	0.010	0.024	0.010	6
2005 Jun 12	3533.66	0.00	...	-0.028	-0.018	0.011	-0.044	...	0.010	0.010	0.024	0.009	4
2005 Jun 12	3533.72	0.06	...	-0.028	-0.007	0.019	-0.008	...	0.010	0.010	0.024	0.009	7
2005 Jun 12	3533.84	0.18	0	-0.027	-0.004	0.016	-0.007	-0.025	0.010	0.010	0.024	0.009	1
2005 Jun 13	3534.73	1.07	-0.011	-0.031	-0.020	-0.006	-0.08	-0.026	0.009	0.009	0.025	0.007	2
2005 Jun 13	3534.84	1.18	0.005	-0.027	-0.004	0.020	-0.010	-0.027	0.009	0.009	0.025	0.007	1
2005 Jun 13	3535.43	1.77	...	-0.018	-0.017	0.067	-0.078	...	0.009	0.009	0.025	0.006	6
2005 Jun 14	3535.72	2.06	...	-0.027	-0.008	0.022	-0.015	...	0.009	0.009	0.026	0.005	7
2005 Jun 14	3535.74	2.08	-0.009	-0.032	-0.020	0.005	-0.090	-0.028	0.009	0.009	0.026	0.005	2
2005 Jun 14	3535.83	2.17	0.015	-0.027	-0.004	0.024	...	-0.028	0.008	0.009	0.026	...	1
2005 Jun 14	3536.44	2.78	...	-0.018	-0.017	0.07	-0.089	...	0.008	0.008	0.026	0.004	6
2005 Jun 15	3536.70	3.04	-0.004	-0.032	-0.020	0.007	-0.103	-0.029	0.008	0.008	0.026	0.003	2
2005 Jun 15	3536.83	3.17	0.017	-0.027	-0.004	0.024	-0.012	-0.030	0.008	0.008	0.027	0.003	1
2005 Jun 15	3537.47	3.81	...	-0.017	-0.016	0.071	-0.101	...	0.007	0.008	0.027	0.002	6
2005 Jun 16	3537.82	4.16	...	...	-0.004	0.025	-0.013	-0.031	0.007	0.008	0.027	1E-3	1
2005 Jun 17	3538.68	5.02	...	-0.025	-0.017	0.019	-0.085	...	0.006	0.007	0.028	-1E-3	4
2005 Jun 21	3542.61	8.95	...	-0.020	-0.015	0.024	-0.104	...	0.002	0.005	0.028	-0.007	4
2005 Jun 21	3542.72	9.06	0.035	-0.015	-0.004	0.021	-0.016	-0.040	0.002	0.005	0.028	-0.007	1
2005 Jun 21	3542.76	9.10	...	-0.024	-0.013	0.022	-0.023	...	0.002	0.005	0.028	-0.007	7
2005 Jun 21	3543.06	9.40	...	...	...	...	...	-0.040	0.002	0.005	0.028	-0.007	3
2005 Jun 22	3543.68	10.02	0.016	-0.024	-0.018	0.015	-0.160	-0.041	1E-3	0.004	0.027	-0.008	2
2005 Jun 22	3543.82	10.16	0.040	-0.013	-0.004	0.021	-0.018	-0.042	1E-3	0.004	0.027	-0.008	1
2005 Jun 23	3544.77	11.11	...	-0.024	-0.014	0.023	-0.020	...	0	0.003	0.027	-0.009	7
2005 Jun 23	3544.80	11.14	0.045	-0.011	-0.004	0.018	-0.019	-0.043	0	0.003	0.027	-0.009	1
2005 Jun 24	3545.82	12.16	0.050	-0.010	-0.004	0.016	-0.020	-0.044	-1E-3	0.003	0.026	-0.009	1
2005 Jun 25	3546.75	13.09	0.058	-0.009	-0.004	0.015	-0.020	-0.045	-0.002	0.002	0.024	-0.009	1
2005 Jun 26	3547.67	14.01	...	-0.014	-0.012	0.026	-0.108	...	-0.003	1E-3	0.023	-0.009	4
2005 Jun 26	3547.82	14.16	0.062	-0.009	-0.004	0.015	-0.019	-0.046	-0.003	1E-3	0.023	-0.009	1
2005 Jun 27	3548.66	15.00	0.029	-0.023	-0.016	0.015	-0.194	-0.046	-0.004	0	0.022	-0.009	2
2005 Jun 27	3548.79	15.13	0.064	-0.009	-0.005	0.014	-0.016	-0.047	-0.004	0	0.021	-0.009	1
2005 Jun 28	3549.71	16.05	0.028	-0.026	-0.016	0.012	-0.196	-0.047	-0.005	-1E-3	0.020	-0.008	2
2005 Jun 28	3549.74	16.08	...	-0.026	-0.013	0.021	-0.007	...	-0.005	-1E-3	0.019	-0.008	7
2005 Jun 28	3549.79	16.13	0.067	-0.011	-0.005	0.013	-0.016	-0.047	-0.005	-1E-3	0.019	-0.008	1
2005 Jun 29	3550.66	17.00	0.031	-0.027	-0.015	0.010	-0.196	-0.048	-0.006	-1E-3	0.017	-0.008	2
2005 Jun 29	3550.67	17.01	...	-0.012	-0.011	0.043	-0.104	...	-0.006	-1E-3	0.017	-0.008	4
2005 Jun 29	3550.79	17.13	0.068	-0.012	-0.005	0.012	-0.015	-0.048	-0.006	-0.002	0.017	-0.008	1
2005 Jun 29	3551.49	17.83	...	-0.015	0	0.044	-0.172	...	-0.007	-0.002	0.015	-0.008	6
2005 Jun 30	3551.73	18.07	0.069	-0.011	-0.005	0.013	-0.014	-0.048	-0.007	-0.002	0.015	-0.007	1

TABLE 15 — *Continued*

UT Date	JD	Phase <sup>a</sup>	$Sc_U$	$Sc_B$	$Sc_V$	$Sc_R$	$Sc_I$	$K_U$	$K_B$	$K_V$	$K_R$	$K_I$	Inst. <sup>b</sup>
2005 Jun 30	3552.07	18.41	...	...	...	...	...	...	-0.007	-0.003	0.015	-0.007	3
2005 Jul 1	3553.44	19.78	...	-0.016	0.0015	0.053	-0.163	...	-0.008	-0.004	0.015	-0.007	6
2005 Jul 2	3553.73	20.07	0.072	-0.010	-0.005	0.013	-0.012	-0.048	-0.009	-0.005	0.015	-0.006	1
2005 Jul 2	3553.83	20.17	...	-0.032	-0.010	0.018	0.006	...	-0.009	-0.005	0.015	-0.006	7
2005 Jul 2	3554.45	20.79	...	-0.017	0.003	0.057	-0.157	...	-0.009	-0.005	0.016	-0.006	6
2005 Jul 3	3554.66	21.00	...	-0.012	-0.006	0.043	-0.091	...	-0.010	-0.006	0.016	-0.006	4
2005 Jul 4	3555.77	22.11	0.075	-0.013	-0.003	0.012	-0.010	-0.049	-0.010	-0.007	0.016	-0.005	1
2005 Jul 6	3557.68	24.02	0.033	-0.04	-0.011	0.020	-0.153	-0.049	-0.012	-0.009	0.016	-0.005	2
2005 Jul 6	3557.73	24.07	0.077	-0.016	-0.003	0.012	-0.008	-0.049	-0.012	-0.009	0.016	-0.004	1
2005 Jul 7	3559.48	25.82	...	-0.020	0.008	0.08	-0.126	...	-0.013	-0.012	0.017	-0.004	6
2005 Jul 8	3559.59	25.93	...	0.035	-0.016	0.006	-0.002	...	-0.013	-0.012	0.017	-0.004	8
2005 Jul 8	3559.61	25.95	...	-0.022	0.003	0.023	-0.074	...	-0.013	-0.012	0.017	-0.003	4
2005 Jul 8	3559.70	26.04	0.073	-0.025	1E-3	0.012	-0.006	-0.049	-0.013	-0.012	0.017	-0.003	1
2005 Jul 8	3559.73	26.07	...	-0.046	-0.002	0.011	0.019	...	-0.013	-0.012	0.017	-0.003	7
2005 Jul 8	3559.76	26.10	...	-0.046	0.010	0.023	0.045	...	-0.013	-0.012	0.017	-0.003	5
2005 Jul 10	3561.73	28.07	0.067	-0.026	0.004	0.011	-0.003	-0.049	-0.013	-0.015	0.017	-0.002	1
2005 Jul 10	3562.42	28.76	...	-0.023	0.010	0.081	-0.118	...	-0.013	-0.016	0.017	-0.002	6
2005 Jul 11	3562.63	28.97	...	-0.023	0.004	0.010	-0.063	...	-0.013	-0.017	0.017	-0.002	4
2005 Jul 11	3562.72	29.06	0.078	-0.048	0.009	0.019	...	-0.05	-0.013	-0.017	0.017	...	5
2005 Jul 11	3563.03	29.37	...	...	...	...	...	...	-0.013	-0.017	0.017	-0.002	3
2005 Jul 11	3563.42	29.76	...	-0.023	0.010	0.08	-0.116	...	-0.013	-0.018	0.018	-1E-3	6
2005 Jul 12	3563.70	30.04	...	-0.055	0.003	0.009	0.022	...	-0.013	-0.018	0.018	-1E-3	7
2005 Jul 12	3563.73	30.07	0.063	-0.024	0.004	0.011	-1E-3	-0.050	-0.013	-0.018	0.018	-1E-3	1
2005 Jul 13	3565.39	31.73	...	-0.025	0.009	0.079	-0.1	...	-0.013	-0.021	0.018	0	6
2005 Jul 14	3565.71	32.05	0.058	-0.026	1E-3	0.010	1E-3	-0.051	-0.013	-0.022	0.018	0	1
2005 Jul 17	3569.40	35.74	...	-0.027	0.006	0.077	-0.089	...	-0.013	-0.020	0.019	0.002	6
2005 Jul 18	3569.54	35.88	...	-0.027	0.003	0	-0.043	...	-0.013	-0.020	0.019	0.002	4
2005 Jul 19	3570.70	37.04	0.047	-0.025	0.003	0.011	0.004	-0.050	-0.013	-0.019	0.019	0.003	1
2005 Jul 19	3570.80	37.14	...	-0.058	0.003	0.009	0.021	...	-0.013	-0.019	0.019	0.003	7
2005 Jul 21	3572.70	39.04	0.046	-0.026	0.003	0.012	0.005	-0.052	-0.013	-0.019	0.020	0.004	1
2005 Jul 22	3573.60	39.94	...	-0.029	0.002	-0.005	-0.036	...	-0.013	-0.018	0.020	0.005	4
2005 Jul 23	3574.70	41.04	0.044	-0.026	0.004	0.012	0.005	-0.051	-0.013	-0.018	0.020	0.006	1
2005 Jul 23	3574.76	41.10	...	-0.058	0.002	0.010	0.025	...	-0.013	-0.018	0.020	0.006	7
2005 Jul 24	3576.40	42.74	...	-0.027	0.006	...	-0.077	...	-0.013	-0.017	...	0.007	6
2005 Jul 25	3576.61	42.95	...	-0.029	1E-3	-0.008	-0.032	...	-0.013	-0.017	0.021	0.007	4
2005 Jul 25	3576.73	43.07	0.044	-0.027	0.004	0.013	0.005	-0.050	-0.013	-0.017	0.021	0.007	1
2005 Jul 27	3578.69	45.03	0.045	-0.028	0.005	0.015	0.007	-0.050	-0.013	-0.016	0.021	0.008	1
2005 Jul 28	3579.55	45.89	...	-0.031	0	-0.004	-0.029	...	-0.013	-0.016	0.021	0.009	4
2005 Jul 29	3580.69	47.03	0.046	-0.029	0.004	0.017	0.007	-0.049	-0.013	-0.015	0.021	0.010	1
2005 Jul 29	3581.00	47.34	...	...	...	...	...	...	-0.013	-0.015	0.021	0.010	3
2005 Jul 31	3582.69	49.03	0.048	-0.027	0.003	0.017	0.006	-0.049	-0.013	-0.015	0.021	0.011	1
2005 Aug 2	3584.69	51.03	0.049	-0.025	0.002	0.016	0.007	-0.048	-0.013	-0.014	0.021	0.013	1
2005 Aug 4	3586.69	53.03	0.05	-0.023	0.002	0.016	0.007	-0.048	-0.013	-0.013	0.021	0.014	1
2005 Aug 6	3588.69	55.03	0.051	-0.021	0	0.017	0.007	-0.047	-0.013	-0.012	0.021	0.016	1
2005 Aug 6	3588.71	55.05	...	-0.046	-0.002	0.018	0.071	...	-0.013	-0.012	0.021	0.016	7
2005 Aug 8	3590.69	57.03	0.05	-0.019	0	0.017	0.006	-0.047	-0.013	-0.011	0.021	0.017	1
2005 Aug 10	3592.69	59.03	0.05	-0.017	-1E-3	0.016	0.006	-0.046	-0.013	-0.011	0.021	0.019	1
2005 Aug 14	3596.68	63.02	...	-0.013	-0.002	0.016	...	...	-0.014	-0.009	0.020	...	1
2005 Aug 17	3599.68	66.02	...	-0.008	-0.002	0.017	0.006	...	-0.014	-0.008	0.019	0.025	1
2005 Aug 18	3601.01	67.35	...	...	...	...	...	...	-0.014	-0.008	0.019	0.026	3
2005 Aug 19	3602.67	69.01	...	-0.005	-0.003	0.016	0.006	...	-0.014	-0.007	0.018	0.027	1
2005 Aug 20	3604.01	70.35	...	...	...	...	...	...	-0.014	-0.007	0.018	0.027	3
2005 Aug 21	3605.11	71.35	...	...	...	...	...	...	-0.014	-0.006	...	...	3
2005 Aug 22	3605.67	72.01	...	-0.002	-0.004	0.017	0.006	...	-0.014	-0.005	0.017	0.03	1
2005 Aug 25	3608.67	75.01	...	0.003	-0.003	0.016	0.006	...	-0.014	-0.004	0.015	0.033	1
2005 Aug 28	3611.67	78.01	...	0.007	-0.003	0.016	0.006	...	-0.014	-0.003	0.013	0.036	1
2005 Aug 31	3614.66	81.00	...	0.011	-0.003	0.016	0.006	...	-0.014	-0.002	0.011	0.039	1
2005 Sept 3	3617.66	84.00	...	0.015	-0.003	0.016	0.007	...	-0.014	-1E-3	0.008	0.042	1
2005 Sept 4	3618.65	84.99	...	0.018	-0.003	0.015	0.008	...	-0.014	0	0.007	0.043	1
2005 Sept 7	3621.66	88.00	...	0.022	-1E-3	0.012	0.009	...	-0.014	1E-3	0.005	0.046	1
2005 Sept 10	3624.65	90.99	...	0.026	0	0.010	0.010	...	-0.014	0.002	0.002	0.049	1

<sup>a</sup> Relative to the epoch of *B*-band maximum (JD = 2,453,533.66).<sup>b</sup> 1 = KAIT 0.76 m; 2 = FLWO 1.2 m; 3 = TNT 0.8 m; 4 = CTIO 1.3 m; 5 = Lick 1.0 m; 6 = Liverpool 2.0 m; 7 = Palomar 1.5 m; 8 = CTIO 0.9 m